

IPICYT

INSTITUTO POTOSINO DE INVESTIGACIÓN CIENTÍFICA Y TECNOLÓGICA, A.C.

División de Ingeniería Ambiental y Manejo de Recursos
Naturales Renovables

Modelación numérica de la dispersión de material
particulado atmosférico y regionalización climática en
México.

Tesis que presenta

LUIS FELIPE PINEDA MARTÍNEZ

Para obtener el grado de

DOCTOR EN CIENCIAS

En la especialidad de CIENCIAS APLICADAS

Director de tesis Dr. José Noel Carbajal Pérez

San Luis Potosí, S.L.P.

Junio, 2009



CARTA DE AUTORIZACIÓN DEL COMITÉ TUTORAL

División de Ciencias Ambientales
Doctorado en Ciencias Aplicadas opción en Ciencias Ambientales




San Luis Potosí, S.L.P., a 14 de Mayo de 2009

Dr. Felipe Alatríste Mondragón

Coordinador Académico del Programa de
Doctorado en Ciencias Aplicadas opción en Ciencias Ambientales
PRESENTE

Por medio de la presente, le informamos que después de haber revisado el trabajo de Tesis de Doctorado del (la) estudiante **Luis Felipe Pineda Martínez**, no encontramos inconveniente alguno para que pueda llevarse a cabo el Examen de Grado ante un jurado.

Atentamente,

COMITÉ TUTORAL	
Nombre de Investigador	Firma de Aceptación
Dr. José Noel Carbajal Pérez	
Dr. Antonio Aragón Piña	
Dr. José Agustín García Reynoso	

*Este formato será entregado por el alumno en el Departamento de Recursos Escolares



Esta tesis fue elaborada en la División de Ciencias Ambientales del Instituto Potosino de Investigación Científica y Tecnológica, A.C., bajo la dirección del Dr. José Noel Carbajal Pérez.

Durante la realización del trabajo el autor recibió una beca académica del Consejo Nacional de Ciencia y Tecnología (**182528**).



Instituto Potosino de Investigación Científica y Tecnológica, A.C.

Acta de Examen de Grado

El Secretario Académico del Instituto Potosino de Investigación Científica y Tecnológica, A.C., certifica que en el Acta 004 del Libro Primero de Actas de Exámenes de Grado del Programa de Doctorado en Ciencias Aplicadas en la opción de Ciencias Ambientales está asentado lo siguiente:

En la ciudad de San Luis Potosí a los 12 días del mes de junio del año 2009, se reunió a las 12:00 horas en las instalaciones del Instituto Potosino de Investigación Científica y Tecnológica, A.C., el Jurado integrado por:

Dr. Antonio Aragón Piña	Presidente	UASLP
Dr. José Agustín García Reynoso	Secretario	UNAM
Dr. Jaime Jesús Carrera Hernández	Sinodal	IPICYT
Dr. José Noel Carbajal Pérez	Sinodal	IPICYT

a fin de efectuar el examen, que para obtener el Grado de:

**DOCTOR EN CIENCIAS APLICADAS
EN LA OPCIÓN DE CIENCIAS AMBIENTALES**

sustentó el C.

Luis Felipe Pineda Martínez

sobre la Tesis intitulada:

Modelación numérica de la dispersión de material particulado atmosférico y regionalización climática en México

que se desarrolló bajo la dirección de

Dr. José Noel Carbajal Pérez

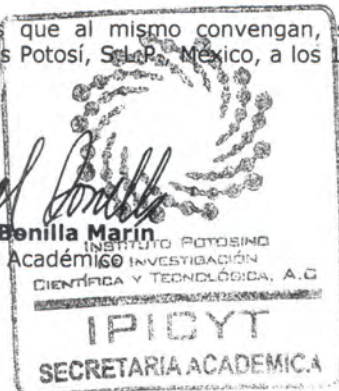
El Jurado, después de deliberar, determinó

APROBARLO

Dándose por terminado el acto a las 13:35 horas, procediendo a la firma del Acta los integrantes del Jurado. Dando fe el Secretario Académico del Instituto.

A petición del interesado y para los fines que al mismo convengan, se extiende el presente documento en la ciudad de San Luis Potosí, S.L.P., México, a los 12 días del mes de junio de 2009.


Dr. Marcial Benilla Marín
Secretario Académico




Mtra. Ivonne Lizette Cuevas Vélez
Jefa del Departamento de Asuntos Escolares

Agradecimientos

Quiero agradecer al Dr. Noel Carbajal por su apoyo y por el buen ambiente de trabajo que mantuvimos. También mi profundo agradecimiento al Dr. José Alfredo Ramos su continuo apoyo y por su sincera amistad.

También, un reconocimiento por su participación y contribución en este trabajo a Arturo Campos Ramos, Cristina Noyola Medrano, Antonio Aragón Piña y Agustín García Reynoso.

A Leonardo Hernández, Jaime Carrera y Sydney Robertson por sus valiosos comentarios sobre este documento.

A todos mis compañeros y amigos que me acompañaron en mi aventura de estudiante de posgrado que sería una lista interminable, a todos gracias.

Contents

Hoja de aprobación de la tesis	ii
Créditos Institucionales	iii
Agradecimientos	iv
Lista de tablas	viii
Lista de figuras	ix
Resumen	xi
Abstract	xii
Chapter 1	1
General introduction	1
Chapter 2	6
Climatology and bioregions of Mexico: A description based on clustering analysis	6
Abstract	6
2.1 Introduction	7
2.2 Methodology	8
2.2.1. Data	8
2.2.2. Principal Components	9
2.2.3. Cluster Analysis	10
2.3 Results	14
2.3.1 Principal component analysis	14
2.3.2 Cluster Analysis	17
2.3.3 Average linkage solutions	18
2.3.4 Ward's solution	20
2.3.5 Temporal analysis	22
2.3.6 Bioclimatic regions	24
2.4 Summary and conclusions	26
References	28
Chapter 3	31
Impact of land vegetation cover on Land Surface Model of Atmospheric	31

Circulation Models in arid regions from central-northern Mexico	
Abstract	31
3.1 Introduction	32
3.2 Model Simulations	34
3.3 Results	36
3.3.1 Moisture availability and land vegetation cover	36
3.3.2 Wind speed and friction velocity	45
3.4 Discussion	46
3.4.1 Vertical structure	51
3.5 Conclusions	52
References	53
Chapter 4	58
Numerical modeling of a dust storm induced by strong winds in the semiarid human impacted zone of Mexico	58
Abstract	58
4.1. Introduction	59
4.2. Description of the dust event	61
4.2.1 Dust dispersion modeling	62
4.2.2 Characterization of PM10	64
4.3 Results	64
4.3.1 Modeled and measured meteorological variables	64
4.3.2 Dust flux emission and dispersion	67
4.3.3 PM10 properties and solar radiation	70
4.4 Discussion	71
4.5 Conclusions	75
References	76
Chapter 5	81
Dispersion modeling of the atmospheric particulate matter in the Urban Area of San Luis Potosi, Mexico.	81
Abstract	81
5.1. Introduction	82
5.1.1. Study area	84
5.2. Methods	85
5.2.1 Dispersion model	85

5.2.2 Data	85
5.2.3 Simulations	85
5.3. Results and Discussion	86
5.3.1 Atmospheric circulation	86
5.3.2 Model validation with observed meteorological data	87
5.3.3 PM10/TSP	90
5.3.4 TSP Characteristic	98
5.4. Conclusions	100
References	102
Chapter 6	107
Conclusion	107

List of Tables

Table 2.1	Summary of the 9 cluster of years applying Ward's method	23
Table 3.1	RMSE for the experiments of MA and VC	41
Table 4.1	RMSE values of MCCM outputs and measurements data for meteorological variables	65
Table 5.1	RMSE values of temperature (RMSE _t), Relative Humidity (RMSE _{rh}) and Wind speed (RMSE _w).	88
Table 5.2	RMSE values of PM10 and modeled PM10 and observed TSP proportion	91

List of Figures

Fig. 2.1	Time series of dataset	9
Fig. 2.2	PC loading plots	14
Fig. 2.3	PC loading horizontal distribution map	16
Fig. 2.4	Clusters histogram	17
Fig. 2.5	Pseudo statistics	18
Fig. 2.6	Link Average solution	20
Fig. 2.7	Ward's solution	21
Fig. 2.8	P/T time series	22
Fig. 2.9	Vegetation and climate regions of Mexico	25
Fig. 3.1	Location map	34
Fig. 3.2	T and RH winter case	37
Fig. 3.3	Latent and sensible heat fluxes	39
Fig. 3.4	T and RH summer case	40
Fig. 3.5	Ground heat flux	43
Fig. 3.6	Wind speed and friction velocity	46
Fig. 3.7	Cold front horizontal plot	47
Fig. 3.8	Warm front horizontal plot	49
Fig. 3.9	Cross section (SW-NE) on 1 Dec 2004	51
Fig. 4.1	Location map of dust storm	61
Fig. 4.2	Horizontal plots of T and V	66
Fig. 4.3	Cross section SW-NE showing wind circulation	67
Fig. 4.4	Observed and modeled PM10 concentration	68
Fig. 4.5	Horizontal plots of PM10 dispersion	69
Fig. 4.6	Diffractogram and micrograph	70
Fig. 4.7	Solar radiation and infrared filtered channel of MODIS image	71
Fig. 4.8	Short down ward radiation horizontal plots	73

Fig. 5.1	Location map of Urban Area of San Luis Potosi	84
Fig. 5.2	Observed and modeled T and RH for UASLP	89
Fig. 5.3	TSP/PM10 observed and modeled for Oct 2008	90
Fig. 5.4	TSP/PM10 ratio	92
Fig. 5.5	TSP/PM10 observed and modeled data	93
Fig. 5.6	Horizontal plots of PM10 dispersion for UASLP	95
Fig. 5.7	Cross section plot of PM10 dispersion for UASLP	97
Fig. 5.8	Horizontal plots of mean PM10 dispersion for UASLP	98
Fig. 5.9	Micrography of atmospheric particles	99

Pineda-Martinez Luis F. (2009) Modelación numérica de la dispersión de material particulado atmosférico y regionalización climática en México.
IPICYT

Resumen

En este trabajo se llevó a cabo la modelación numérica de la circulación atmosférica en la región centro-norte de México en la zona de transición de la Sierra Madre Oriental. Se estudiaron los efectos de frentes fríos y calidos y proceso convectivos forzados por barreras topográficas sobre el clima de la región. También, se investigaron otros efectos como las propiedades de la superficie del suelo, cobertura vegetal y humedad disponible del suelo en la circulación atmosférica. Una vez conocidos estos fenómenos meteorológicos se investigó estos procesos recurrentes en la zona del Altiplano Mexicano, particularmente en la región del semidesierto de Zacatecas. La erosión del suelo por efectos de fuertes vientos y severas tormentas de polvo fueron estudiadas por su importancia en pérdida de suelo y calidad del aire en zonas urbanas como en las ciudades de Zacatecas, San Luis Potosí, Torreón y Monterrey. Los experimentos numéricos fueron capaces de reproducir las plumas de polvos y su dispersión por grandes zonas de México. Otra aplicación de los modelos de circulación y dispersión fue el estudio del origen y dispersión material particulado urbano de la fracción menor a los 1×10^{-6} m en la ciudad de San Luis Potosí. Fue posible explicar el transporte de partículas desde la zona industrial hacia la zona urbana. En estos experimentos hubo buen acuerdo entre datos observados y modelados. Para entender mejor la climatología de México, se procedió a establecer regiones climáticas aplicando técnicas estadísticas y de métodos agrupamiento jerárquico de datos climáticos. Se utilizó una base de datos de cerca de 2000 estaciones climáticas de México. Los climas resultantes se aproximan adecuadamente a regionalizaciones anteriores así como a la vegetación característica de cada región. Todas estas investigaciones contribuyen a entender mejor un gran número de fenómenos atmosféricos recurrentes en la región del norte de México.

Palabras Clave: Modelos numéricos, Propiedades de la superficie, Dispersión de contaminantes, Regiones climáticas,

Pineda-Martinez Luis F. (2009). Numerical modeling of the dispersion of atmospheric particulate matter and climatic regionalization in Mexico. IPICYT

Abstract

In this work was carried out numerical modeling of atmospheric circulation in central and northern Mexico in the transitional zone of the Eastern Sierra Madre. We studied the effects of cold and warm fronts and convective process induce by topographic barriers on the climate of the region. Also, other effects were investigated as land surface properties, vegetation and soil moisture availability on the atmospheric circulation. Once known these meteorological phenomena we investigate the processes of recurring weather events in Mexican Altiplano area, particularly in the region of the semi Zacatecas. Soil erosion by strong winds and severe dust storms were studied for their importance on soil loss and air quality in urban areas in the cities of Zacatecas, San Luis Potosi, Torreon and Monterrey. The numerical experiments were able to reproduce the plumes of dust and its dispersion through large areas of Mexico. Another application of circulation and dispersion models was to study the origin and deposition of urban particulate matter of the fraction less than 1×10^{-6} m in the city of San Luis Potosi. It was possible to explain the transport of particles from the industrial area into the urban area. In these experiments there was good agreement between modeled and observed data. In order to better understand the climate of Mexico, was established climatic regions by applying statistical techniques and hierarchical clustering methods of climatic data. A database of over 2000 climatic stations in Mexico was used. The resulting climates were approximated to previous regionalization and to characteristic vegetation of each region. These investigations contribute to a better understanding many recurring atmospheric phenomena in the region of northern Mexico.

Keywords: Numerical Models, Land surface properties, Dispersion of pollutants, Climatic regions

Chapter 1

General Introduction

This thesis aims to link aspects of climate and vegetation cover with land surface properties on land-atmosphere interactions and other environmental concerns. In this work we develop a study of the climatic regions of Mexico by applying multivariate statistical techniques. These techniques are based on matrix calculation and grouping for regional and seasonal climatic characteristics from temperature and precipitation database. The heterogeneous spatial distribution and high variations in the variables cause that standardization processes is carry out by applying principal component method which by its nature gives a new array with no correlation of each component (orthogonal). This new component-based matrix is grouped in terms of its variance to create clusters where intra-group variance is minimized. Hence climatic regions are deduced with similar characteristics between members of each group. To complement this climatic study we analyze the vegetation cover. This gives us a distribution of climates for each vegetation type (bioclimates). Defining such bioclimatic zones is important because the modification of land use and cover may produce a direct effect on regional climate change by altering the physical parameters that determine the absorption and disposition of energy at the Earth's surface (Feddema et al, 2005).

The effect of land surface properties on atmospheric circulation models is analyzed on the third chapter of this thesis. We studied the effects of cold and warm fronts and convective process induce by topographic barriers on the climate of the region. Also, other effects were investigated as land surface properties, vegetation and soil moisture availability on the atmospheric circulation. The change in land surface properties has immediate impacts on

the weather and climate (Chase et al, 2000). These alterations have larger potential change in mid-latitude semiarid regions as well as implications on solar radiation, vegetation cover, albedo, soil moisture, aerodynamic roughness and other surface properties (Chang et al, 2000). Although, there are other factors affecting the global climate such as greenhouse gases, the growth of urban areas, and changes in land vegetation cover at different scales; it is difficult to obtain a separate effect of each of these factors (Kalnay and Cai, 2003). These combined effects cause changes in climate over the medium and long term as well as soil and biodiversity loss.

Changes in land vegetation cover by conversion into agricultural land affect the radiation balance by altering the albedo and also cause soil loss by erosion (Chase et al 2000, Koster et al. 2000). The factors directly related to effects on surface properties are associated with two major impacts on the weather and climate. The first impact is related to climate changes at global and regional scale by altering the balance of radiation fluxes and the land-atmosphere exchange energy (Feddemma et al, 2005; Chen and Dudhia 2001). The second one, linked to abrupt discontinuities in soil properties that induce mesoscale circulations (Garrat, 1993; Sud et al, 1988, Segal et al, 1989). These changes in the surface have been studied from a meteorological point of view for its importance in atmospheric circulation models. Some studies have shown the importance of the variability of land surface properties at different scales. This variability governs surface processes in extreme weather conditions (Miao et al; 2007).

The vegetation cover loss affects the structure of plant communities and soil physical properties (Collado et al; 2002). In the semi-arid zones of Mexico the largest soil loss is due

to wind erosion. In addition, there is a combined effect of the cold and dry winter season, when scarce vegetation cover is present with influence of strong winds that occur at this time of year. Thus, dust storms events are common in the region of the Mexican Highland. The soil loss can reach hundreds of tons per hectare during a single event in the most vulnerable agricultural regions (Hagen 1999). The loss of vegetation cover has also caused that large land surface in the semiarid region of Mexico present large problems of soil loss during the dry season. We have selected a case study in the north-central state of Zacatecas, Mexico to perform a study based on dispersion numerical model of an extreme wind event which caused an extraordinary dust storm.

The effect of land vegetation cover change on long term climate (regional and global) is an important issue and affects on several scales as well as other environmental concerns, for instance urban growth. Human impacted areas lead to increases in environmental pollution. Another application of circulation and dispersion models was to study the origin and deposition of urban particulate matter of the fraction less than 1×10^{-6} m in the city of San Luis Potosi. The air quality in urban areas is affected by some aspects related to daily urban activities. The urban area of San Luis Potosi has a population of nearly one million, with a large number of vehicles and an industrial zone of considerable size. There are few studies of air quality that give insight about the pollution problem associated with particulate matter emissions. This study case will be discussed in the last chapter of this thesis as an example of pollutant dispersion by a numerical model approach.

References

Chang DH, Jiang L, Islam S (2000) Issues of Soil Moisture Coupling in MM5: Simulation of the Diurnal Cycle over the FIFE Area. *J. Hydrometeor.* 1: 477–490.

Kalnay, E. and M. Cai (2003), Impact of urbanization and land-use change on climate, *Nature*, 423, 528-831.

Chase, T. N., R. A. Pielke, T. G. F. Kittel, R. R. Nemani, and S. W. Running (2000), Simulated impacts of historical land cover changes on global climate, *Clim Dyn.*, 16, 93–105.

Chen F, Dudhia J (2001b) Coupling an advanced Land Surface–Hydrology Model with the Penn State–NCAR MM5 modeling system. Part II: Preliminary model validation. *Mon. Wea. Rev.*, 129: 587–604.

Collado, A.D., E. Chuvieco, and A. Camarasa (2002), Satellite remote sensing analysis to monitor desertification processes in the crop-rangeland boundary of Argentina. *J Arid Environ*, 52, DOI:10.1006/jare.2001.0980

Feddema J.J., K. W. Oleson, G. B. Bonan, L.O. Mearns, L.E. Buja, G.A. Meehl, W.M. Washington, (2005), The importance of land-cover change in simulating future climates. *Science*. 310, 1674-1678.

Garratt, J. R. (1993), Sensitivity of climate simulations to land-surface and atmospheric boundary-layer treatments A review, *J. Clim.*, 6, DOI: 10.1175/1520-0442(1993)006

Koster RD, Suarez MJ, Heiser M (2000) Variance and Predictability of Precipitation at Seasonal-to-Interannual Timescales. *J. Hydrometeor.*, 1: 26–46.

Miao JF, Chen D, Borne K (2007) Evaluation and Comparison of Noah and Pleim–Xiu Land Surface Models in MM5 Using GÖTE2001 Data: Spatial and Temporal Variations in Near-Surface Air Temperature. *J. Appl. Meteor. Climatol.* 46: 1587–1605.

Segal, M., W. E. Schreiber, G. Kallos, J. R. Garratt, A. Rodi, J. Weaver, and R. A. Pielke (1989), The impact of crop areas in northeast Colorado on midsummer mesoscale thermal circulations, *Mon. Weather Rev.*, 117, DOI: 10.1175/1520-0493(1989)117.

Sud, Y. C., J. Shukla, Y. Mintz (1988), Influence of land surface roughness on atmospheric circulation and precipitation: A sensitivity study with general circulation model, *J. Appl. Meteorol.*, 27, 1036–1054.

Chapter 2

Climatology and bioregions of Mexico: A description based on clustering analysis

Abstract

Climate regions of Mexico are delimited using Hierarchical Clustering Analysis (HCA). We assign the precipitation and temperature variables to groups or clusters based on similar statistical characteristics. Since meteorological stations in Mexico are heterogeneously distributed, we used Principal Components Analysis (PCA) to obtain a standardized reduced matrix to conveniently apply HCA. We consider monthly means of both maximum and minimum temperatures as well as monthly accumulated precipitation. HCA defines groups of stations that delimit regions of similar climate. In addition, the methodology describes the dominant vegetation for each climate region.

Pineda-Martinez L F and Carbajal N (2009) Climatology and bioregions of Mexico: A description based on clustering analysis. *Manuscript to be submitted to Int J Climatol*.

2.1 Introduction

Delimitation of climate regions introduces a series of the objective criteria to make regionalization based on multivariate statistical analysis of long-term meteorological data. In Mexico the climatology has been described by some authors (Garcia, 1989; Comrie and Glenn 1998; Englerth and Douglas, 2002; Nieto et al 2004; Giddings et al. 2005). To introduce new criteria is indispensable to understand climate zoning based on statistical data handling, nevertheless. In general, a set of meteorological observations from several stations of long term monthly means is used to define climate regions. In this case, is not only possible to define groups of stations delimiting a region but also time periods with similar behavior, for instance seasons (Kalkstein et al, 1987). We aim to describe climate regions based on hierarchical clustering analysis. Cluster analysis is used to assign a set of variables into groups or clusters based on similar characteristics (Mimmack et al, 2001). Cluster analysis has become a useful tool to define groups of objects within a dataset and allows finding meteorological regions. As meteorological stations are heterogeneously distributed we employed principal components analysis to generate a standardized matrix that may be suitable as an input to the cluster algorithm.

Although there are some methods of performing cluster analysis we compare Ward's minimum variance technique and average linkage results as described by Kalkstein et al (1987). Both methods showed similarities but with differences in estimating the matrix variables. We will present both results and a brief discussion. Finally, we attempt to describe the principal phenomena that affect climate distribution based only on results of the statistical analysis. Patterns obtained through these statistical tools show a consistent

correspondence with regional topographic attributes and physical obstacles such as mountain formations and the latitude effect, which are sketched by the results.

2.2 Methodology

2.2.1. Data

We employed data from the National Water Commission (CNA, 2007), which is the most complete climatic dataset for Mexico. In this particular case we consider maximum averaged temperature, minimum averaged temperature and accumulated precipitation on a monthly basis (36 variables total), from 1940 to 2004. A total of 2324 stations were used across Mexico considering only those with the most complete time series and discarding those with more than 10 years of missing data (Fig. 2.1). In addition, an algorithm was applied to every station to verify data quality, proceeding in the following way: in the first place a rough climatic classification was made to discard or accept each station, this was, applying criteria to exclude those stations that presented incongruent climate, for instance polar climate in middle latitudes. This is related to missing or errors in the time series. The second criterion was related to precipitation-temperature ratio; those stations exceeding more than 10 times this ratio were discarded. High precipitation values and cold temperature mean a data error. Finally, we verified a not zero average in the precipitation and temperature time series (not empty series). This study considers a two dimensional matrix from the dataset reduced by calculating monthly means through the total period. Although this reduction may imply a loss of detailed information, it is a practical procedure for cluster analysis without loss of tempo-spatial variability. The variables were standardized to mean 0 and standard deviation 1.

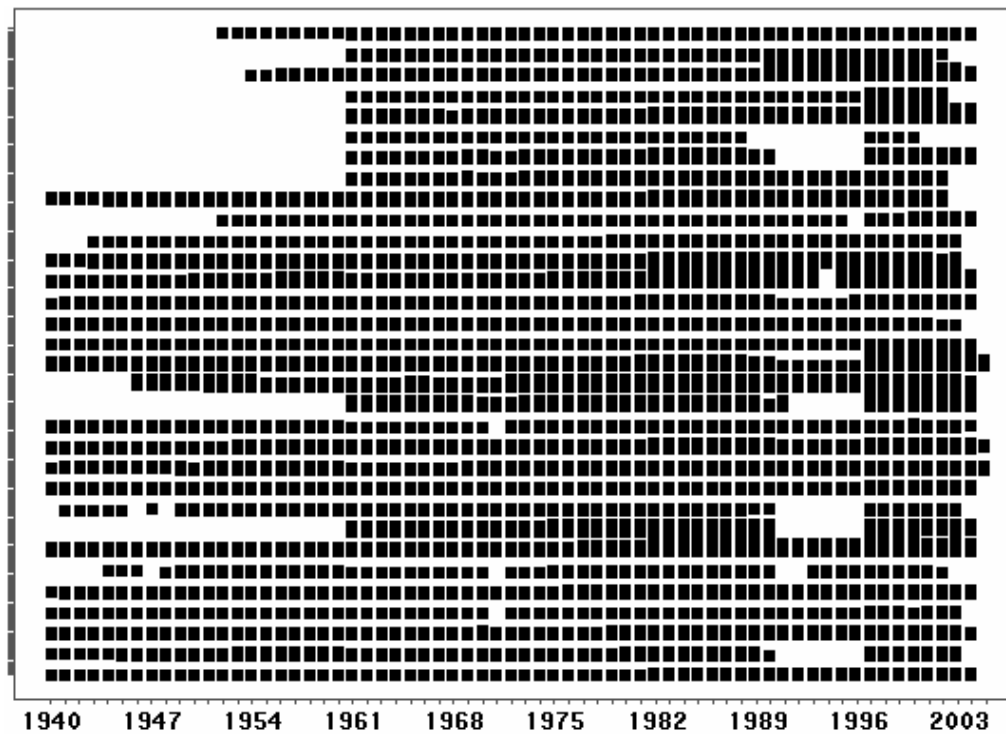


Fig. 2.1 Retained stations for clustering (2324) considering the most complete time series with at least 20 years of records. Squares represent stations groups for each State of Mexico in the vertical axis.

2.2.2. Principal Components

We conveniently used PCA to obtain a standardized reduced matrix that could be used in a hierarchical cluster analysis as described by Fovell and Fovell (1993). Spatial heterogeneous distribution of the stations motivated us to include this multivariate analysis to the dataset. Since PCA provides a set of new variables sorted by their explained variance we can reduce the dimensionality preserving the maximum possible variability (Fovell and Fovell, 1993).

The method of principal components is a multivariate statistical technique that involves linear transformations of a matrix of ‘standardized’ observed variables, based on the eigenvalues and eigenvectors of either a correlation matrix or a covariance matrix

(Ehrendorfer, 1987; Richman, 1981). The principal analytical purpose of PCA is to reduce the dimensions of the observed information, compiled in a data set, preserving the original data variability. Eigenvectors define a new coordinate system which is orientated in such a way that every new axis points to the maximum variability of the information (Wilks, 1995; Richman, 1981). The raw data matrix X contains n entities and m variables (2324x36). A rotate Varimax principal component analysis is carried out based on a covariance matrix components loadings matrix A ($m \times n$). It has been argued that the use of the correlation matrix, as opposed to covariance matrix, allows a direct comparison between dry and wet stations, but it is not useful to distinguish geographical effects (Comrie and Glenn, 1998).

This PCA has the goal of replacing the correlated original variables with new components mutually uncorrelated based under the principle of each component defined by an orthogonal base. The Rotate Varimax method assures major certainty of major variance inside the first components. This represents an advantage since the grouping will be on the basis of a minor number of variables (Richman, 1985). The eigenvector matrix resulting from PCA is often then truncated, which involves the omission of some non zero components of A that can be redundant information. Errors could exist for omission of residual variance and we also must consider the introduction of redundant information. The decision of truncation may be based in a priori considerations. Although the variables present a tempo-spatial heterogeneous distribution, PCA makes an efficient work avoiding the non-normal behavior in data.

2.2.3. Cluster Analysis

Cluster analysis allocates a set of objects into groups or clusters on the basis of measurements of similarity. This similarity or distance for a metric data is basically an

Euclidean measurement, which is a simple square difference between two objects (Fovell and Fovell, 1993; Mimmack et al, 2001). Agglomerative hierarchical clustering is an algorithm which starts with n clusters each containing one member or observation. In the next step the method combine the nearest cluster pairs to create a new multi-object cluster. Hierarchical methods produce clusters that are not allowed to overlap and the objects in one level are combined with objects in a superior level.

Several combination options are possible depending of the metric used to define similarity among groups. In our case we tested two different possibilities: the average linkage method and the Ward method. The average linkage method defines the inter-group distance as an average distance between every possible pair of elements of the compared groups. This method creates groups with similar variance. The Ward method merges those elements that minimize the dispersion of the resultant group. Both methods use the average squared distance to combine different clusters.

The Ward method is described to illustrate these techniques.

Give a matrix of data (v_1, v_2, \dots, v_n) the Ward method separate the total variance V on intra-groups variance. For actual groups C_i with centroid c_i and mass m_i in a specific iteration the variance among groups is:

$$V = \sum_q m_q \|c_q - c\|^2 + \sum_q \sum_{i \in C_q} m_i \|v_i - c_q\|^2 \quad (2.1)$$

Where c is the global centroid (mean of the data).

If two groups C_i and C_j with mass m_i and m_j respectively, are merged in a new group, D , with mass $m_i + m_j$ and centroid:

$$d = \frac{c_i m_i + c_j m_j}{m_i + m_j} \quad (2.2)$$

Then, the variance V_{ij} of C_i and C_j respect to D can be computed by

$$V = m_i \|c_i - d\|^2 + m_j \|c_j - d\|^2 + m \|c - d\|^2 \quad (2.3)$$

The last term is constant even changing C_i and C_j by the centroid D . Thus, the reduction of the variance is

$$\Delta V_{ij} = m_i \|c_i - d\|^2 + m_j \|c_j - d\|^2 \quad (2.4)$$

Using 2.2, we have

$$\begin{aligned} \Delta V_{ij} &= m_i \left\| c_i - \frac{c_i m_i + c_j m_j}{m_i + m_j} \right\|^2 + m_j \left\| c_j - \frac{c_i m_i + c_j m_j}{m_i + m_j} \right\|^2 \\ &= \frac{m_i m_j}{m_i + m_j} \|c_i - c_j\|^2 \end{aligned} \quad (2.5)$$

The process of this method is the join, in every step of groups C_i and C_j that minimize ΔV_{ij} (initially every element is considered as a group). Therefore, ΔV_{ij} is considered as a measurement of similitude and those elements with less mass are merged first.

The number of clusters continues reducing by one each step and this procedure end when one cluster containing every object is created. This process should be examined to determine which step or clustering level represents the optima solution. Although delimitation of climate regions is our final goal it is important to discern a reliable number of clusters. The optimal number of clusters is determined by using “stopping rules” *pseudo-F* and *pseudo-t²* scores to determine cluster cohesiveness (Kalstein et al, 1987; Fovel and Fovell, 1993; Degaetano 1996). Pseudo *F* is given by the formula:

$$pseudoF = \left[\frac{A}{W} \right] * \left[\frac{(n-k)}{(k-1)} \right] \quad (2.6)$$

where A and W are the among and within clusters sum of squares respectively, n is the number of objects and k is the number of existing clusters.

The pseudo t^2 statistic for joining C_i and C_j is

$$pseudot^2 = \left[\frac{(W_i - W_j) / \left(\left[\frac{(W_i + W_j)}{(n_i + n_j - 2)} \right] \right)}{\left(\left[\frac{(W_i + W_j)}{(n_i + n_j - 2)} \right] \right)} \right] \quad (2.7)$$

Guidance for the selection of the final number of clusters is to observe a local maximum of the *pseudo-F* followed by a local maximum of the *pseudo-t²* as the number of clusters decreases. The local maximums of *pseudo-F* and *pseudo-t²* are considered to be the optimal number of clusters (Kalstein et al, 1987). This issue is less problematic in the current study since our goal is to define climatically homogenous regions rather than the true cluster data structure.

Hierarchical cluster analysis was carried out to group the first components after truncation. Average linkage and Ward's are similar agglomerative hierarchical cluster methods merging pairs with smallest inter-cluster distance differing in their designation of this distance. Ward's method gives inter-clusters minimum variance, and is the most frequently used method for climatic classification (Kalkstein et al, 1987). For average linkage method, the distance between clusters is the average of two other linking clustering from all possible pairs of elements in the two evaluated clusters. In other words, the distance is the average distance between possible pairs of elements in two clusters compared, similar to Ward method. Thus average linkage method tends to generate clusters with similar variance and has little influence on cluster size. In addition, is more efficient working with compact groups and defectively separated clusters (Degaetano, 1996; Fovell and Fovell, 1993).

2.3 Results

2.3.1 Principal component analysis

PCA result showed a distribution of temperature in component 1 and precipitation in component 2. Figure 2.2 presents loading distributions which are characterized by presenting temperature variables mainly by component 1 that represents 55 % of the explained variance while component 2 is related to precipitation variables with 23.5 % of explained variance. In this study we decided to retain components with eigenvalues greater than 1 based on concurrence of rule N (Kalstein et al, 1987). Were retained four components which explained a 91% of variance when summed. The rest of the components were scarcely significant (each with eigenvalue<1).

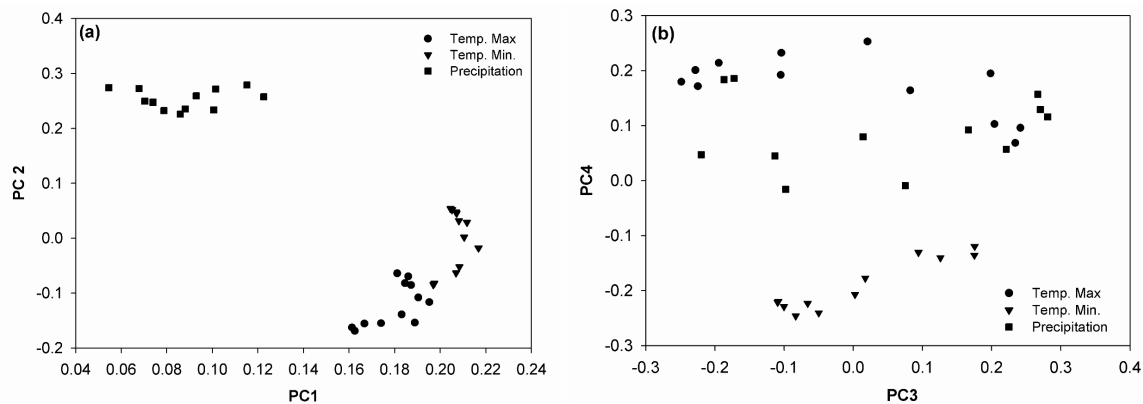


Fig. 2.2 Plot of principal components (a) PC1 versus PC2 scores, and (b) PC3 versus PC4 scores for the 1940-2004 dataset.

Minimum temperatures have the major contribution in PC1 mainly because they have a major variability within the winter season. In contrast, we observed some points near zero in PC2 axis which correspond to May and October minimum temperatures due to a lower fluctuation in minima temperatures. Maximum temperatures tend to a negative influence in PC2 possibly due to less variability on fluctuations in maximum temperatures trough all

stations. Principal component 2 is dominated by precipitation and describes 23.5 % of the variance. All precipitation variables are grouped within a small range of the loadings. This reduces discrepancies of each parameter and makes it possible to identify significant points that represent rainy months from August to October in PC1 axis. A clear influence of the mid-summer drought or ‘canicula’, associated to July when this phenomena take place. PC3 shows a clear seasonal influence based on temperatures and precipitation, describing a cool dry season from November to April and a warm rainy season for the remaining months. Of the rest of PC’s analyzed, only PC6 shows that the first half of the year is the most warm-dry while the second one is colder and wetter. Thus, our grouping will be attained to a four-dimensional space context defined by temperature maxima and minima (PC1), precipitation (PC2) and a combined contribution of both in PC3 and PC4. Although clustering might be made by retaining additional components, this would introduce redundant information.

Since the distribution on PC loadings are very constricted, tracing regions with similar variance is no practical by several reasons. As regions corresponding to different climates may have a similar PC loading, this tracing may group discrepant stations together. Also the northwestern of Mexico represents its driest part, in the Sonora Desert region; in contrast the southeastern is the wettest part, where the tropical forests can be found. While the Sonora Desert dominantly presents high temperature and scarce precipitation, the Yucatan Peninsula is characterized by presenting high precipitation, nevertheless the covariance as a group of climatic variables is very similar so PC loadings are close each together (Fig. 2.3). Since the distances between stations with low mean and variance are likely to be small simply because differences in rainfall are small in absolute terms, these stations are likely to be clustered together (Mimmack et al, 2001). As discussed by

Englehart and Douglas (2002), summer precipitation defines principal climate regions in Mexico (five in their study), but they did not consider the quantity and the seasonal variability of rainfall. As a result, stations placed in contrasting climatic regions were grouped together; for instance the Yucatan peninsula and semiarid region of highland in the central part are put in the same region. This is not a statistical error since the variability and correlation of loadings of PC's is very high as shown in Fig. 2.3. Hence in our calculation, we introduce an additional criterion in order to avoid stations with similar climate characteristics drop into different climate classification and vice versa. As a result we introduced a standardized cumulated average annual precipitation to scatter the loadings of PC's (see Fig. 2.2a). This was done in both clustering methods resulting in a better regionalization.

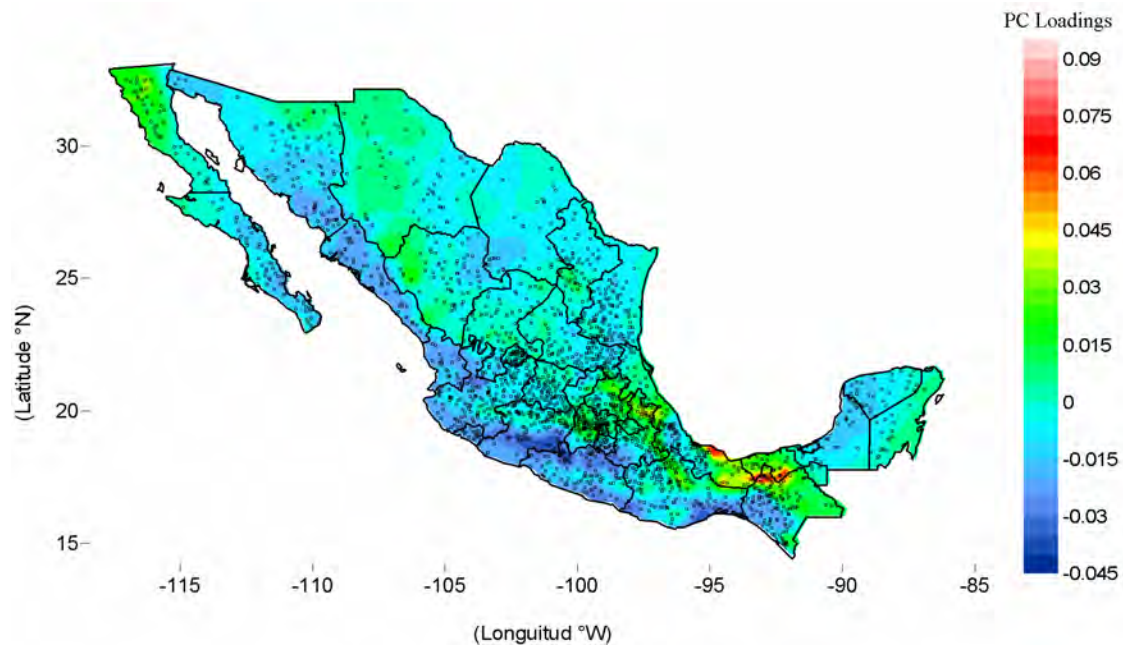


Fig. 2.3 Spatial distributions of the four retained components (shaded color), and climatic stations distribution in Mexico.

2.3.2 Cluster Analysis

The second step in the procedure involves the delineation of natural groupings of stations which share similar meteorological characteristics. The classification is carried out by using clustering techniques through the retained PC. Once that the number of retained PC has been decided clustering methods are applied in order to make a grouping of stations. Average linkage and Ward's methods were carried out in a fourth PC base. Spatial interpolation was done by using geostatistical ordinary kriging method and a linear variogram in order to represent each cluster into the geographical context.

The number of clusters needs to adequately delineate the climate regions for Mexico, which is the main goal. This is not a trivial exercise since we need to examine the behavior of clustering process step by step principally to know which level is the adequate subdivision, thus representing better the climate distribution. In our case we stopped when each cluster represented the principal climate region since the terrain distribution is very complex in Mexico. Thus we make calculations of the number of clusters from 8 to 22 in both methods. Figure 2.4 outlines the number of stations by clusters for Ward's and Average Linkage methods where a better distribution in Ward's method can be observed.

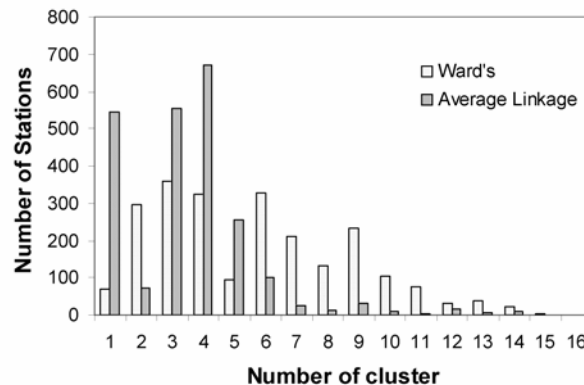


Fig. 2.4 Cluster size distributions histogram of in Ward's and Average linkage methods.

Making a pseudo statistics analysis (Fig. 2.5) we have been able to choose a level of clustering for both methods. For average linkage there is an abrupt increase in pseudo t^2 statistic associated with the formation of 10 and 11 clusters joined to subtle variations in pseudo F . Pseudo statistics suggest that a 12 level clustering for average linkage method is a reasonable point to stop the process, representing a good distribution of regions as is showed in the next section.

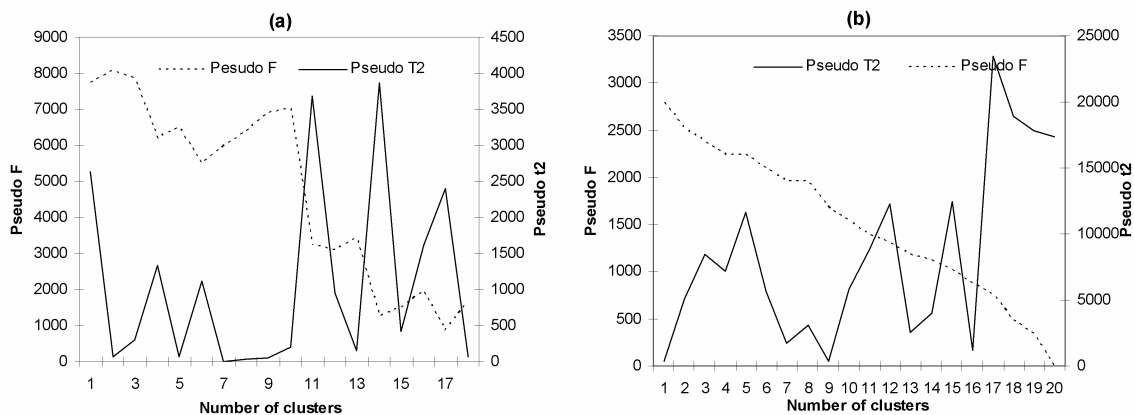


Fig. 2.5 Pseudo statistics (a) Average Linkage (b) Ward's

Ward's method displays a quite different behavior. Pseudo F decrease more smoothly than average linkage; while pseudo t^2 has an abrupt increase in cluster 17 and R^2 drops in 16 cluster levels. Based in these statistics we analyzed some solutions in different levels of clustering. For average linkage a 10 cluster solution was selected while for Ward's we examined 14 clusters which are not discussed here due to similitude between both results.

2.3.3 Average linkage solutions

The solution at the 10-cluster level is shown in Fig. 2.6, Average Linkage method produces an acceptable rough climate division in the context that almost all geographic regions are

approximately well represented. This suggests that the delimitation of clusters is concordant with topographic gradients and vegetation. Arid zones represent a great part of the territory, going from the south-central part to Chihuahua Desert, continuing to Texas and New Mexico in the south of the United States, as shown by Fovell and Fovell (1993). It can also be observed that the Sonora Desert and arid parts in the Baja California Peninsula enclose the northwestern part. Within the desert region is included the semi-desert zone through the highlands in the middle part of Mexico. The great Mountains formations are displayed in the West and East delimited in the cluster 5 although the method tends to merge some transition regions in the cluster 4. Cluster 5 represents wet climates, but there are clear differences between the temperatures range; while the Yucatan Peninsula is warmer, the Sierra Madre Occidental presents colder temperatures. Clusters 8, 9 and 10 represent rainy and warm zones in the region of the temperate-tropical forest in the southeastern between 15° and 17° of North Latitude. There is not a clear definition of the central mountains (Mesa Central), right from lowlands to the high plains region which is a transition zone at 20° N. Although cluster 2 capture some regions as lowlands (El Bajío), these does not have all similar climates, consequently joining together unrelated climatic regions (even different vegetation types). Overall, we can discuss Average Linkage denote the principal regions but cannot capture enough detail in the transitions. This is caused by the complexity of the data, which translates into a great covariance precisely because this method is not efficient reducing the inter-cluster variance as Ward's does.

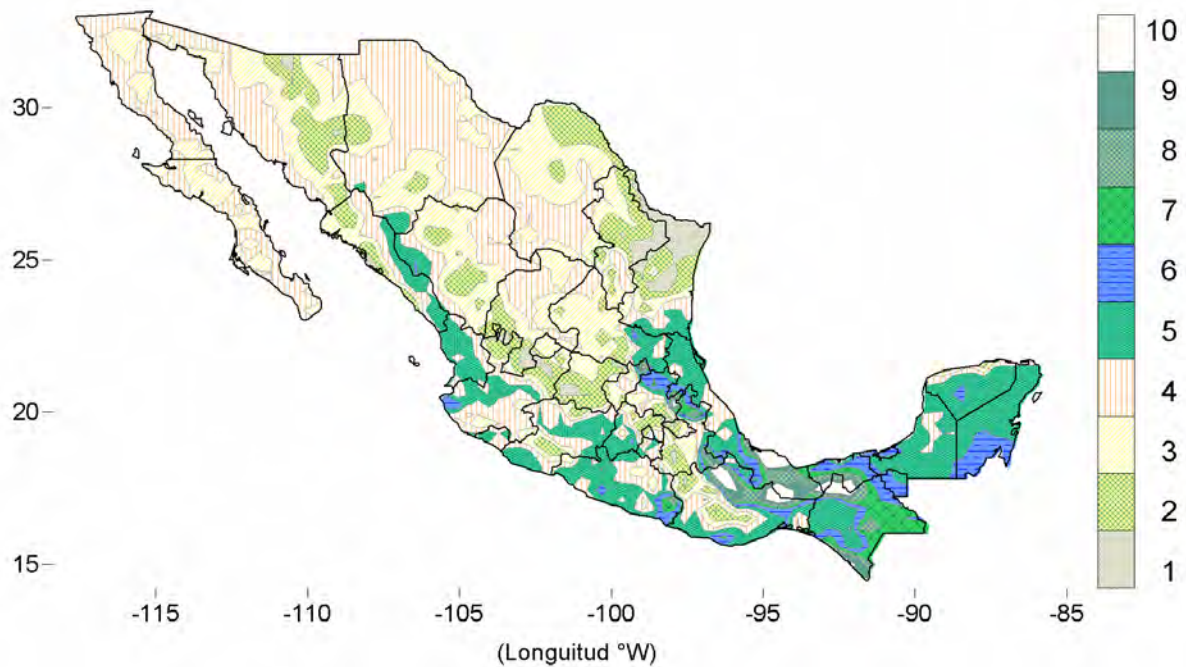


Fig. 2.6 Clusters solution of the 12 climate regions in Mexico by average linkage method.

2.3.4 Ward's solution

Figure 2.7 show a 12 clustering solution for Ward's method. Taking into account that there are other criteria (for instance vegetation) we found better results on Ward's than Average Linkage because Ward's solution capture more detail of all climate regions. Desert and arid climatic regions are well defined in the Chihuahuan desert area including the transition in the southern most part of the highlands and the transition between mountains and highland near to the isthmus. In addition, clusters 3, 4 and 5, also represent the degree of semi-arid climates in agreement with geographic position, for instance 3 and 4 represent almost all Mexican highlands in the central-northern part; cluster 5 not only represent arid zones (more arid) but also includes the Sonora Desert and California's Peninsula indicating a delimitation in range of precipitation. Cluster 6 defines regions near cluster 5 in arid regions despite to statistical similitude but with differences in precipitation regimes. Cluster 2 delimits the transition between temperate and humid climates in the plains of low lands

(El Bajío and Northeast plains). This gives us an idea about the climate gradient related to spatial distribution. Most of the wetter climates are located in the in the southeastern, after Cluster 7 humid and temperate climates are defined. These are located in the mountain regions and in the Peninsula of the Yucatan. Cluster 7 delineates all of the central mountains formations from Sierra Madre Occidental to lowland in the central part. Cluster 8 is almost all within of Peninsula of Yucatan and some regions in costal zone of the Gulf of Mexico which show humid climates. Clusters 9 and 10 are located in the regions of Tropical Forest with summer rainy regime and temperate climate. The wettest climate regions are delimited by Clusters 11 and 12 in the Sierra Alta regions of the Tehuantepec isthmus.

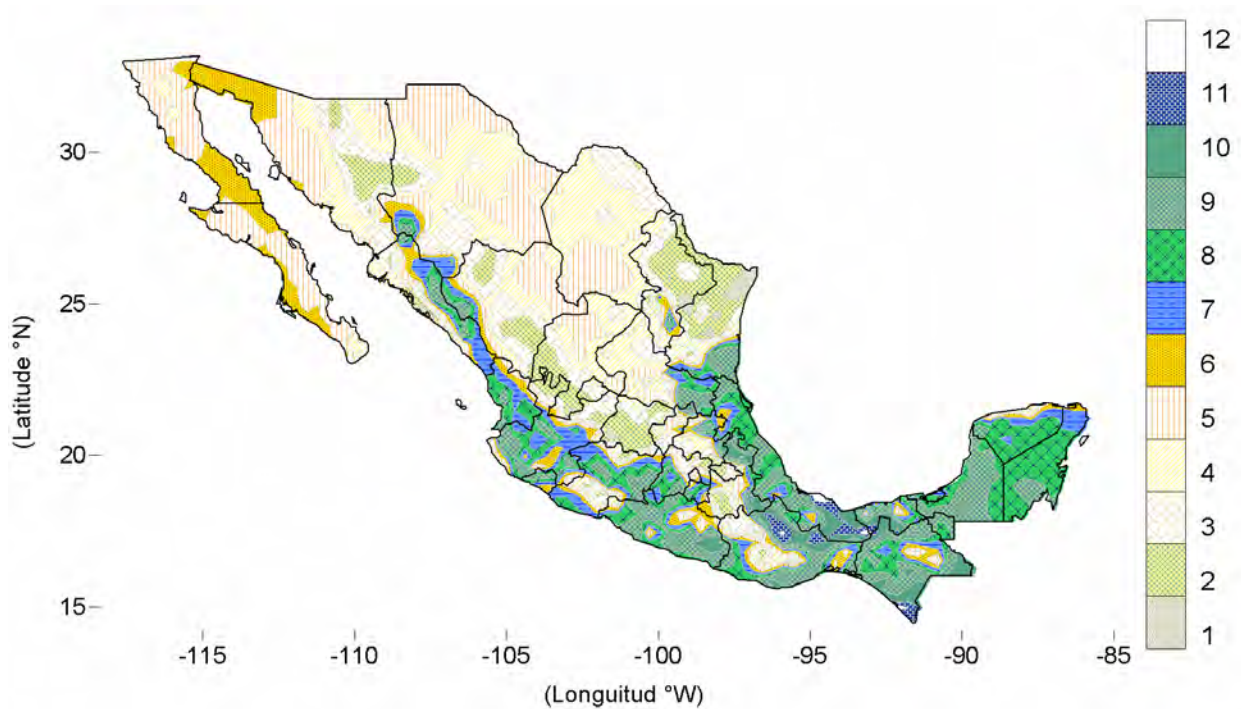


Fig. 2.7 Clusters solution of the 12 climate regions in Mexico using Ward's method

2.3.5 Temporal analysis

Since that the datasets, may be re-organized this permit to achieve different analysis depending of each case. Thus, we performed an analysis in terms of the temporal variation; it is possible to identify either climatic periods or extreme events such as drought. We analyzed time series by applying PCA-HCA methodology to find out years which presented large anomalies. Figure 2.8 shows time series and the ratio of precipitation and temperature from 1940 to 2004 period averaged from a total of 2324 stations in whole Mexico area. From a simple analysis; it is evident a series of peaks, the majority of them related to ENSO events. Nevertheless, we distinguish three principal periods determined by differences between precipitation and temperature (P/T ratio). These periods represent a major separation of both lines indicating a first period from 1940 to 1961. After 1961 precipitation and temperature lines keep near each other in a period of climatic stability, although also in this period there were a major introduction of industrial development and a quick increase in land use change during the 70's these are not revealed in these period (INEGI, 2000). It is possible that those anthropogenic forcing had had a delayed influence in the regional climate variation after the 90's, when the amplitude of both lines increase again, indicating an increase in mean temperature and less precipitation.

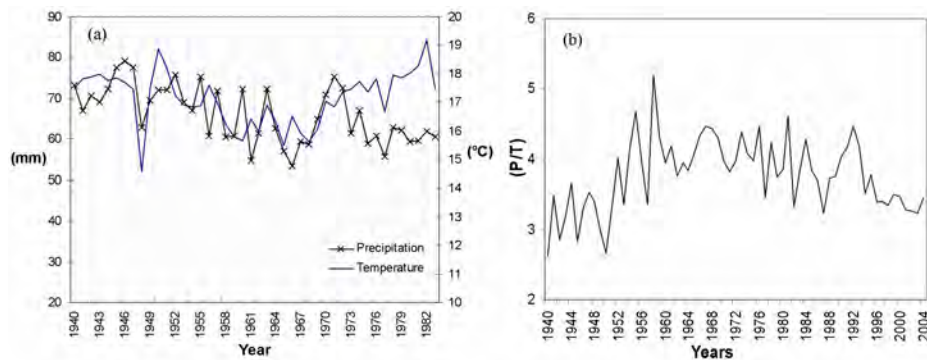


Fig. 2.8 (a) Time series of precipitation (crossed line), and temperature (continue line), and (b) P/T ratio for the same period.

Cluster analysis could give us a major idea of the delimitation of periods by doing an analysis of a recomputed matrix of the data. Therefore, if we take every variable considered in the last analysis but now averaged for the same 2324 used stations, we can build a matrix of years (64) in terms of maxima and minima temperature and monthly accumulated precipitation (36 variables). The raw data matrix Y contains now n entities (years) and m variables (64x36). Also was carried out a rotate Varimax PCA based on a covariance matrix components loadings matrix B ($m \times n$). Following the same idea we applied only Ward's method for clustering analysis based on 9 retained components which explain 73% of variance.

Table 2.1 Summary of the 9 cluster of years applying Ward's method.

Cluster Name	Years											
A	2000	2001	1999	1997	2002	2003	2004					
B	1956	1974	1975	1976	1984	1985	1986	1991				
C	1941	1943	1946	1948	1949	1952	1954	1959	1962	1977	1981	1982
D	1940	1951	1953	1979	1987							
E	1942	1945	1947	1957	1980	1988	1989	1990	1993	1994	1995	
F	1965	1967	1971	1973	1996	1998						
G	1955	1958	1960	1961	1963	1970	1972					
H	1944	1966	1968	1969	1978	1983						
I	1950	1964	1992									

Table 2.1 presents the grouping and distribution of the years; there is a clear influence of amplitude between precipitation and temperature (cluster A). Consequently, years with major amplitude appear away from the principal group, further represent the same clusters (G, H, I). Although, exist few years with an extraordinary behavior which are concurrent on ENSO events; for instance 1950 and 1988 (Fig. 2.8a). Clusters B, C and F correspond to stable years in the Fig. 2.8a; although some years with high values in temperature are

discriminated. Transitions are captured by clusters C and E, these represent the rest of years in the period of change. These do not represent a firm evidence of climate change but there is a clear increase in the variability of precipitation and temperature anomalies. Probably in the first period there was an influence by scarce and not optima distribution of the meteorological stations, but in the last period anomalies may be explained by the influence of global tendencies. We can do a quantitative analysis by an examination of the ratio between precipitation and temperature P/T shown in the Fig. 2.8b, where there is a clear negative tendency to decrease in the last period.

2.3.6 Bioclimatic regions

The land vegetation cover is defined by several criteria such as physiognomy and floristic composition and show a strong relationship with climate (Karlsen et al, 2003; Hessburg et al, 2005; Piovesan et al, 2005). Defining such bioclimatic zones is important because the modification of land use cover may produce a direct effect on regional climate change by altering the physical parameters that determine the absorption and disposition of energy at the Earth's surface (Feddema et al, 2005). Further we compare our result of climate regions with land vegetation cover of data form year 2000 (INE, 2000). In Fig. 2.9, it is shown the map of vegetation and the climate region based in Ward's solution.

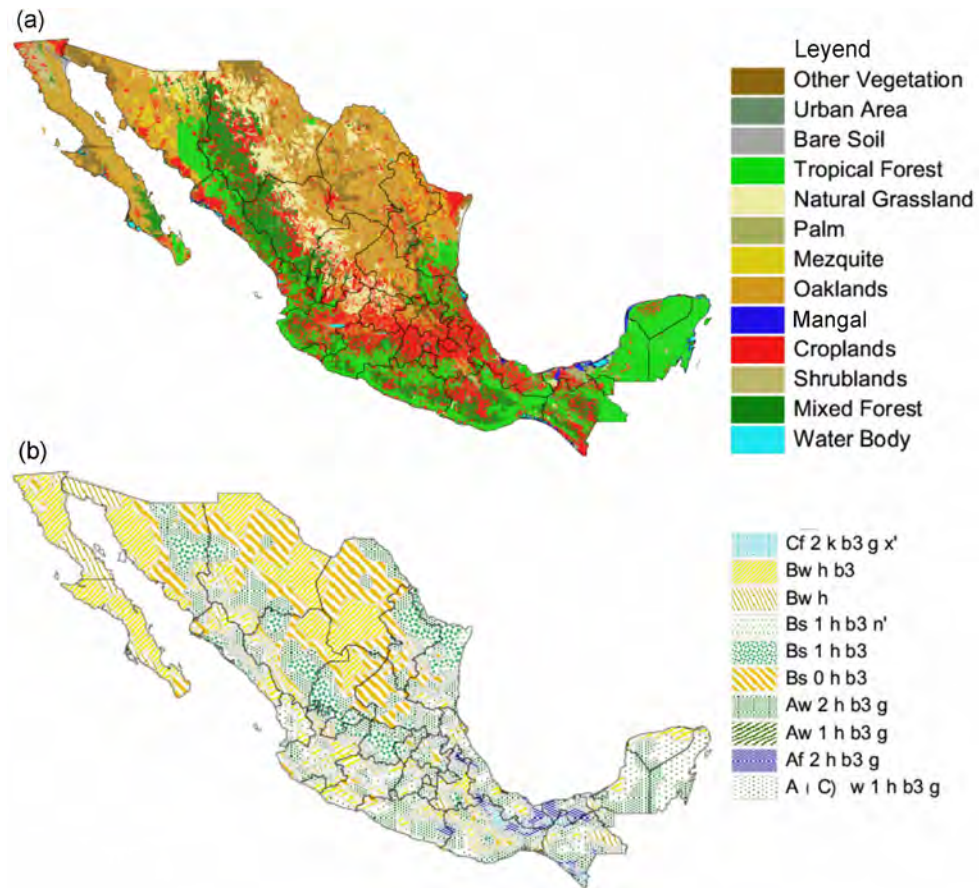


Fig. 2.9 (a) Vegetation of Mexico of the forestry national inventory, and (b) Climate regions using Ward's method

By using Geographic Information System (GIS) we defined the relative cover of each type of vegetation for climate regions (bio-climates). Dry climates (**Bs** and **Bw**) are located in the Altiplano region and in the Peninsula of Baja California. Shrublands domain the arid climates cover with 52 %, Mixed Forest 12.6% and 8.35 % of natural Grasslands. Croplands represent the 14 % of the whole of the territory of Mexico and are widely distributed in climates **A(w,c,f)**. In croplands we have included induced grassland, forestry and range managements. Climates **A** extend along of costal plains in both sides of continental land and in the slopes of the Western and Eastern Sierra Madre. The dominant vegetation is the tropical and mixed forest (55.7 percent). Temperate climates **C** are

characterized by being covered with perennial forest (mainly pine-oak forests) and some patches of deciduous tropical forest. There are some regions with semi-desert shrublands representing only 1.5 percent of the whole area of Cw climates.

The land cover changes are likely modifying the long-term climate by altering the solar energy balance and it is likely having effects on other regional climatic variables such as precipitation (Lean and Warrillow, 1989, Shukla et al., 1990). However, we are aware that the effects of land-cover change on climate are not well understood because regional impacts are not correctly represented in annual global statistics (Feddemma et al, 2005). Decreases in natural vegetation may also be affecting regional weather and climate by altering some surface properties, mainly in arid regions.

2.4 Summary and conclusions

The approach of including multivariate analysis into climate regionalization is not a new issue, nevertheless exercises as this is important to Mexico since they represent an advantage in the context of future ecosystems management and planning. The development of such a regionalization of climate presented in this study is based on clustering analysis modifying conventional techniques and including major statistical criteria as objectively as possible. Originally, techniques including combination of principal components analysis and hierarchical clustering were used to reduce the dimensions of the original variables even though there are some exceptions by truncation. Due to large number of stations we consider to make a rough grouping based on the number of principal climate regions by retaining a major accuracy in the level of clustering. Further, main criterion for clustering has been selected considering that all principal climate regions were represented.

Standardized cumulated average annual precipitation was introduced as a weight criterion considering constricted distribution of their PC loadings. This gives well results since climate regions were better represented in the final spatial distribution compared to Garcia (1988) map for climate types and vegetation. Cluster analysis results correspond to inherent bias, for instance variance intra and inter clusters. Criteria of homogeneity for each cluster is different for each of both methods used.

For this exercise Ward's represent more confident climate regionalization than Average Linkage Method because captured in a better way spatial variability, for instance topographic gradients and land vegetation cover. Probably heterogeneous spatial distribution of the meteorological stations influenced the clustering despite of the treatment given to the data by PCA and previous standardizations so many stations may have high correlation to each other, influencing also the covariance matrix. Finally climate regionalization is purely a way of classifying the climate variability and there exist many methodologies to approach it. The effect of land vegetation cover change on long term climate (regional and global) is an issue discussed by several authors (Sut et al, 1988, Segal et al, 1989; Chase and Pielke, 1999; Kalnay and Cai, 2003; Feddema et al, 2005). These implications will affect on several scales. Human impacted areas are leading to desertification processes by soil loss, fertility loss or alterations in surface energy balance. Land surface properties will be discussed in the following chapters in a context of numerical modeling approach for some application in environmental pollution.

References

- Anderberg, M. R., 1973: Cluster Analysis for Applications. Academic Press, 359 pp..
- Beaver, S. and Palazoglu, A. 2006: Cluster analysis of hourly wind measurements to reveal synoptic regimes affecting air quality, *J. Appl. Meteorol. Climatol.*, 45, 1710–1726
- Bunkers MJ, Miller JR, DeGaetano AT (1996) Definition of climate regions in the northern plains using an objective cluster modification technique *J. Climate* 9:130–146
- Cavazos, T., A.C. Comrie, and D.M. Liverman, 2002: Intraseasonal Variability Associated with Wet Monsoons in Southeast Arizona. *J. Climate*, 15, 2477–2490.
- Crane RG, Hewitson BC (2003) Clustering and upscaling of station precipitation records to regional patterns using self-organizing maps (SOMs). *Clim Res* 25: 95-107
- De Gaetano A.T., (1996) Delineation of mesoscale climate zones in the Northeastern United States using a novel approach to cluster analysis, *J. Clim.* 9 1765 .1782.
- Davis, R. E., and L. S. Kalkstein, 1990: Development of an automated spatial synoptic climatological classification. *Int. J. Climatol.*, 10, 769–794.
- Davis, R. E. and D. R. Walker, 1992: An upper-air synoptic climatology of the western United States. *J. Climate*, 5, 1449–1467
- Douglas, M. W., R. A. Maddox, K. W. Howard, and S. Reyes, 1993: The Mexican monsoon. *J. Climate*, 6, 1665–1677.
- Englehart P. J., and A. V. Douglas, 2002a: Mexico's summer rainfall patterns: An analysis of regional modes and changes in their teleconnectivity. *Atmosfera*, 15, 147–164.
- Elmore, K.L., and M.B. Richman, 2001: Euclidean Distance as a Similarity Metric for Principal Component Analysis. *Mon. Wea. Rev.*, 129, 540–549.
- Fovell, R. G., and M.-Y. C. Fovell, 1993: Climate zones of the conterminous United States defined using cluster analysis. *J. Climate*, 6, 2103–2135.

- Garcia, E., 1988. Modificaciones al sistema de clasificación climática de Köppen. Quinta Edición Instituto de Geografía UNAM
- Gong X., and M. B. Richman, 1995: On the application of cluster analysis to growing season precipitation data in North America east of the Rockies. *J. Climate*, 8, 897–931.
- Hewitson BC, Crane RG (2002) Self-organizing maps: applications to synoptic climatology. *Clim Res* 22: 13-26
- Kalkstein L.S., Tan G. and J.A.Skindlov, (1987) An evaluation of three clustering procedures for use in synoptic climatological classification, *J. Clim. Appl. Meteorol.* 26 717–730.
- Negri, A.J., R.F. Adler, R.A. Maddox, K.W. Howard, and P.R. Keehn, 1993: A Regional Rainfall Climatology over Mexico and the Southwest United States Derived from Passive Microwave and Geosynchronous Infrared Data. *J. Climate*, 6, 2144–2161.
- Magaña, V., J. A. Amador, and S. Medina, 1999: The midsummer drought over Mexico and Central America. *J. Climate*, 12, 1577–1588.
- Mimmack, G.M., S.J. Mason, and J.S. Galpin, 2001: Choice of Distance Matrices in Cluster Analysis: Defining Regions. *J. Climate*, 14, 2790–2797.
- Mitchell VL (1976) The regionalization of climate in the western United States. *J Appl Meteorol* 15:920–927
- Pavia, E.G., F. Graef, and J. Reyes, 2006: PDO–ENSO Effects in the Climate of Mexico. *J. Climate*, 19, 6433–6438.
- Richman M, Lamb PJ (1985) Climatic pattern analysis of 3- and 7-day summer rainfall in the central United States: some methodological considerations and a regionalization. *J Clim Appl Meteorol* 24:1325–1343

- Richman M. B., 1986: Rotation of principal components. *J. Climatol*, 6, 293–335.
- Richman M, Lamb PJ (1987) Pattern analysis of growing season precipitation in southern Canada. *Atmos Ocean* 25(2): 137–158
- Sirabella, P., Giuliani, A., Colosimo, A. & Dippner, J. (2001). Breaking down the climate effects on cod recruitment. *Marine Ecology Progress Series* 216, 213– 222
- Unal, Y., Kindap, T. & Karaca, M. (2003) Redefining the climate zones of Turkey using cluster analysis. *Int. J. Climatol.* 23, 1045–1055.
- Vega, A. J., R. V. Rohli, and K. G. Henderson, 1998: The Gulf of Mexico midtropospheric response to El Niño and La Niña forc-ing. *Climate Res.*, 10, 115–125.
- von Storch H., and F. W. Zwiers, 1999: *Statistical Analysis in Climate Research*. Cambridge University Press, 499 pp
- White D, Richman M, Yarnal B (1991) Climate regionalization and rotation of principal components. *Int J Climatol* 11: 1–25

Chapter 3

Impact of land vegetation cover on Land Surface Model of Atmospheric Circulation Models in arid regions from central-northern Mexico

Abstract

A series of numerical experiments were carried out to study the effect of meteorological events such as warm and cold air masses on climatic features and variability of a understudied region with strong topographic gradients in the northeastern part of Mexico. We applied the mesoscale model MM5. We investigated the influence of soil moisture availability in the performance of the model under two representative events for winter and summer. The results showed that a better resolution in land use cover improved the agreement among observed and calculated data. The topography induces atmospheric circulation patterns that determine the spatial distribution of climate and seasonal behavior. The numerical experiments reveal regions favorable to forced convection on the eastern side of the mountain chains Eastern Sierra Madre and Sierra de Alvarez.

Adapted of :

Pineda-Martinez L F and Carbajal N, (2009) Mesoscale numerical modeling of meteorological events in a strong topographic gradient in the northeastern part of Mexico. *Climate Dynamics in press*

3.1 Introduction

Cold fronts, moving from middle latitudes into Mexico are frequent during the winter season causing a temperature decrease and strong changes in weather conditions. Highlands (Altiplano), in the northern part of Mexico (Fig. 3.1), are characterized by daily and seasonal thermal contrast with high temperatures during the day and low at night. These patterns are modified by the arrival of cold air masses which have an important impact on weather and climate of the region (Fitzjarrald 1986; Schultz et al 1998). For the complex topography of the Altiplano, the dynamics of cold fronts induces noteworthy phenomena in the atmosphere (Fitzjarrald 1986). The presence of topographic barriers, humidity and convection strongly modify the atmosphere structure during the passage of these extreme events contributing to the spatial variability of temperature and precipitation (Cavazos and Hastenrath 1990; Steenburgh et al 1998). Winter events such as cold air outbreaks (called Nortes in Mexico) are associated with anomalies of precipitation and temperature over continental lands in Mexico (Brown et al 1999; Cavazos 1999). Topographically induced channeling of winds occurs often in the Altiplano controlling to some extent the incursion of cold air masses.

In summer, the weather in the northeastern part of Mexico is influenced by air masses moving from the Gulf of Mexico into the mainland. This process is reflected in high temperatures and precipitation values. Furthermore, hot summer events and tropical waves propagating in the Gulf of Mexico modify the precipitation and temperature distributions of the adjacent land regions. Humid and warm air masses moving from the coast into the Altiplano lead often to extreme muggy weather conditions. At a regional scale, the importance of these severe conditions may cause illnesses by cold temperatures in winter or

dehydration in summer, predominantly in children and older persons. The socioeconomic significance embraces agricultural losses by freezing in early winter season and periods of prolonged drought together with excess of heat in summer time (Magaña et al 1999; Perez 1996). Although every year these phenomena affect the low lands near the coast and sometimes even the Altiplano, there is a lack of studies investigating their effect on the structure of the atmosphere, on the regional climate and vegetation.

Some studies have shown the importance of land use variability and topographic heterogeneity at different scales (micro/meso) of circulation. The topographic variability governs intense surface weather processes on the lee side, like precipitation, temperature and local atmospheric circulation (Pielke and Avissar 1990; Dickinson 1995; Dimri 2004). Therefore, Dimri and Mohanty (1999) showed that different altitude and orientation of the barriers induce different thermodynamical and dynamical forcings. In this context, some analyses of precipitation and topography in the western United States have shown significant impact of surface terrain on the spatial distribution of precipitation and temperature by strong shadow effects along the Cascades and Sierra Range. (Mass and Albright 1987; Leung et al. 2003)

Although there are a few studies on the climatology of the region (Pineda-Martinez et al 2007), there is not emphasis on the interaction among the mesoscale atmospheric circulation of cold air masses and the complex topography characterized by the transition from flat lowlands near the coast (called Huasteca) to the highlands of the Altiplano (Fig. 3.1b). From a meteorological point of view, this research gives insight about the implication on modeling the interactions between the circulation and topography that

determine the climate distribution. Thus, the climate in the study zone is strongly influenced by the topography and the dominant synoptic circulation from the Gulf of Mexico into the continental land. Additionally, some surface properties such as albedo, roughness length, moisture availability influence the weather at local and regional scale (Chase et al 2000; Koster et al. 2000). In this chapter, we describe the results of a 3D numerical mesoscale simulation of a number of meteorological events. The experiments include extreme cold and warm fronts for different vegetation categories (VC) and soil moisture availability (M). Further, we analyze the simulations in relation to the implications of the frequency of these events on regional climate patterns obtained from historical meteorological data.

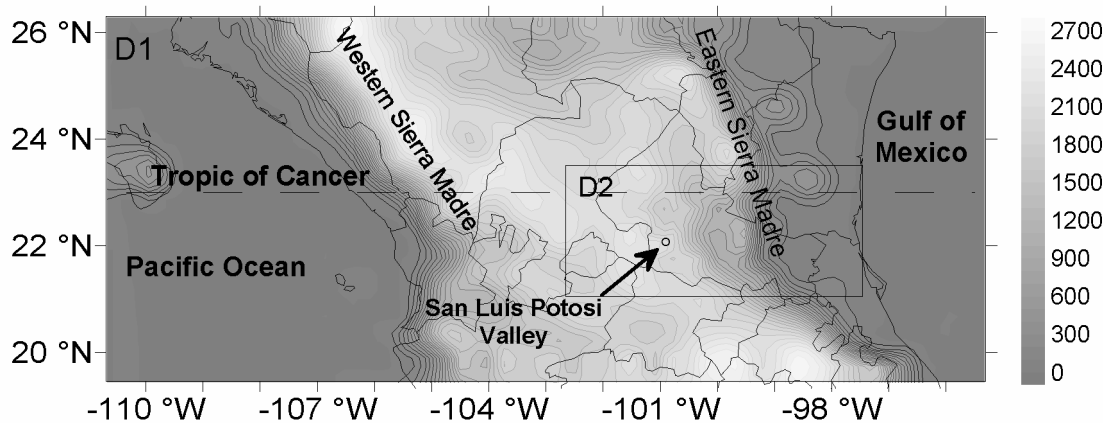


Fig. 3.1 Nested-grid domains and contours of terrain elevation (m) D1 and D2

3.2 Model Simulations

In this chapter we investigate the ability of the Mesoscale Model version 5 (MM5), developed by the Pennsylvania State University and the National Center for Atmospheric Research (NCAR) in simulating extreme weather events. The MM5 is a non-hydrostatic, three-dimensional and prognostic numerical model (Grell et al 1994). The sigma (σ)

coordinate is considered in the basic equations of the model to determine the vertical levels. The model MM5 included the parameterization for convection of Grell et al. (1994), the Blackadar boundary layer scheme, the radiation scheme of Dudhia (1989) and the microphysics of warm rain scheme.

The model was initialized with the National Centers for Environmental Prediction (NCEP) final analysis data as initial conditions (Kalnay et al. 1996). The numerical simulations were initialized at 00Z with duration of 72 hours with hourly outputs. The mother domain (D1 in Fig. 1) was established at central coordinates 25° N and 103° W, with a horizontal grid resolution of 27 km on 60x30 grid points. A second nested domain (D2) was defined with a 9km horizontal resolution, 30x60 grid points. Additionally, there are two inner domains (D3 3km and D4 1km) of high resolution. These included only the topographic transition into the highlands to evaluate the MM5 ability for capturing the regional circulation. We selected a vertical resolution of 27 sigma levels (\mathbf{s}).

Recent estimations in the region suggest that the soil moisture for desert grassland and shrublands does not reach 16 % (Medina-Roldan et al 2007). To investigate the sensitivity of the results to this parameter, we performed two basic numerical experiments in order to establish the influence of land vegetation cover and soil moisture on the results. To specify the relative humidity at the surface accurately is very difficult. For this reason, the concept of moisture availability was introduced (Carlson and Boland 1978). In the Land Surface Model (LSM) coupled to MM5, the moisture availability is represented as a constant parameter. Moisture availability has been applied to predict surface fluxes, which are a function of land use and it is invariant during the simulation. In the first experiment, we use

the 1km resolution U.S. Geological Survey's (USGS) classification, which has 25 land use categories. This land cover dataset is derived from the 1km satellite Advanced Very High Resolution Radiometer (AVHRR). In the second experiment, we use uniform land vegetation cover for the inner domain (grassland). For each land cover experiment, M was varied with three different values expressed as a decimal fraction, 0.11, 0.22 and 0.30.

3.3 Results

3.3.1 Moisture availability and land vegetation cover

In order to investigate the sensitivity of the model to selected values of moisture availability and land use cover, we carried out a series of numerical experiments for three M values and two VC configurations. Soil moisture availability is a major factor controlling the amount of surface evaporation taking place in the model. Therefore, changing the soil moisture availability is equivalent to changing the latent heat flux in the surface budget; which affects the land surface temperature (Lam et al 2006). We compare the results of the lowest sigma level (0.995) of temperature and relative humidity with superficial observed data.

We firstly discuss a winter case of a cold front event moving through the Highland topography of the northern part of Mexico and reaching the San Luis Potosi Valley on December 2nd 2004 approximately at 11:00 local time causing a significant temperature decrease during the passage of the air mass (Fig. 3.2). At this time of year, the temperature values vary typically from about 4-6°C at 6:00 in the early morning to 22-25°C at 15:00 in the afternoon. Inspection of Fig. 3.2a reveals that the passage of the cold front leads to a net decrease of the observed temperature of about 11 °C (from 20°C to 9 C°). This kind of relatively unexpected temperature changes have health consequences for the inhabitants.

Furthermore, if one considers that in the winter season about 45 cold fronts reach this part of Mexico (SMN 2007); the significance of these temperature decreases on climate are very important. The best agreement among observed and calculated temperature data is obtained for $M=0.3$. This result does not agree with simple estimations of Medina-Roldan et al (2007). Since M represent a parameterization, it is quite sensible to changes in soil thermal and hydraulic conductivities. M is always better approximated by iterative calculations in the MM5 (Oncley and Dudhia 1995; Chen and Dudhia 2001b).

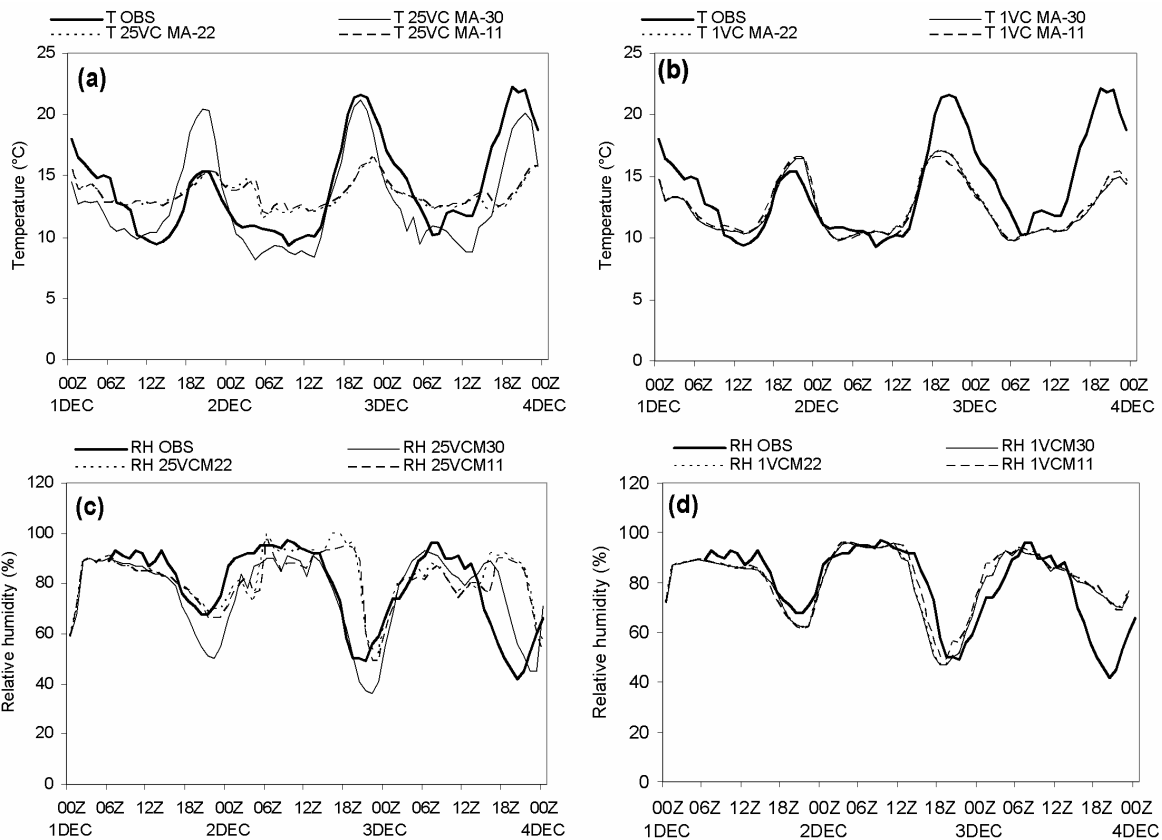


Fig. 3.2 Comparison of observed and modeled data with different moisture availability values and two different vegetation categories (VC) (initialized 00Z 1 DEC 2004). (a) Temperature (25VC), (b) Temperature (1VC), (c) Relative humidity (25VC) and (d) Relative humidity (1VC).

In Figs. 3.2a and 3.2b, we distinguish a decrease in the daily temperature oscillation for low M values. This fact has been reported by Carlson and Boland (1978). They suggested that while the soil moisture availability is dominantly responsible for the daytime temperature, the thermal inertia influences the nighttime temperature. In the LSM (slab model) of MM5, the surface temperature is estimated from a slab of soil maintained at constant temperature. The change in the temperature of this slab is determined by the energy balance between net radiation, the transfer of heat with the underlying substrate and the sensible heat and latent heat fluxes (Grell et al. 1994; Chen and Dudhia 2001b). Therefore, errors in the sensible and latent fluxes will be reflected in surface temperature errors. An increase of the latent heat flux implies a decrease of the surface energy available for sensible heat, which cause MM5 to predict low air and surface temperature (Oncley and Dudhia, 1995). The calculations showed that latent heat flux presented higher variations than sensible heat flux. This can be seen in the results for soil moisture values and 25 land vegetation categories (Fig. 3a). It is interesting to mention that the largest latent heat flux was reached for $M=0.22$, even larger than for $M=0.3$, however the best agreement for the temperature was obtained for $M=0.3$ (see Figs. 3.2a and 3.3a). These unusual variations are related to parameterizations in slab model for urban surface. When it was modified to grassland (1VC), heat fluxes and temperatures showed less variation (Figs. 3.3c and 3.3d). Since the field data were measured at an urban meteorological station, our expectation is to appreciate the heat island effect, such as is captured in the 25VCM30 experiment (Fig. 3.2a).

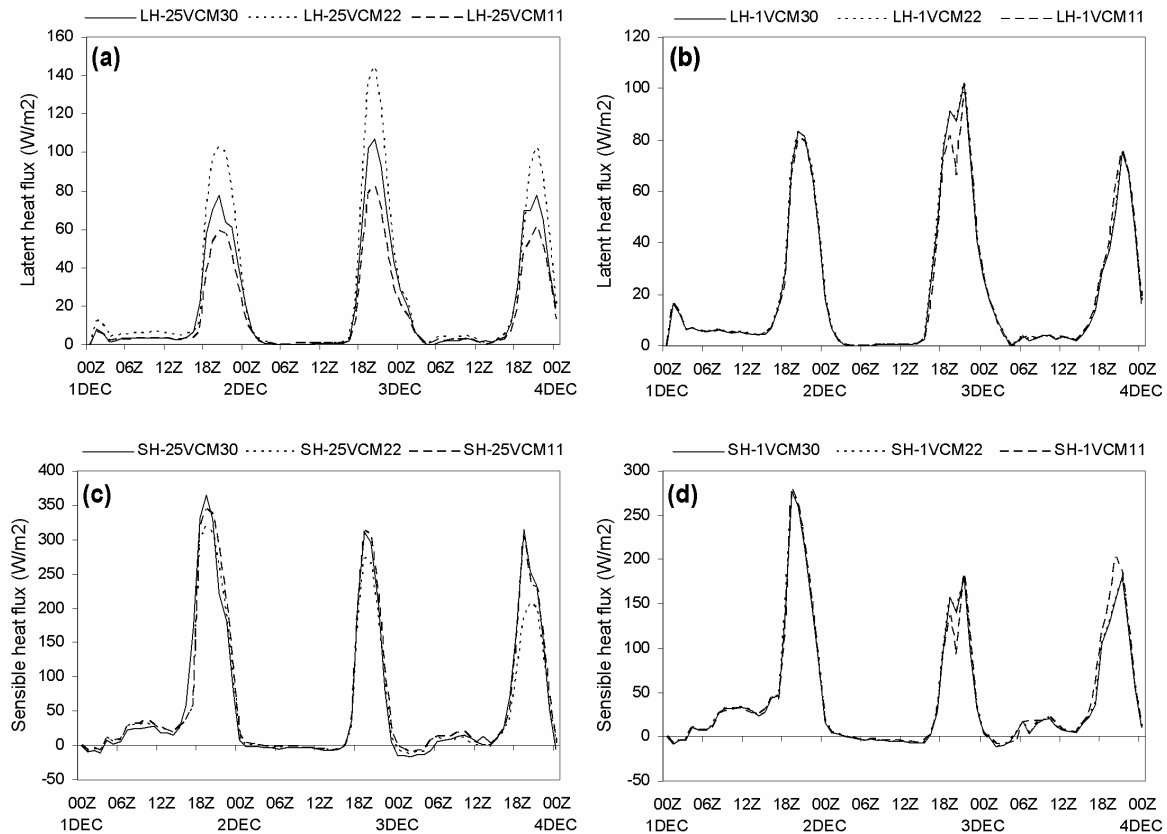


Fig. 3.3 Comparison of calculations for different soil moisture values and two different vegetation categories (VC). (a) latent heat flux (25VC), (b) latent heat flux (1VC), (c) sensible heat flux (25VC) and (d) sensible heat flux (1VC).

During the intrusion into the Altiplano on Dec 1, the cold front presented a high relative humidity value, which did not fall to the normal minimum value of about 40-50% (Fig. 3.2b). Instead it diminished to 70% at the time when the relative humidity minimum occurs, i.e. at about 15:00, in the afternoon. The entering air mass was characterized by high humidity values and cloud cover on Dec 1. The presence of a jet from the Pacific flowing eastward to the Gulf of Mexico is the dominant circulation during the boreal winter in the upper troposphere (Cavazos and Hastenrath 1990; Shultz, 2005). This is a mechanism for humidity transport into highland regions.

We describe the results of a similar experiment realized for a warm air mass moving on 1 May 2004 from the Gulf of Mexico into the Altiplano. The inflowing air mass reached the Valley of San Luis Potosi at 14:00 local time causing extraordinary changes in the normal behavior of temperature and relative humidity (Fig. 3.4). The first effect of the warm front was an increment of the temperature to about 30 °C at 15:00, local time. An outstanding phenomenon is that during the entrance of the warm front, the relative humidity decreased from 80% to 18% at high temperatures. After that it increased rapidly to 95%. The presence of this humid air mass caused a decrease in temperature due to cloud cover, reducing energy fluxes and the incoming solar radiation.

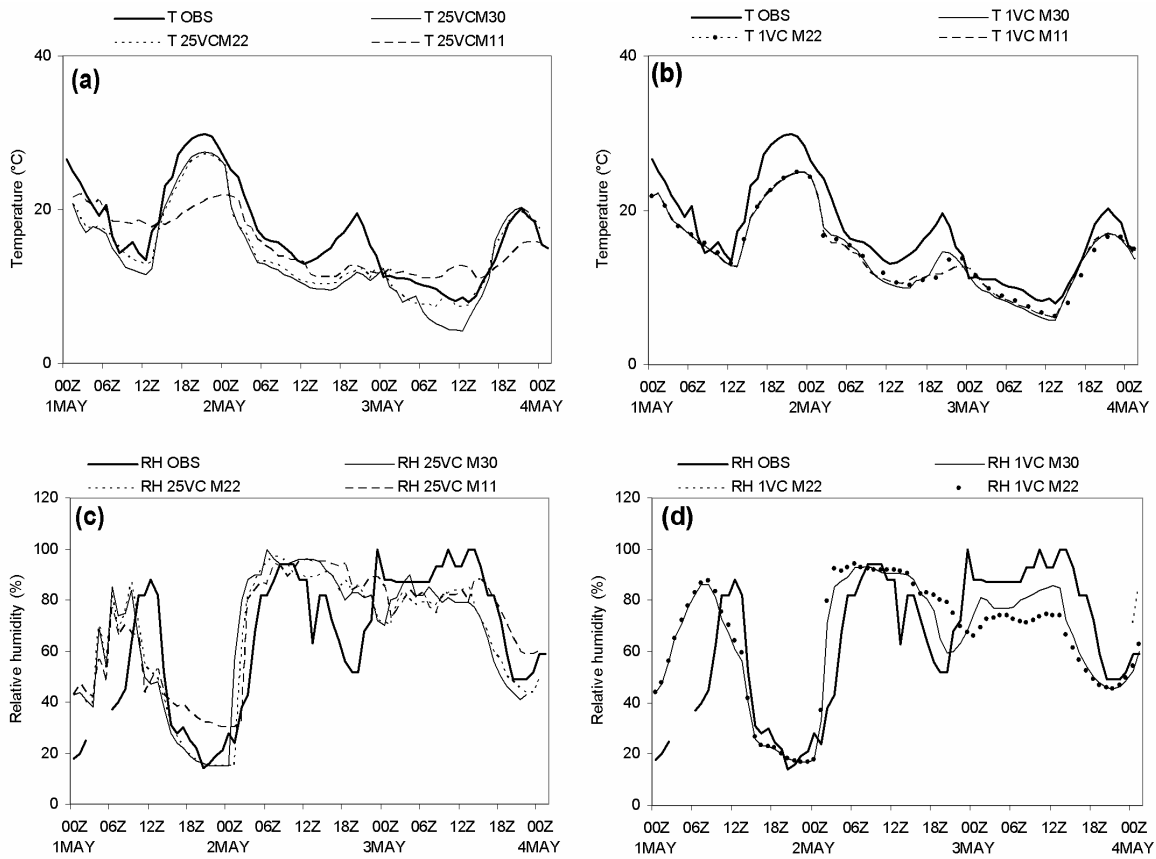


Fig. 3.4 Same as Fig. 2 but for 00Z 1 MAY 2004

In general terms, we show in Fig. 3.4 how the different applied soil moisture values affect the curve behavior of temperature and relative humidity. We also reached the best agreement with a $M=0.3$ and 25 land vegetation categories for the summer event, primarily in phase and intensity where we obtained acceptable values of Root Mean Square Error (RMSE) (Table 3.1). Furthermore, we found in our calculations that urban areas are more susceptible to changes in moisture availability than rural areas. It suggests that soil moisture $M=0.30$ and 25 land cover vegetation categories, which include urban areas, are the most appropriate in the contribution of energy balance.

Table 3.1 Root mean square error values for the experiments of MA and vegetation categories (VC) shown in Fig. 3.2.

Experiment ID	Winter event	Summer event
RH 1VC MA-30	10.44	14.51
RH 1VC MA-22	9.87	15.35
RH 1VC MA-11	9.90	19.12
RH 25VC MA-30	9.80	14.97
RH 25VC MA-22	12.31	14.93
RH 25VC MA-11	12.31	14.81
T 1VC MA-30	3.18	3.21
T 1VC MA-22	3.04	3.45
T 1VC MA-11	3.05	3.40
T 25VC MA-30	2.87	3.60
T 25VC MA-22	3.18	3.12
T 25VC MA-11	3.13	3.97

A simple analysis shows that in all calculations, the model underestimates the temperature values, specifically at the time when the maximum temperature occurs. The estimated RMSE values are of the same order as those reported by other authors (Colle et al 2000; Hanna and Yang 2001). The surface temperature is mainly controlled by the surface energy budget, especially the sensible heat during the day. The underestimated daytime temperatures indicate that the models either underestimate the absorbed solar radiation at

the surface or underestimate the upward sensible heat flux. An additional numerical experiment, with an increased albedo from 15 to 20, indicated that additional reflectance enhances errors in the underestimation of daytime temperatures in about 4.16°C with respect to observed values; whereas for the control experiment (25VCM30) the error was about 2.35°C . The numerical experiments also indicated that the impact of a varying M on the ground heat flux was not significant. But, for the increased albedo experiment, the ground heat flux (Fig. 3.5) grew in average 32.86 W/m^2 . For the nighttime temperatures, the intensities of outgoing radiation and upward heat release from the underlying surface determine the temperature changes. Thus, the overestimation may be an indication that either heat flux at surface is overestimated or the outgoing longwave radiation is too strong. In fact, the albedo experiments indicate that heat fluxes play a major role in estimating nighttime temperatures and the impact is larger on land urban surface. It has been mentioned above, in the numerical experiments for two vegetation categories (urban and rural areas), that M variations had a smaller impact on surface heat fluxes in areas with vegetation cover. Finally, for an increased albedo (from 15 to 20), the temperature mean error was visibly higher ($\text{RMSE} = 4.63$). This model behavior has been reported by others authors (Oncley and Dudhia 1995; Miao et al 2007); unfortunately, we did not have energy measurements to clarify this particular issue for this study. Beside these deficiencies, it was possible with the actual applied model inputs to satisfactorily reproduce the temperature daily cycle, with a maximum value at 14:00 and a minimum at 6:00 local time and acceptable values for the RMSE.

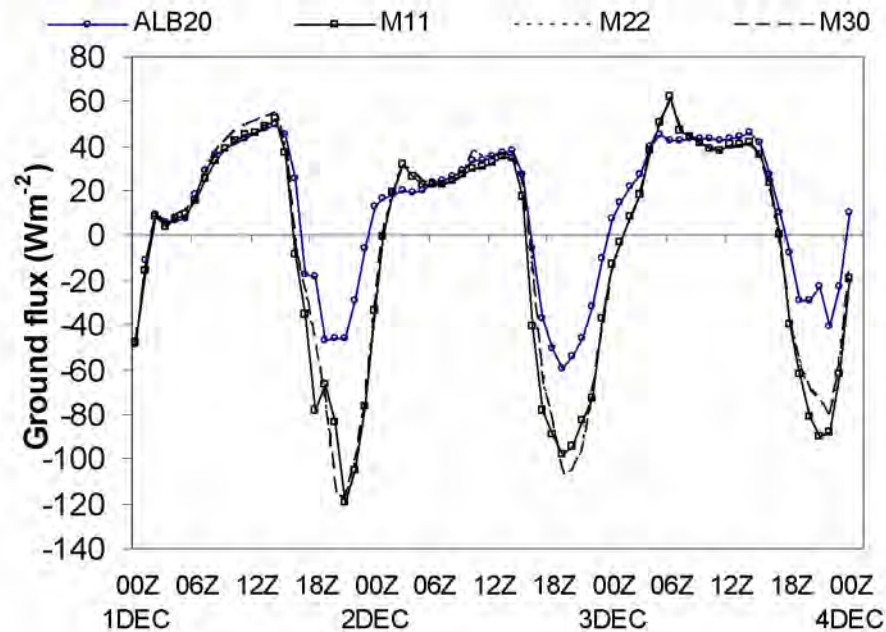


Fig. 3.5 Comparison of modeled data of 25VC configuration of ground flux with different moisture availability values and albedo 20 (initialized 00Z 1 DEC 2004).

Although there are some gaps in measured data, the model adequately reproduced the behavior of the relative humidity; the curves of simulated and observed data are quite similar. The surface temperature is largely determined by heat fluxes and intrinsically related to variations in humidity. This variation is closely related to the surface moisture flux, to schemes for the planetary boundary layer (PBL) and to schemes for the parameterization of the cumulus convection (Grell et al 1994). In cumulus scheme, the amount of convection is determined by the vertically integrated moisture convergence. The feedback to the larger scale is determined by mean of the normalized vertical profiles of convective heating and moistening, and a vertical eddy-flux divergence of water vapor associated with cumulus convection (Anthes 1977). Hence, cloud fraction is based on vertical profiles of relative humidity. The results of additional experiments for two different PBL schemes (Blackadar and Medium-Range Forecast MRF) showed the dependence of

relative humidity on the PBL height. We obtained the best agreement among calculated and observed data with the Blackadar scheme ($RMSE_{MRF}=16.65$, $RMSE_{BLK}=9.80$). At the surface level, variations in RH are strongly related to evaporation processes and surface temperature (Carlson and Boland 1978; Grell et al 1994; Chen and Avissar, 1994). A discussion of vertical profiles of temperature and relative humidity are not possible because there is not sounding in the studied domain. However, the model results give some insight about the behaviors of relative humidity and temperature.

Under normal conditions, in these regions of the Altiplano there are daily temperatures fluctuations with a range of about 20 °C, from about 22-25 °C at 15:00 local time to 4-6 °C early in the morning. This oscillating pattern changes drastically during the passage of cold air masses. The range of temperature fluctuations decreases and, in some cases, the temperature falls almost linearly with time. The frequency of these cold air masses in the whole season significantly determines the winter climatology of the region. The observed and modeled data in the winter season reveal that cold fronts cause strong weather changes, i.e. the passage of cold air masses produces anomalous time series of temperature, relative humidity and strong winds. Though there are model discrepancies in the estimation of maximal and minimal values, the daily cycle of the variables is well calculated. This represents a great advantage, since the use of model-generated information for the prognostic of horizontal and vertical atmospheric sequences is of fundamental importance for the region.

3.3.2 Wind speed and friction velocity

Another important parameter associated with front dynamics is the intensity of winds. In Fig. 3.6, show observed wind speed and modeled data of wind and friction velocity (U^*), for the same experiments of M and VC. The root means square error of the wind speed varies between 1.4 and 2.1 m/s. Besides the complexity of large and small chain mountains, highland plains and valleys the agreement is quite good. Typically, wind speeds of about 7-9 $m \cdot s^{-1}$ can be reached in the Altiplano, although gusts with wind speeds of more than 11 $m \cdot s^{-1}$ occur frequently. Considering that large areas of the Altiplano are characterized as desert regions, the prediction of these strong winds has ecological implications such as soil losses by wind erosion. Additionally, we analyze the friction velocity for its importance in wind erosion, which will be discussed in the following chapter. The U^* is defined as a function of the momentum flux parameterization of the fluctuations of mean wind (U) and the vertical component, specifically to fluctuant term (w') at a height z above the earth's surface. The importance of using U^* is that also considers the stability conditions of the atmosphere.

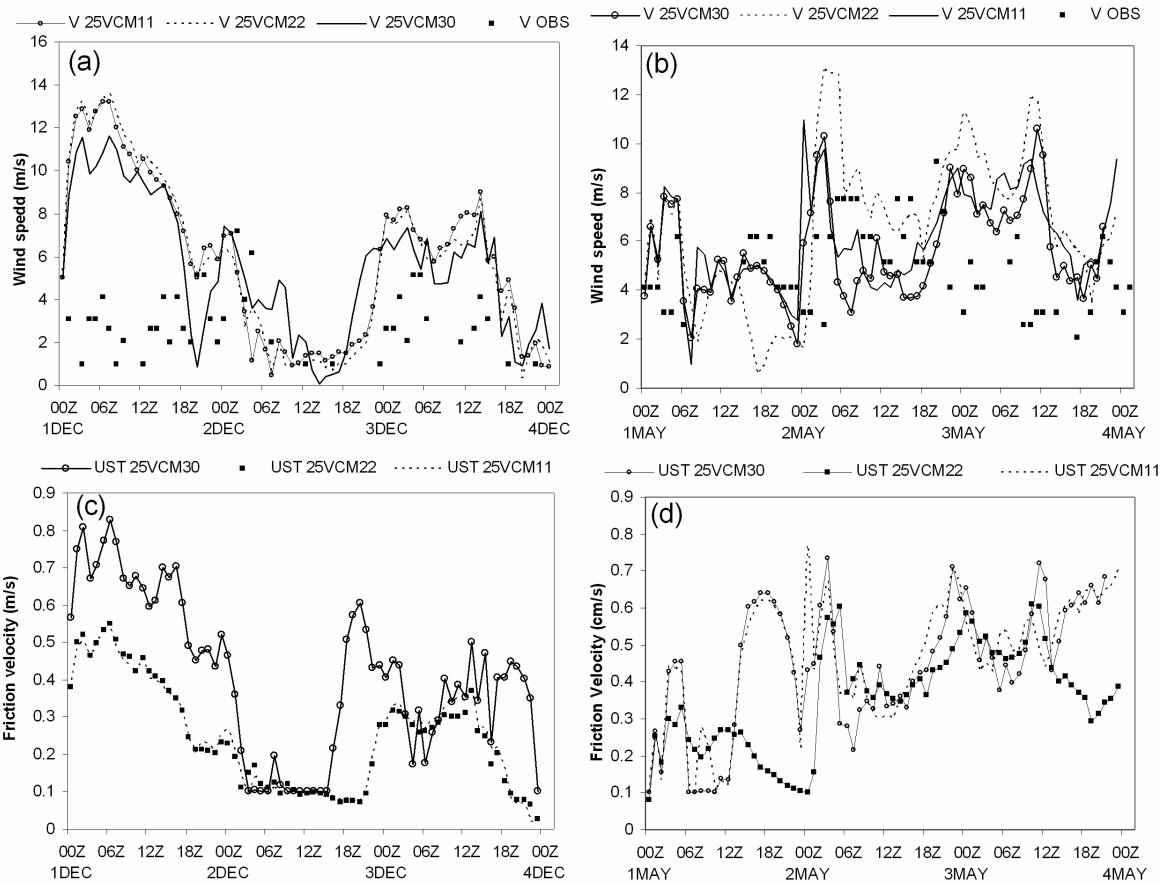


Fig. 3.6 Comparison of wind speed among measured data and modeled results for different M values on: (a) 1-4 Dec and (b) 1-4 May. Calculated friction velocity for different M values on: (c) 1-4 Dec and (d) 1-4 May.

Since friction velocity is totally related to surface properties, variations in M imply changes in U^* . It is clear the influence of changing M in the prediction of U^* (Fig. 3.6c and 3.6d), as it has discussed above the model is quite sensible to M and intrinsically has large impact in the estimation of surface variables.

3.4 Discussion

We have presented results of some numerical simulations of the atmospheric circulation. Since the model results agree well with observations at the meteorological stations, we

discuss and diagnose with some confidence horizontal structures associated to fronts and processes occurring in the atmosphere during these outstanding events.

Figure 3.7 shows the horizontal progression of a cold front on the Mexican Highland. It reflects the fact that cold air masses enter through the central plain located between the two principal chain mountains, the Eastern Sierra Madre and the Western Sierra Madre. There are also other smaller mountain chains where the air is channeled. The lowlands along both the Atlantic and Pacific oceans coasts are distinguished by higher temperature values. The passage of the cold air masses and their interaction with the complex topography radically modify the prevailing temperature pattern. It also introduces climatic features which influence synoptic conditions.

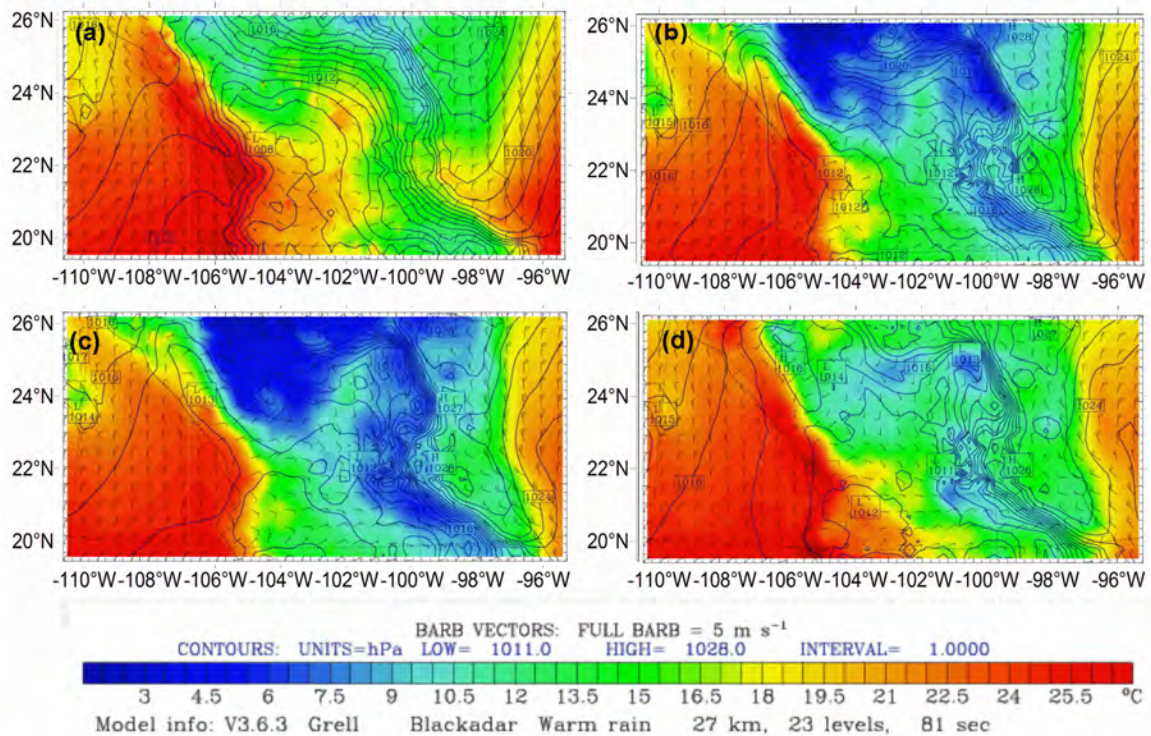


Fig. 3.7 Sea Level Pressure (SLP) (contours), wind vectors and temperature in °C (shaded) during the passage of four cold fronts on the Mexican Altiplano on 1 Dec 2004, (a) 00Z (b) 06Z, (c) 12Z and (d) 18Z .

The near-surface structure and evolution of the cold air mass is illustrated by a sequence of maps of sea level pressure (SLP), surface (lowest sigma level $\sigma = 0.995$) air temperature and wind (Fig. 3.7). The cold front is strong enough to reach the southern part of Mexico with temperatures ranging between 6 and 8 °C and the major strong cold incursion occurs with temperatures of about -4 °C in regions of the northern part of Mexico. The passage of the air mass reflects through temperature gradients the highland topographic influence on the propagation of the cold front. The temperature gradients along the Eastern and Western Sierra Madre produce narrow zones of strong density gradients causing baroclinic currents. This circulation can be observed in the slopes of the Eastern and Western Sierra Madre. In the cold area of the Highland, strong ageostrophic winds (~10 m/s) take place. The narrow strip of surface wind transition (maximum of horizontal relative vorticity) is used to trace the leading edge of the cold surges. The band of robust temperature and pressure gradients acquires a curved shape and is consistent with spreading surface winds (diffluent flow) on both sides of the Altiplano region, precisely where the topography is characterized by strong gradients. The diffluent flow is a wind flow pattern in which the air moves outward from a central axis of the front, generally in the Altiplano region (Fig. 3.7). Cold events are usually initiated as a developing cyclone over the Gulf of Mexico in connection with an anticyclonic circulation brought on by topographic barriers and a dynamical forcing in the central part of the United States inducing the transport of cold air southwards at least until 10°N (Schultz et al 1998).

On another hand, warm fronts are produced when marine air masses advance towards higher latitudes and the thermal ridges ascend through the mountains into the inland affecting cooler air masses. Some mechanisms for warm air masses sources are warm sector mid-latitude cyclone motions (Chien et al 1997). However, the dominant factor is that trade easterly winds find mountainous obstacles producing forced convection, temperature gradients and rainfall. Annual rainfall in these regions varies from 1400 mm in Veracruz, on the coastal side of the Eastern Sierra Madre, and 400 mm in the high plains (Fitzjarrald 1986).

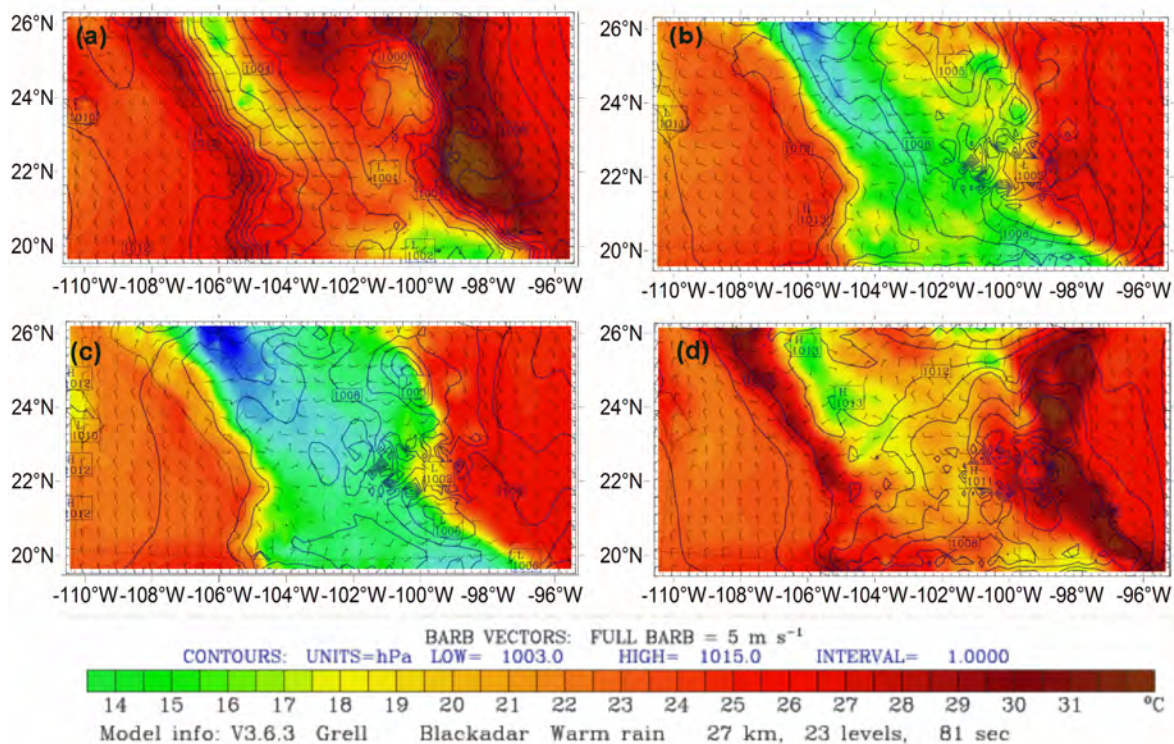


Fig. 3.8 Sea Level Pressure (SLP) (contours), wind vectors and temperature in °C (shaded) of warm events moving from the Gulf of Mexico into highland regions on 1 May 2004 (a) 00Z, (b) 06Z, (c) 12Z and (d) 18Z.

The modeled summer event shows the behavior of very warm air masses reaching the highland regions (Fig. 3.8). It can be observed that topography plays an important role as

the warm marine air mass circulates from the Gulf of Mexico into the Altiplano. The air mass propagates through lowlands and over the topographic complexity of the Eastern Sierra Madre. This can be seen in the band of warm air mass reaching the middle zone in the area formed approximately by the coordinates 22°-23° N and 98°-100° W. An important quantity of humidity is able to arrive to the middle zone in this way. Additionally, the Sierra de Álvarez, located on the western side of the middle zone, constrains the passing of this humidity in direction of the Highlands. Only when the atmospheric circulation is favorable, the warm humid air coming from the Gulf of Mexico is able to reach the region of the San Luis Potosi Valley (Pineda-Martinez et al 2007). The arid zone of the Altiplano is mainly associated with these topographic barriers and to the deficient moisture transport in subsidence zones close to Tropic of cancer. This complex interaction between topography and the atmospheric circulation causes an important geographical distribution of climate and vegetation types (Karlsen and Elvebakk 2003). The warm summer events may produce long periods of excessive heat, exceeding average temperature maxima during several days and weeks in the summer months. They often are typified by high humidity values (Chien et al 1997; Zhang and Fritsch 1988b). It is clear that variations in surface properties, such as moisture, influence the weather through impacts on evaporation and other surface energy fluxes, as we have discussed in Figs 3.2, 3.3 and 3.4.

3.4.1 Vertical structure

To illustrate the evolution of the meteorological variables in the vertical direction as the air masses interact with the topography, we discuss the wind intensity, the temperature and pressure at different sigma levels across a selected vertical section. The analyzed cross section extends SW to NW. In Fig. 3.9, the vertical structure of the winter reveals the influence of the cold air mass in wind circulation and temperature.

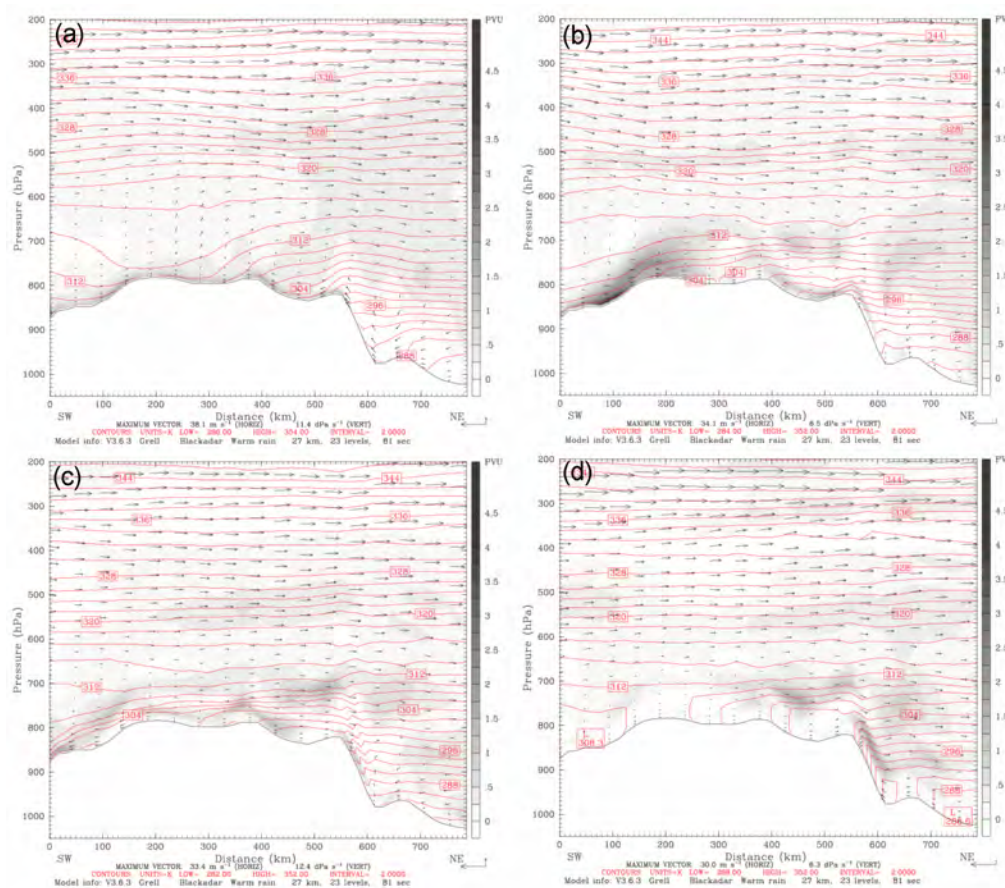


Fig. 3.9 Cross section (SW-NE) on 1 Dec 2004 at: (a) 00Z, (b) 06Z, (c) 12Z and (d) 18Z. The solid lines represent the temperature at 2 °C intervals. Shading represents potential vorticity in wind vectors.

At high levels (200 hPa), a winter dominant synoptic easterly jet exists and humidity is transported from the Pacific Ocean to the Gulf of Mexico (Cavazos and Hastenrath 1990;

Shultz 2005). In the lower layer the circulation pattern is dominated by regional effects caused by interactions with terrain. An additional feature is a flow in the direction of the Altiplano, which flows through the mountain slope (upslope flow) causing strong potential vorticity stratified (Schultz 2005). The motion of these cold air masses alters the structure of the atmosphere causing a minor influence of regional effects such as katabatic and anabatic winds. Thus, strong winds associated with cold front passages are frequent events that determine the circulation in winter season. This has implications that will be discussed in the next chapter.

3.5 Conclusions

We presented a series of numerical simulations of the land surface properties and its effect atmospheric circulation in a semiarid region of Mexico. The experiments for moisture availability and land vegetation cover revealed their importance for the performance of models LSM-MM5, since we found that a land vegetation cover of 25 categories yielded the best results. The variation of the soil moisture clearly generated differences between urban and grassland surfaces affecting the model calculations and consequently the estimated local weather conditions. For this not-well characterized region, it is important to obtain more detailed information about surface properties in order to improve the LSM parameters. We now have a better understanding about the interaction among land properties and cold and warm fronts, about the role played by these processes in the regional circulation and, principally, about the importance of natural barriers to induce regional flow.

References

Anthes RA (1977) A cumulus parameterization scheme utilizing a one-dimensional cloud model. *Mon. Wea. Rev.*, 105: 270-286.

Brown MJ, Stoelinga MT, Hobbs PV (1999) Numerical modeling of precipitation cores on cold fronts. *J. Atmos. Sci.* 56: 1175–1196

Carlson TN, Boland FE, (1978) Analysis of urban–rural canopy using a surface heat flux/temperature model. *J. Appl. Meteor.* 17: 998–1013.

Cavazos T, Hastenrath S (1990) Convection and rainfall over Mexico and their modulation by the Southern Oscillation. *Int. J. Climatol.* 10:377–386

Cavazos T (1999) Large-scale circulation anomalies conducive to extreme precipitation events and derivation of daily rainfall in northeastern Mexico and southeastern Texas. *J. Clim.* 12: 1506-1523.

Chase T, Pielke NR, Kittel TF, Nemani RR, Running SW (2000) Simulated impacts of historical land cover changes on global climate. *Clim Dyn.*, 16: 93-105.

Chen F, Avissar R (1994) Impact of land-surface moisture variability on local shallow convective cumulus and precipitation in large-scale models. *J Appl Meteorol* 33:1382–1401.

Chen F, Dudhia J (2001b) Coupling an advanced Land Surface–Hydrology Model with the Penn State–NCAR MM5 modeling system. Part II: Preliminary model validation. *Mon. Wea. Rev.*, 129: 587–604.

Chien FC, Mass CF, Kuo YH (1997) Interaction of a warm-season frontal system with the coastal mountains of the western United States. Part I: Prefrontal onshore push, coastal ridging, and alongshore southerlies. *Mon. Wea. Rev.* 125: 1705–1729

Colle BA, Mass CF, Westrick KJ (2000) MM5 Precipitation Verification over the Pacific Northwest during the 1997–99 Cool Seasons. *Wea. Forecasting* 15: 730–744

Dickinson RE (1995) Land atmosphere interaction. *Rev Geophys* 33(Suppl):917–922.

Dimri AP, Mohanty UC (1999) Snowfall statistics of some SASE field stations in J&K and a case study of western disturbance. *Def Sci J* 49(5):437–445

Dimri AP (2004) Impact of horizontal model resolution orography on the simulation of a western disturbance and associated precipitation. *Meteorol Appl* 11(2):115–127.

Dudhia J (1989) Numerical study of convection observed during the winter monsoon experiment using a mesoscale two-dimensional model. *J. Atmos. Sci.* 46: 3077–3107

Fitzjarrald DR (1986) Slope winds in Veracruz. *J. Climate Appl. Meteor.* 25: 133–144

Grell GA, Dudhia J, Stauffer DR (1994) A description of the fifth generation Penn State/NCAR mesoscale model (MM5), Natl. Cent. for Atmos. Res. TN-398+STR: 138 pp

Hanna SR, Yang R (2001) Evaluations of Mesoscale Models' Simulations of Near-Surface Winds, Temperature Gradients, and Mixing Depths. *J. Appl. Meteor.* **40**: 1095–1104

Kalnay E, Kanamitsu M, Kistler R, Collins W, Deaven D, Gandin L, Iredell M, Saha S, White G, Woollen J, Zhu Y, Leetmaa A, Reynolds B, Chelliah M, Ebisuzaki W, Higgins W, Janowiak J, Mo K, Ropelewski C, Wang J, Jenne R, Joseph D (1996) The NCEP/NCAR 40-Year Reanalysis Project. *Bull. Amer. Meteor. Soc.* *77*: 437–471

Karlsen SR, Elvebakk A (2003) A method using indicator plants to map locale climatic variation in the Kangerlussuaq/Scoresby Sund area, East Greenland. *J. Biogeography* *30*: 1469-1491.

Koster RD, Suarez MJ, Heiser M (2000) Variance and Predictability of Precipitation at Seasonal-to-Interannual Timescales. *J. Hydrometeor.*, *1*: 26–46.

Lam JSL, Lau AKH, Fung JCH (2006) Application of refined land-use categories for high resolution mesoscale atmospheric modelling, *Bound.Layer Meteor.* *119*: 263–288.

Leung LR, Qian Y, Bian X (2003) Hydroclimate of the Western United States Based on Observations and Regional Climate Simulation of 1981–2000. Part I: Seasonal Statistics. *J. Climate.* *16*(12): 1892–1911.

Magaña V, Amador J, Medina S (1999). The mid-summer drought over Mexico and Central America. *J. Climate*. 12: 1577-1588

Mass CF, Albright MD (1987) Coastal southerlies and alongshore surges of the west coast of North America: Evidence of mesoscale topographically trapped response to synoptic forcing. *Mon. Wea. Rev.*, 115: 1707–1738.

Medina-Roldan E, Arredondo JT, Garcia E, Huerta FM (2007) Soil Water Content Dynamics Along a Range Condition Gradient in a Shortgrass Steppe. *Rangeland Ecology & Management* 60: 79–87

Miao JF, Chen D, Borne K (2007) Evaluation and Comparison of Noah and Pleim–Xiu Land Surface Models in MM5 Using GÖTE2001 Data: Spatial and Temporal Variations in Near-Surface Air Temperature. *J. Appl. Meteor. Climatol.* 46: 1587–1605.

Oncley SP, Dudhia J (1995) Evaluation of Surface Fluxes from MM5 Using Observations. *Mon. Wea. Rev.* 123: 3344–3357.

Perez I (1996) Major cold air outbreaks affecting coffee and citrus plantations in the eastern and northeastern Mexico. *Atmosfera* 9: 47-68

Pielke R, Avissar R (1990) Influence of landscape structure on local and regional climate. *Landsc Ecol* 4:133–155.

Pineda-Martinez L F, Carbajal N, Medina-Roldan E (2007) Regionalization and classification of bioclimatic zones in the central-northeastern region of México using principal component analysis (PCA). *Atmósfera* 20: 111-123

Servicio Meteorológico Nacional (SMN) (2007) Productos climáticos. Comisión Nacional del Agua, Mexico

Steenburgh WJ, Schultz DM, Colle BA (1998) The structure and evolution of gap outflow over the Gulf of Tehuantepec, Mexico. *Mon. Wea. Rev.* 126: 2673–2691

Schultz DM (2005) A review of cold fronts with prefrontal troughs and wind shifts. *Mon. Wea. Rev.* 133: 2449–2472

Schultz DM, Bracken WE, Bosart LF (1998) Planetary- and synoptic-scale signatures associated with Central American cold surges. *Mon. Wea. Rev.* 126: 5–27

Zhang DL, Fritsch JM 1988b A numerical investigation of a convectively generated, inertially stable, extratropical warm-core mesovortex over land. Part I: Structure and evolution. *Mon. Wea. Rev.* 116: 2660–2687.

Chapter 4

Numerical modeling of a dust storm induced by strong winds in the semiarid human impacted zone of Mexico

Abstract

We provide evidence of a recurrent strong wind erosion process of soil which occurs as a consequence of land use change and land cover change in the arid zones of the Mexican highlands. We applied an algorithm based in the friction velocity for estimating the flux of particulate matter less than 10 μm (PM₁₀) and numerical modeling to investigate the regional impact of a dust storm induced by strong winds during the passage of a cold front on March 18 2008. We show how the band of high concentration of particulate matter propagates through the complex topography of the highland and of the Eastern Sierra Madre to reach large urban zones in the northern part of Mexico. The morphological characteristics of the collected particles reveal the effects of the interactions associated with a continuous surface transport. The direct effect of dust particles is appreciated in the reduction of measured solar radiation data at stations placed right on the track of the dust storm. In our numerical simulation we estimated roughly that the fraction of PM10 emitted during this event was of the order of 9162.72 ton.

Pineda-Martinez L F, Carbajal N, Noyola-Medrano M C, Campos-Ramos A A and Aragon-Piña A (2009) Numerical modeling of a dust storm induced by strong winds in the semiarid human impacted zone of Mexico. *Manuscript submitted to Environmental Research Letters.*

4.1. Introduction

Land use change (LUC) and land cover change (LCC) have been identified as having a potential impact on local and global climate. The effects of LUC and LCC on air quality and more generally on global climate change are seen through changes in the atmospheric circulation by altering the balance in solar radiation, albedo, soil moisture and texture, aerodynamic roughness and other surface properties (Chase et al 2000). Although, there are other factors affecting the global climate, such as green house gases and growing urban areas (Kalnay and Cai 2003), some of the effects of LUC on climate are strong dust storms in arid and semiarid regions. There is a lack of information about the impact of factors linked directly to land surface properties and their relationship with weather and climate at several scales (Chase et al 2000, Stohlgren et al 1998). The factor of vegetation cover change affects the synoptic climate by causing regional changes in radiation budgets and surface fluxes modifying the land-atmosphere energy exchange. Furthermore, abrupt discontinuities in land surface properties may lead mesoscale circulations. In fact, this circulation can be compared to the sea breeze and mountain-valley circulations. It directly affects local atmospheric circulation regimes (Garratt 1993, Sud et al 1988, Segal et al 1989).

The most important impact of LUC and LCC in arid zones is linked to soil loss by wind erosion effects. This spatial and temporal desertification process is related to recurrent strong wind events in the dry season in semiarid human-impacted zones (Collado et al, 2002). Furthermore, dust storm occurrence affects the radiation budget by increasing the air turbidity. Some assessments indicate that the incoming radiation is scattered back to space due to dust particles (Ramanathan et al, 2001; Menon et al, 2002; Loeb and Kato, 2002;

Natsagdorj et al, 2003). It has been documented that in summer the direct effect is due to remote marine aerosol and aerosol produced by biomass burning. However, the dust induced by wind storms in semiarid regions acquires, in winter, more importance as a contribution to air turbidity. This kind of dust emission occurs in the northern part of Mexico, but its environmental effect has not been investigated. Soil loss in this region has almost totally an anthropogenic origin, in contrast to the Sahara and other natural desert zones of the world (Prospero et al 2002, Prospero et al 2003, Smirnov et al 2002, In and Park 2003, Slingo et al 2006).

The soil loss is on the order of hundreds of tons per hectare in a single strong wind event over the most vulnerable semiarid agriculture regions (Hagen 2004, Hupy 2004). The north-central part of Mexico has experienced some transformations in land management from mining to rainfed agriculture, barely irrigated lands and grazing. In the State of Zacatecas (Fig. 4.1), crops and induced grassland increased from 23.72% in 1976 to 32.49% in 2000 (INEGI 2008). The decrease of land vegetation cover and natural barriers has caused serious problems of soil loss in this highland region of Mexico. It is important to mention that under wind events, with the interaction between a flat topography and scarce vegetation cover, the soil loss is intensified. This erosion process occurs recurrently and dominantly in the dry winter season, with several events per season and is very variable depending on the intensity of the winds.

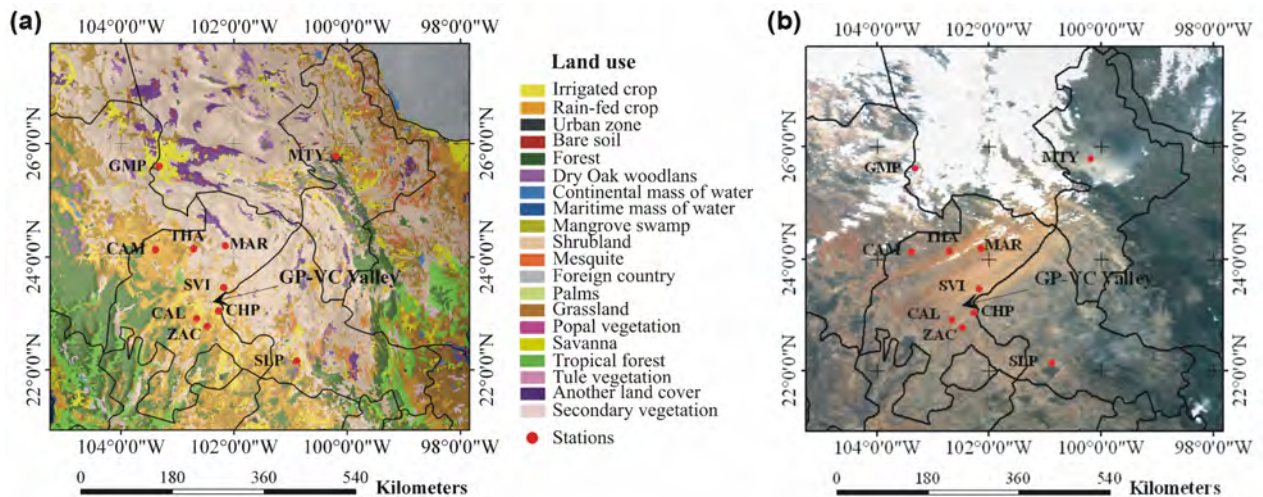


Fig. 4.1 (a) Land use classification map for Mexican Highlands (Source: INEGI, 2008) and (b) MODIS image of 18 March 2008. It is possible to observe the dust storm in the central part of Mexico.

To document the dust storms in the central northern part of Mexico, we selected a case study in the State of Zacatecas, in the Mexican highlands. We carried out a numerical simulation for an extreme wind event which caused a severe dust storm. The source of dust is situated in the valley of Guadalupe-Villa de Cos (GP-VC), near the city of Zacatecas (Fig. 4.1a). The principal land use in the valley is the rainfed crops. There are also some areas of irrigated crops with some patches of secondary grassland and shrublands (Fig. 4.1a).

4.2. Description of the dust event

The event occurred on 17 and 18 March 2008 during the passage of a cold front, oriented from southwest to northeast, which propagated along the highlands of the northern part of Mexico (cold front No. 39, (SMN 2008)). The circulation was governed by the presence of a high pressure (H) region in the southwest of USA and a low pressure (L) region in the

central-northwestern part of Mexico moving eastward. This synoptic situation caused an intensification of winds right at the leading edge of the front. These southwesterly winds were channeled by the topography, reaching gusts of up to 30 m/s. These strong winds originated the removal of soil particles from agricultural areas generating a dust storm around the City of Zacatecas. The agricultural areas of Calera (CAL), Guadalupe and Villa de Cos Valleys are characterized by a flat topography, 2200 m above the sea level, without the presence of natural topographical barriers. Due to the poor vegetation cover, these regions show a high vulnerability to soil loss in conditions of strong winds (>10m/s) which are frequent in the dry winter season (December to March).

4.2.1 Dust dispersion modeling

The event was simulated by applying a dispersion numerical modeling of the respiratory particles or particulate matter less than 10 μm (PM_{10}) by applying the Multiscale Climatic Chemistry Model (MCCM), which is based on the Mesoscale Model MM5 (Grell et al 2000). The MCCM includes multiple nesting capability, non-hydrostatic dynamic and data assimilation in four dimensions; in addition, it offers options for modeling microphysics processes (Grell et al, 1994). In opposition to non-coupled transport models, the coupling of meteorology with PM transport gives consistent results without interpolation of data (Stockwell et al, 1990; Wesley, 1989). The simulation domain was established at central coordinates 24° N and 101.3° W, with a horizontal grid resolution of 12 km on 70x70 grid points. The model was initialized with the National Centers for Environmental Prediction (NCEP) final analysis data as initial conditions (Kalnay et al 1996). The numerical

simulation was initialized at 00Z on March 16 2008 with a duration 96 h producing hourly outputs.

The dust emission flux was determined by applying the proposed vertical mass flux for PM10 equation by Choi and Fernando (2008) based in the approach of Westphal et al (1987). The algorithm consists in a simple estimation of the emitted dust when the friction velocity exceeds the threshold of dust emission.

$$Fa = 0.13 \times (1 - R) \times 10^{-14} \times U_*^4 \quad (1)$$

$$\text{when } U_*^4 \geq U_{*t}^4$$

where Fa is dust emission flux ($\text{g cm}^{-2} \text{ s}^{-1}$), R is a vegetation reduction factor, U_* is the friction velocity (cm s^{-1}), U_{*t} represents the threshold friction velocity.

The source areas were limited to bare soil, dry grassland and rainfed agriculture lands in the highlands. The friction velocity is estimated using the land surface model of MM5 (Oncley and Dudhia, 1995):

$$u_* = \frac{kU}{\ln\left(\frac{z}{z_0}\right) - \mathbf{y}_m\left(\frac{z}{L}\right)} \quad (2)$$

where k is the Von Karman constant (0.4), U the wind speed at the height of Z , Z_0 the surface roughness length, \mathbf{y}_m the stability function for the momentum and L the Monin-Obukhov length scale.

The threshold friction velocity is determined based on the observed wind speed and dust-rise at the surface. During the dust storm event the friction velocities are calculated at each model grid using the observed wind speed and PM10 concentrations in a 1hr intervals.

4.2.2 Characterization of PM₁₀

In order to obtain specific characteristics of the dust particles, we obtained samples of PM₁₀ in the study zone. The obtained data have been used to increase knowledge about the soil properties and the dust emissions in the region. The particles were collected with PM₁₀ high-volume Tich Environment equipment in quartz fiber filters. The gathering time for each sample was during 24 hours and a constant air flow 1.3 m³/min over a period of 72 hrs. To determine the chemical composition and morphology of particles at the individual level, a scanning electron microscope (SEM) Phillips XL30 model coupled with an energy dispersed spectrometry (EDS) microanalysis EDAX DX4 were used. An X-ray diffractometer was employed (DRX) (Rigaku MAX D-2200) to characterize the principal crystalline phases of the collected atmospheric dust.

4.3 Results

4.3.1 Modeled and measured meteorological variables

The meteorological data were obtained from stations in the surroundings of the source area as well as from stations located on the track of the dust cloud. The wind speed data were obtained from the station located in the GP-VC Valley; they showed two cycles during the event which lasted from 1000UTC on 17 March 2008 to 1800UTC on 18 March 2008 (Fig. 4.2). The topographic forcing channeled the leading edge of the cold front causing intense winds in the central part of the highlands (see ZAC in Fig. 4.1a). In northern regions (MTY), the wind was also very intense (Fig. 4.2a). To the south, the event of intense wind was also recorded at the meteorological station in SLP after a delay of almost six hours.

We calculated the root mean square error (RMSE) of the difference between observed and modeled variables for the same period. The RMSE of temperature, relative humidity and wind speed are depicted in Table 4.1. Under extreme atmospheric circulation conditions the numerical models have some difficulty capturing the spatial variation and magnitude of almost all parameters, even though the calculated RMSE is acceptable. The main variations in temperature (T °C) and relative humidity (RH %) are associated with atmospheric features such as the cold front passage and the direct effect of mineral dust since they tend to reflect solar radiation as well as to absorb environmental moisture by the presence of quartz and silica (Zobeck and Fryrear 1986).

Table 4.1 RMSE values of MCCM outputs and measurements data for meteorological variables.

ID	T	HR	V
ZAC	7.74	37.74	4.70
SLP	5.87	20.70	6.92
GMP	7.06	20.99	4.35
MTY	9.28	29.42	4.69
Mean	8.05	30.41	5.09

Figure 4.2 shows a simulation of the passage of the cold air mass through the highlands on 18 March 2008. The horizontal plots show the wind intensification in the highlands being associated to ageostrophic circulations in the leading edge of the front. In general terms, the mesoscale atmospheric circulation is well represented by the model, since the channeling of winds through the topography from the central highlands to the northeast region where the city of Monterrey is located, are well reproduced in the entire event.

These changes affect the vertical and horizontal structure of the meteorological variables.

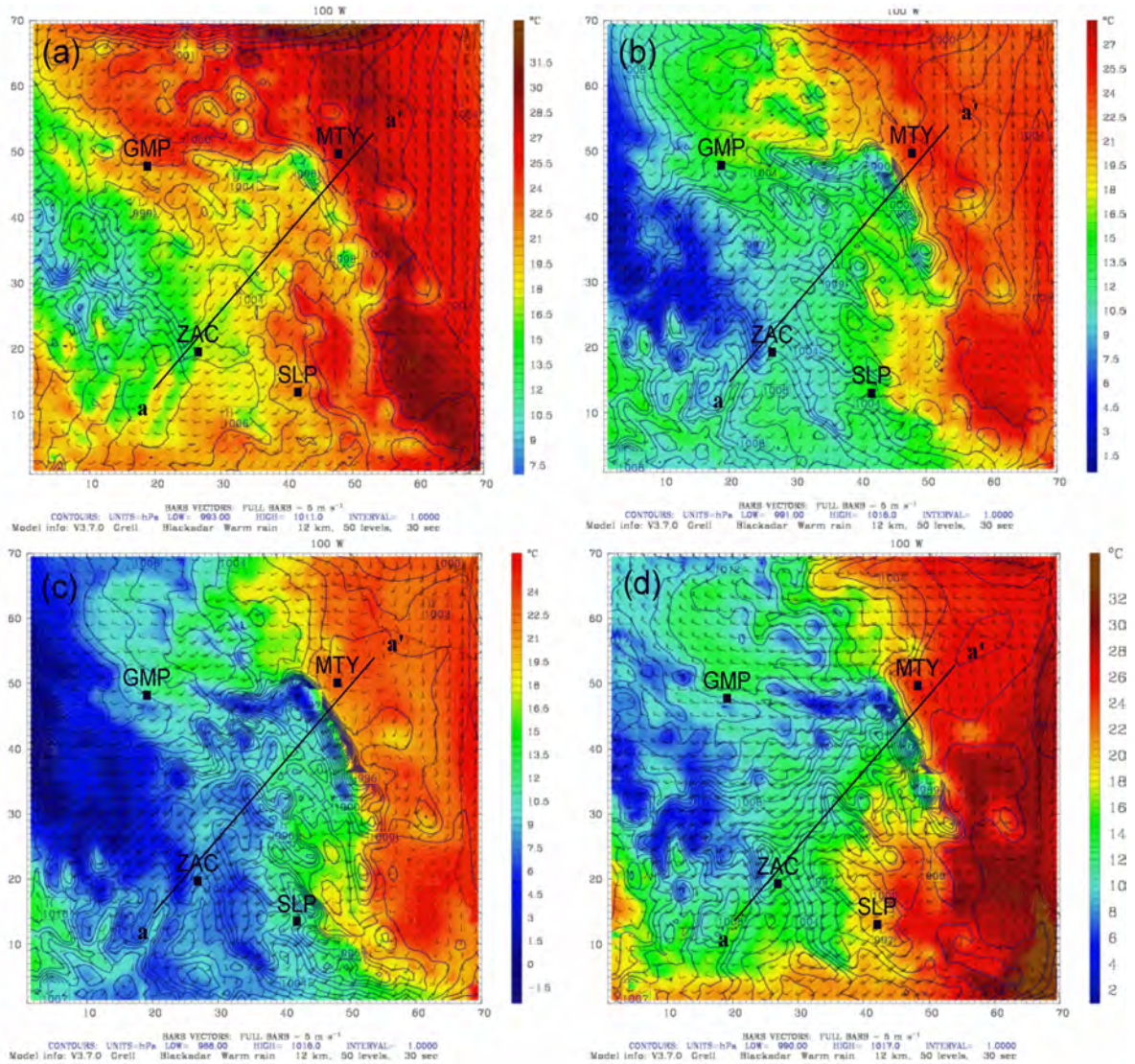


Fig. 4.2 Sea Level Pressure (SLP) (contours), wind vectors and temperature in °C (shaded) of the event moving from the Northwest into highland region on 18 March 2008 at: (a) 00Z, (b) 06Z (c) 12Z and (d) 18Z. Line (a-a') indicates the cross section in figure 4.3.

The intensification of the winds was associated to low-level strong winds circulation from the Pacific to Gulf of Mexico, including the upper level jet circulation. The cross sections in Fig. 4.3 illustrate this motion. The maximum winds are reached in the transition from the highlands to costal lands near Gulf of Mexico. The potential vorticity is displayed in this section to provide evidence of the effect of the gust of winds in topographic transitions. In

some cases the discontinuities in surface properties or elevation gradients induce vertical turbulent fluxes.

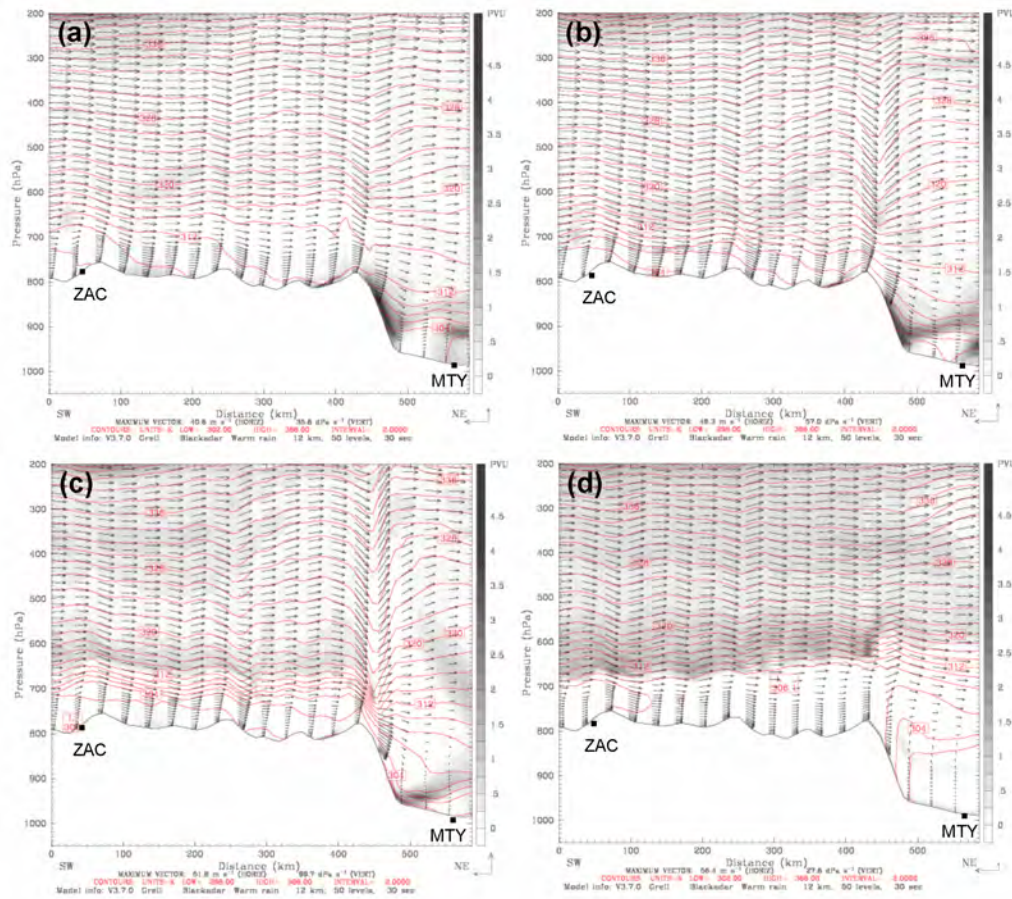


Fig. 4.3 Cross section SW-NE showing wind circulation on 18 March 2008 at: (a) 00Z, (b) 06Z (c) 12Z and (d) 18Z. Solid line represents the potential temperature at 2 K intervals. Shading represents potential vorticity.

4.3.2 Dust flux emission and dispersion

The estimated threshold friction velocity was of 60 cm^{-1} for the areas of rain-fed agriculture, semi-arid grassland and bare soil (30 Grid points). The results of the dust emission flux algorithm reveal that the maximum friction velocities were reached in flat topography regions and as consequence the dust flux was larger, $234.45 \text{ (Kg/Km}^2 \text{ h)}$ in bare soil. These values are comparables with those reported for other studies in natural deserts

(Wetspal 1987, In and Park 2003; Choi and Fernando, 2008). Although, the semiarid regions have influence of the scatter vegetation cover, this can be analyzed like a human-induced desert in dry season in single areas (i. e rainfed agriculture lands). The Fig. 4.4 presents a time series of PM₁₀ for 3 sites. These varied mainly by some aspects such as cover vegetation and topography.

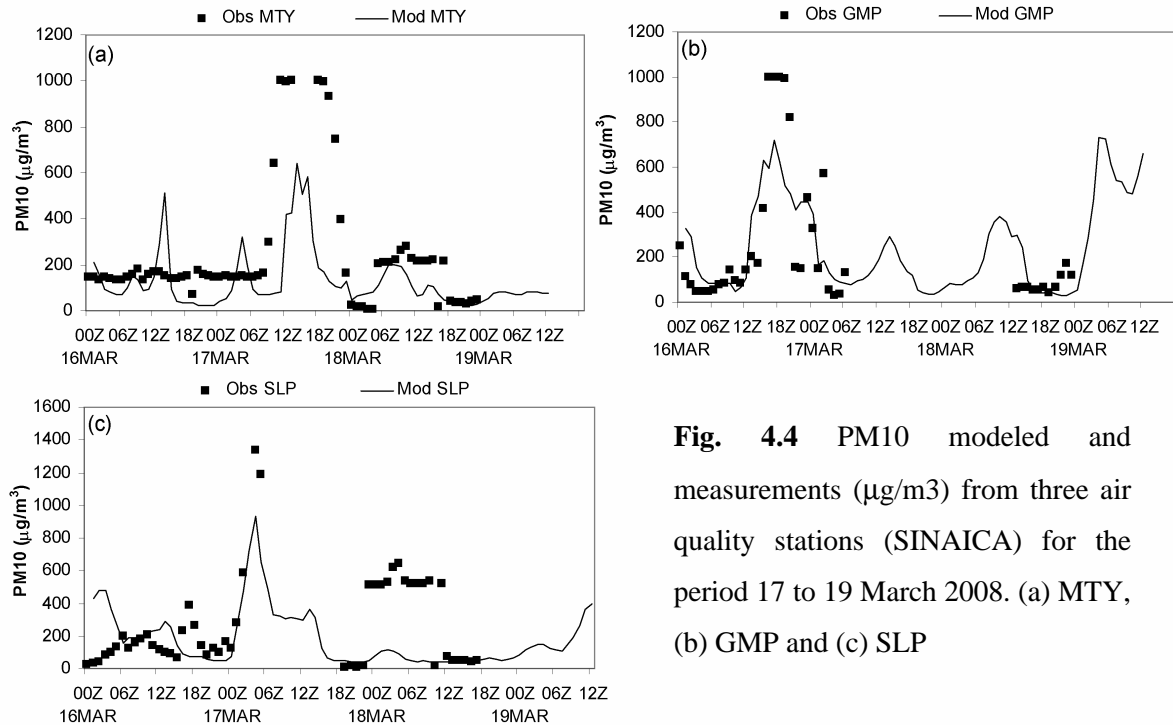


Fig. 4.4 PM₁₀ modeled and measurements (µg/m³) from three air quality stations (SINAICA) for the period 17 to 19 March 2008. (a) MTY, (b) GMP and (c) SLP

Figure 4.5 shows a simulation of the passage of the front through the highlands on 18 March 2008. The circulation and mobility of PM₁₀ is well captured by the simulation. The dust emitted was transported from the highlands to northeast across of the eastern Sierra Madre reaching the southeast of the Texas, USA.

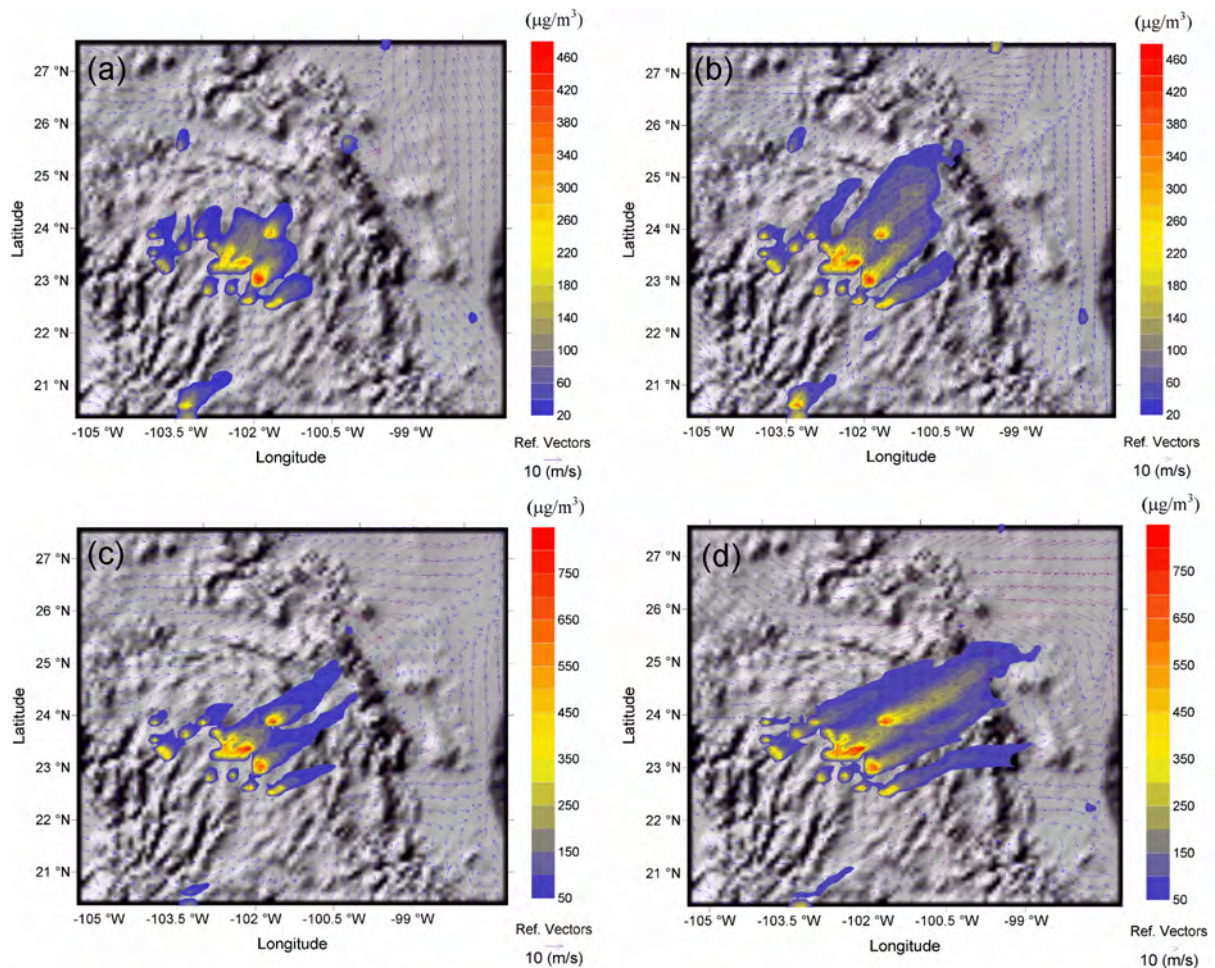


Fig. 4.5 Dust dispersion modeling of PM₁₀ horizontal distribution (shaded color) and wind vectors on 18 March 2008 at: (a) 09Z, (b) 12Z (c) 15Z and (d) 18Z.

As the cold front propagated southwards, it caused the suspension of dust with several intensities at different sites. Data of concentrations of PM₁₀ from Torreon station (GMP), is located to the northwest of the study area, reveal a maximum value on 17 March 2008 about of 1900UTC. The station located in the city of Monterrey (MTY) registered the arrival of the dust storm by the afternoon of 18 March 2008 increasing the PM₁₀ concentration during three hours. Additional data of PM₁₀ concentrations were obtained from the station located in the city of San Luis Potosi (SLP). The highest concentrations of PM₁₀ were reached in SLP earlier than in Monterrey (MTY).

4.3.3 PM₁₀ properties and solar radiation

In field collected PM₁₀, we distinguish the mineral phases of abundant quartz (SiO₂), microcline (KAlSi₃O₈) and particles related to anorthite (CaAl₂Si₂O₈). These particles are mainly well rounded, with shapes close to spheres. The principal morphology of the particles is possibly due to friction processes caused by transport at the land surface (Goltsyn, et al 2003) (Fig. 4.6a).

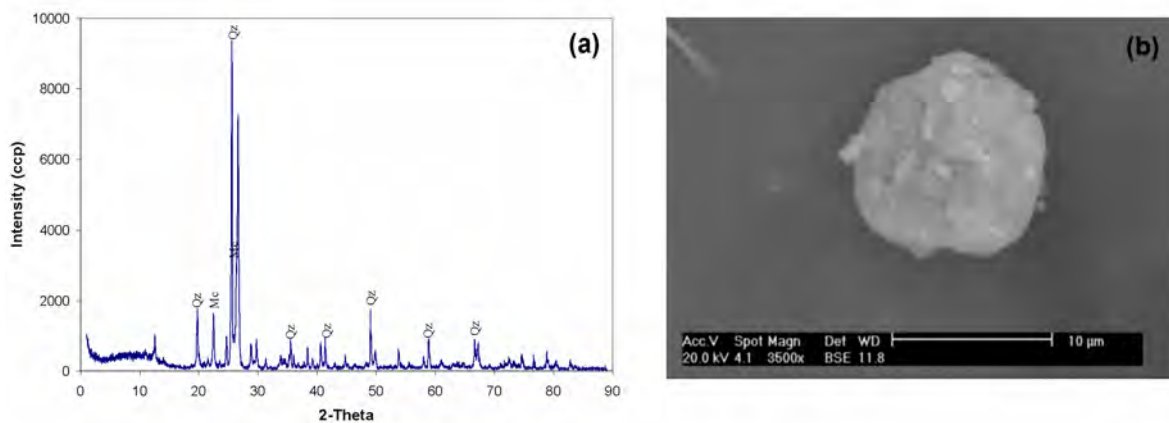


Fig. 4.6 (a) Diffractogram of the atmospheric particles from the study area. (b) Photomicrography of the particle of Microcline (KAlSi₃O₈), and is possible to perceive the rounded edges.

The large quantity of dust transported in the atmosphere modified the incidence of solar radiation, which is reduced by aerosols feedback mechanisms. In Fig. 4.7a, we show that the measured solar radiation decreased in about 50 W/m² during the passage of the dust storm. The high concentrations of particles in the region (more than 400 µg/m³) and its chemical characteristics give an idea of the impact on the surface solar radiation. The whole field stations recorded a diminution in solar radiation during passage of the dust. The geographical position of the stations determined their register in the shadow effect while the dust travels through the highland.

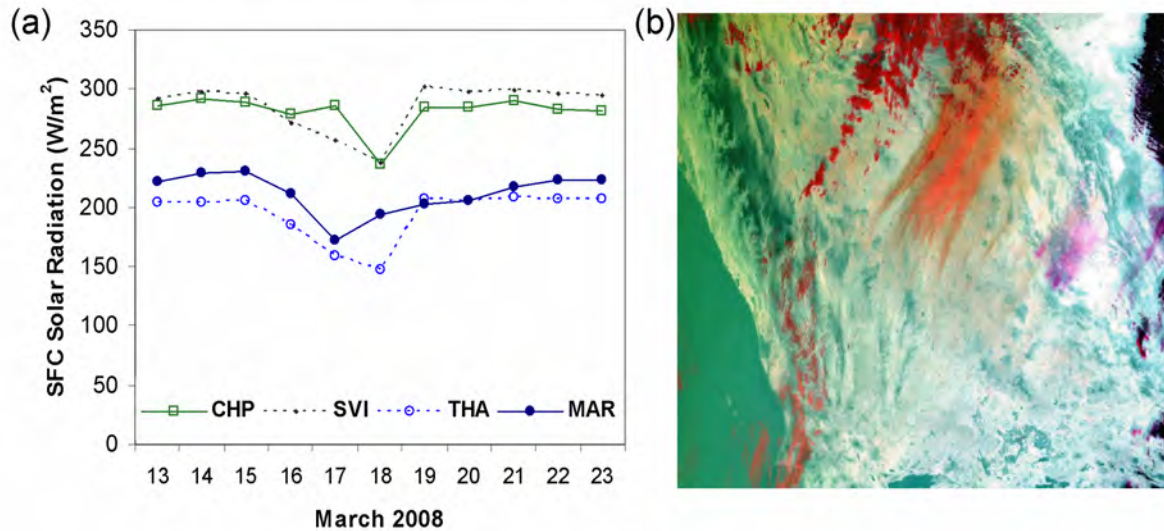


Fig. 4.7 (a) Surface (SFC) total radiation from meteorological stations placed in the rural zone in central-northern of Mexico: Calera (CAL), Chaparrosa (CHP), Sierra Vieja (SVI), Mazapil 1 (THA), Mazapil 2 (MAR) and Campo Uno (CAM) (Also shown in Fig. 4.1) (INIFAPZAC, 2008). (b) Infrared channel of MODIS image.

Figure 4.7b show a dust diagnostic derived from infrared channel from MODIS landsat image. It is possible to observe some dust plumes in light red; which appeared to propagate close to the surface as the mixtures of density currents and light flow flowing northernward through highlands. Clouds appear in dark red. An event of wildfire was occurred at the same time and is appreciated in magenta. It is interesting to note that dust plumes agree quite well with the simulation.

4.4 Discussion

The results of our numerical calculations show the progression of events on 18 March 2008. The emission began during the morning and continued throughout the day, finishing near the 1900 UTC. The direct effect of dust particles is noted in the reduction of solar radiation. Since the radiation data were measured at stations placed just on the track of the

dust storm, it is possible to infer the net reflectivity effect of mineral dust particles (dominantly quartz). The measured solar radiation data showed clearly a minimum during the development of the dust storm. In addition, these stations have no influence from large urban areas. Similar effects have been previously reported for the Sahara and other natural desert zones where emitted mineral dust diminished the solar radiation at the surface level (Prospero et al, 2002; Smirnov et al, 2002; Slingo et al, 2006).

Additionally, numerical experiments showed the differences in shortwave downward radiation under clear and dusty sky (Fig. 4.8). These results indicate that the presence of suspended mineral material alters the solar radiation incidence. In Fig. 4.8, the first serial of plots shows the model result without PM10 emission in the model. The second ones show the influence of the presence of the atmospheric dust during its passage for the Mexican highlands. Effects of clouds cover are appreciated in both cases.

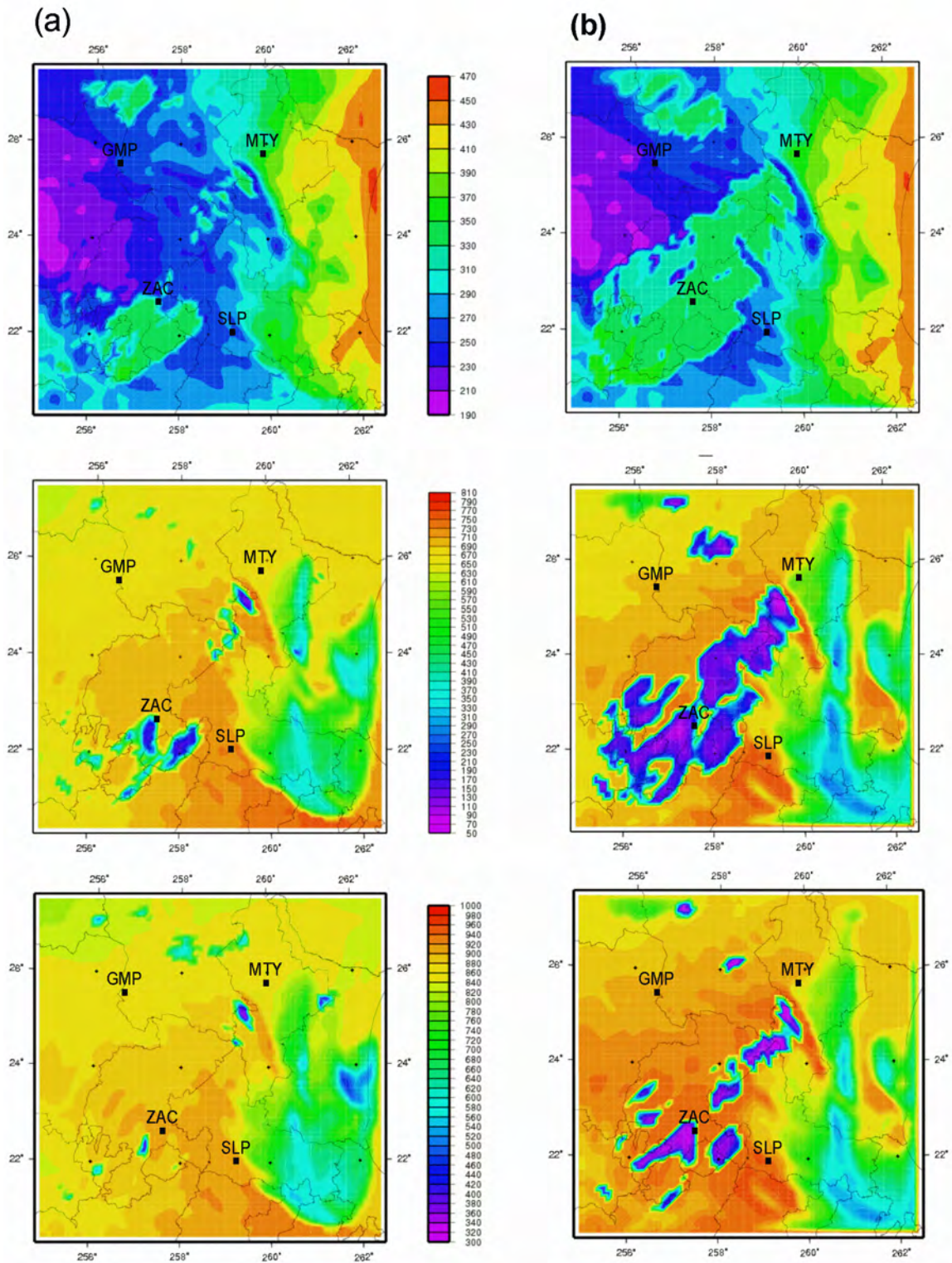


Fig. 4.8 Shortwave downward radiations for tow numerical experiments. (a) MM5 running without considers PM10 emissions and (b) MCCM including PM10 particles transported trough Mexican highlands.

The process of dust emission occurs mainly by suspension of fine material (<10mm) followed by transport by saltation of the aggregates of superior diameter (>0.01mm). Once the friction velocity threshold is reached the advection process transports finer material (Hagen et al 1999). The influence of wind and soil conditions in the semi-desert area being studied lead to the suspension of fine particles into the atmosphere. The friction velocity, wind speed, soil type, soil density and physical properties play an important role in the process of suspension, but under extreme wind conditions, joined with exposed agriculture land, the soil loss is radically increased (Woodruff and Siddoway 1965, Hagen 2004).

Although the maximum wind intensity lasted for a period of 8 hours the friction velocity threshold for dust suspension was reached about 7:00 hrs (Local Time). It began with moderate levels of concentration, reaching its maximum value in the afternoon and ending this process at about 19:00 hrs LT. The average dust flux estimated was on the order of 176.75 (Kg/ km² h). With this value, a rough estimation of the soil loss for a period of 12 hours for a source area of 4320 (km²) was 9162.72 ton of PM₁₀ fraction. These results show the significance of this recurrent problem in the dry winter season.

The transport of huge quantities of dust shows how relatively small local factors such as land cover change may affect the air quality in large areas and urban zones such as the city of Monterrey, located 400 km from the source area. Further, LCC generates a local environmental impact through desertification and loss of productivity in cultivated land and affects the weather in the arid Mexican highlands.

4.5 Conclusions

We discussed physical and dynamic aspects of a recurrent dust storm in the highlands of the central-northern part of Mexico. We applied observed data of meteorological variables, concentrations and characterization chemical of PM_{10} and numerical modeling to investigate the development of this phenomenon. We were able to reproduce spatial and temporal characteristics of the event as well as the emissions and concentrations of PM_{10} under a well-modeled atmospheric circulation. The analysis of SEM indicated that the morphological characteristics of the collected particles reflect the effects of continuous surface transport in semiarid regions. The physical properties of the mineral phases of quartz, microcline and anorthite cause changes in the local weather conditions by reducing the surface total solar radiation. The management strategy to mitigate the soil loss must consider policies for agricultural areas by developing programs of rotating crops and natural barriers. We showed that a relatively small human impacted area, by desertification process, is converted a source of dust affecting large regions, including urban zones.

References

Collado, A.D., E. Chuvieco, and A. Camarasa (2002), Satellite remote sensing analysis to monitor desertification processes in the crop-rangeland boundary of Argentina. *J Arid Environ*, 52, DOI:10.1006/jare.2001.0980

Garratt, J. R. (1993), Sensitivity of climate simulations to land-surface and atmospheric boundary-layer treatments A review, *J. Clim.*, 6, DOI: 10.1175/1520-0442(1993)006

Grell, G. A., S. Emei, W. R. Stockwell, T. Schoenemeyer, R. Forkel, J. Michalakes, J. R. Knoche, and W. Seild (2000), Application of a multiscale, coupled MM5/chemistry model to the complex terrain of the VOLTAP valley campaign. *Atmos. Environ.*, 34, 1435–1453.

Chase, T. N., R. A. Pielke, T. G. F. Kittel, R. R. Nemani, and S. W. Running (2000), Simulated impacts of historical land cover changes on global climate, *Clim Dyn.*, 16, 93–105.

Choi Yu-Jin, Fernando H.J.S. (2008) Implementation of a windblown dust parameterization into MODELS-3/CMAQ: Application to episodic PM events in the US/Mexico border. *Atmos. Environ.*, 42, 6039–6046.

Hagen, L. J., L. E. Wagner, E. L. Skidmore (1999), Analytical solutions and sensitivity analyses for sediment transport in WEPS, *Ame. Soc. Agr. Engr*, 42(6), 1715-1721.

Hagen, L. J. (2004), Evaluation of the Wind Erosion Prediction System (WEPS) erosion submodel on cropland fields, *Env. Mod & Sw.*, 19, DOI:10.1016/S1364-8152(03)00119-1

Hogan, T. F., and T. E. Rosmond (1991), The description of the Navy operational global atmospheric prediction system's spectral forecast model, *Mon. Wea. Rev.*, 119, DOI: 10.1175/1520-0493(1991)119.

Hupy, J. P. (2004), Influence of vegetation cover and crust type on wind-blown sediment in a semiarid climate, *J Arid. Environ.*, 58, DOI: 10.1016/S0140-1963(03)00129-0.

In, H. J., Park, S. U. (2003). Estimation of dust emission amount for a dust storm event occurred in April 1998 in China. *Water, Air and Soil Pollut.*, 148, 201–221.

Instituto Nacional de Investigaciones Forestales, Agrícolas y Pecuarias (INIFAP) (2008) Red de monitoreo agroclimático del estado de Zacatecas.

Instituto Nacional de Estadística Geográfica e Informática (INEGI) (2008), Principales tipos de vegetación de México. Sistemas nacionales estadísticos de información geográfica, available at <http://www.inegi.gob.mx/>

Kalnay, E. and M. Cai (2003), Impact of urbanization and land-use change on climate, *Nature*, 423, 528-831.

Loeb, N. G., and S. Kato (2002), Top-of-atmosphere direct radiative effect of aerosols over the Tropical Oceans from the Clouds and the Earth's Radiant Energy System (CERES) satellite instrument, *J. Clim.*, *15*, DOI: 10.1175/1520-0442(2002)015.

Menon, S., J. Hansen, L. Nazarenko, and Y. Luo (2002), Climate effects of black carbon aerosols in China and India, *Science*, *297*, 2250– 2252.

Natsagdorj, L., D. Jugder, and Y. S. Chung (2003), Analysis of dust storms observed in Mongolia during 1937–1999. *Atmos. Environ.*, *37*, DOI:10.1016/S1352-2310(02)01023-3.

Prospero, J. M., and P. J. Lamb (2003), African droughts and dust transport to the Caribbean: Climate change implications, *Science*, *302*, 1024-1027.

Prospero, J. M., P. Ginoux, O. Torres, and S. Nicholson (2002), Environmental characterization of global sources of atmospheric soil dust derived from the NIMBUS 7 Total Ozone Mapping Spectrometer (TOMS) absorbing aerosol product, *Rev. Geophys.*, *40(1)*, doi:10.1029/2000RG000095.

Ramanathan, V., P. J. Crutzen, J. T. Kiehl, and D. Rosenfeld (2001a), Aerosols, climate, and the hydrological cycle, *Science*, *294*, 2119–2124,

Segal, M., W. E. Schreiber, G. Kallos, J. R. Garratt, A. Rodi, J. Weaver, and R. A. Pielke (1989), The impact of crop areas in northeast Colorado on midsummer mesoscale thermal circulations, *Mon. Weather Rev.*, *117*, DOI: 10.1175/1520-0493(1989)117.

Servicio Meteorológico Nacional (SMN) (2008), Climatic Products, available at <http://smn.cna.gob.mx>

Sistema Nacional de Información de la Calidad del Aire (SINAICA v4.0) (2008) Consulta de datos en tiempo real. Instituto Nacional de Ecología (INE) available at <http://sinaica.ine.gob.mx/>

Slingo, A., T. P. Ackerman, R. P. Allan, E. I. Kassianov, S. A. McFarlane, G. J. Robinson, J. C. Barnard, M. A. Miller, J. E. Harries, J. E. Russell, and S. Dewitte (2006), Observations of the impact of a major Saharan dust storm on the atmospheric radiation balance, *Geophys. Res. Lett.*, 33, L24817 doi:10.1029/2006GL027869.

Smirnov, A., B. N. Holben, Y. J. Kaufman, O. Dubovik, T. F. Eck, I. Slutsker, C. Pietras, and R. Halthore (2002), Optical properties of atmospheric aerosol in maritime environments, *J. Atmos. Sci.*, 59, DOI: 10.1175/1520-0469(2002)059.

Stohlgren, T. J., T. N. Chase, R. A. Pielke, T. G. Kittel, and J. Baron (1998), Evidence that local and land use practices influence regional climate and vegetation patterns in adjacent natural areas, *Global change Biol*, 4, 495-504.

Sud, Y. C., J. Shukla, Y. Mintz (1988), Influence of land surface roughness on atmospheric circulation and precipitation: A sensitivity study with general circulation model, *J. Appl. Meteorol.*, 27, 1036–1054.

Woodruff, N. P., and F. H. Siddoway (1965), A wind erosion equation, *Soil Science Soc. of Amer. Proc.* 29(5), 602-608.

Westphal, D.L., O.B. Toon, T.N. Carlson (1988) A Case Study of Mobilization and Transport of Saharan Dust. *J. Atmos. Sci.*, 45, 2145–2175.

Zobeck, T. M., and D. W. Fryrear, (1986), Chemical and physical characteristics of windblown sediment: I. Quantities and physical characteristics, *Trans. Am. Soc. Agric. Engin.*, 29(4), 1032-1036.

Chapter 5

Dispersion modeling of the atmospheric particulate matter in the Urban Area of San Luis Potosi, Mexico.

Abstract

A numerical study of the spatial-temporal evolution of concentrations of particulate matter from May 2003 to April 2004 in the Urban Area of San Luis Potosi was carried out. Although there is a considerable annual variability of the atmospheric circulation, the analysis of the results indicates preferential seasonal circulation patterns; northeasterly winds in winter and southeasterly in summer. High concentration values of particulate matter were closely connected with local characteristics of the atmospheric circulation. A net transport from the industrial zone into the urban area is one of most important outcomes of the investigation. Total Suspended Particle (TSP) samples were collected in order to obtain information about their size ranges and chemical composition. By Scanning Electron Microscopy (SEM) it was possible to identify the types of polluting sources. Measurements of total suspended particles revealed that the Mexican Official Standard (annual guideline $75 \mu\text{g m}^{-3}$) was exceeded in 43 days. Atmospheric circulation description by numerical modeling for high concentration of TSP allow us to conclude that effects of bad ventilation cause the diminution of air quality in Urban Area of San Luis Potosi.

Pineda-Martinez L F, Campos-Ramos A A, Carbajal N, Aragon-Piña A, García A (2009) Numerical modeling of dispersion and characterization of atmospheric particulate matter (PM10) in the Urban Area of San Luis Potosi, Mexico. *Manuscript to be submitted to WaterAir and Soil Pollution.*

5.1. Introduction

There is considerable uncertainty about the effects of atmospheric particulate matter (PM) on the global climate; hence it is important to know their physicochemical characteristics and to evaluate the dispersion phenomena that contribute to the presence of high concentrations of particulate matter (Leyva et al, 1996; Kulmala et al, 2003, IPCC, 2007). In addition, the origin and transport mechanisms of particles give information about its final properties; they are continuously controlled by many physical and chemical processes that influence their composition, shape and distribution (Korhonen et al, 2004). Particulate matter effects on atmospheric pollution have been documented in several fields, which highlight the relation between its exposure and various health effects, such as cardiovascular and respiratory diseases (WHO, 2002). In the Urban Area of San Luis Potosi (UASLP), previous studies have revealed some morphological characteristics and chemical composition of particles and it has been possible to distinguish their natural and anthropogenic origin (Aragón-Piña et al., 2000, 2002, 2006). Nevertheless, these studies did not consider atmospheric circulation, pollutants dynamics and their interaction with topographic effects. Due to the complex nature of the particulate matter, it is important to identify sources of emissions in order to make local and regional detailed plans, as well as developing strategies for estimating the impact on the population caused by particulate matter exposure (Jazcilevich et al, 2002; Chen et al, 2005).

Important factors in the particles dispersion are wind patterns and the regional circulation which determine their main mechanisms of transport and deposition. The final product of these processes is a heterogeneous spatial distribution (Querol et al, 2004b). Atmospheric circulation is an important indicator to make decisions about the location of the best

monitoring stations from which information will be obtained on specific characteristics of particles and mechanisms to determine the influence of pollutants sources. The Mesoscale Model of fifth generation MM5 (Grell et al, 1994) and the Multiscale Climate Chemistry Model (MCCM) (Grell et al, 2000) have been applied successfully to study the pollution in Mexico City (Jazcilevich et al, 2002; 2003).

The urban area of San Luis Potosi consists of a city with a large number of vehicles and of an industrial zone (IZ) of considerable size (Fig. 1). In the west part of the city, there is an intense activity of the metallurgical industry (MMZ). Nowadays, in the Industrial Zone, located in southern side of the UASLP, there are in operation more than 356 companies: working industrial automotive manufacture, melting iron, steel and non-ferrous metals and chemical industry. Airborne particulate matter represents a complex mixture of organic and inorganic substances. Total suspended particles (TSP) include any particle suspended in air in a wide range of sizes. There are few studies of air quality that propose strategies to control the pollution problem associated with particulate emission (Leyva et al, 1996). It has motivated the interest for understanding the physicochemical characteristics of the atmospheric particulate matter. There are signs that TSP values are, several times in a year, above the Mexican Regulation Concentrations Guideline. In this chapter is carried out a numerical study of the spatial distribution of TSP generated in the industrial zone from May 2003 to April 2004. As well as, the polluting sources that contribute to the urban area (UASLP) are identified by comparing characteristics of the particles sampled at the monitoring and punctual sampling by applying Scanning Electron Microscopy (SEM).

5.1.1. Study area

The urban area of San Luis Potosi is located at 22.15° N and 100.98° W, in the central part of Mexico, about 500 km to the north of Mexico City (Fig. 5.1a). The climate is arid with a rainy season in summer. The UASLP is located in the San Luis Potosi Valley surrounded by two mountain chains that work as natural barriers channeling wind between the Sierra San Miguelito on the West side and the Sierra de Alvarez to the East of the city. The valley is approximately 1877 m above sea level, it is topographically flat and it is oriented in the Southwest-Northeast direction (Fig. 5.1b) (INEGI, 2002; Pineda-Martínez et al, 2007).

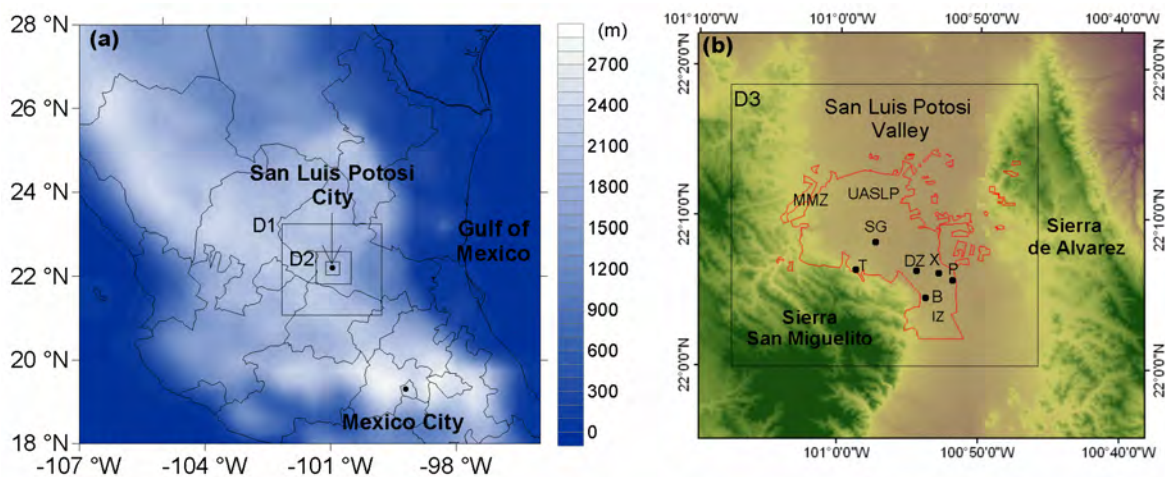


Fig. 5.1 (a) Location map of the City of San Luis Potosí in the central part of Mexico. Terrain elevation is in meters and nested domains configurations are centered in the UASLP. The mother domain has a resolution of 27km (30X30), 9 km,(31X31) the middle, 3 km (20X20) and the interior 1km (40X40). (b) The domain D3 presents the Urban Area of San Luis Potosi (irregular contour line). The image shows two main topographic barriers: on the west part the Sierra San Miguelito and on the east the Sierra de Alvarez. Dots represent the field-stations position, four in the Industrial Zone (IZ), Tangamanga Park (T) and in urban zone (SG).

5.2. Methods

5.2.1 Dispersion model

In order to know about the distribution of particles under the prevailing meteorological conditions, we applied the model Multiscale Climate Chemistry Model (MCCM). It was implemented for the central region of Mexico, specifically to study the Urban Area of San Luis Potosi (UASLP), located in the central Mexican highlands (Fig. 5.1). The configuration of the domains is shown in Fig 5.1a.

5.2.2 Data

We obtained concentration data of TSP from a previous campaign, which included five sampling urban field-stations and another suburban station in an area with extensive vegetation inside the park Tangamanga (T), about 10 Km distant from industrial sources (Fig. 1). The samples were collected during the period from May 2003 to April 2004 (242 days) (Aragon-Piña et al, 2006). Additionally, particulate matter less than 10^{-6} m (PM10) and TSP concentrations data were obtained from simultaneous sampling (SG station). From PM10-TSP samplers we calculate their proportion. This comparison is useful for validating the model since the dispersion is computed in terms of the PM10 fraction.

5.2.3 Simulations

By applying the MCCM model, we modeled the atmospheric circulation in the UASLP and the dispersion of particles for some months in the years 2003 and 2004, right for the same period in which TSP data concentrations were measured. Additionally, it has been performed a model run test for recent PM10 data using the same initial emissions conditions discussed below. The numerical experiments were performed by including a PM10 background concentration in whole urban area and including constant rate of

emission in the industrial zone. The numerical simulations covered the monitoring period which includes the principal seasonal variations. We modeled 242 days with outputs every 3 hours and we calculated daily averages. 23 sigma levels with vertical high resolution near the surface were incorporated, with an increasing thickness until the level pressure of 100 mb. The model was initialized using NCEP/NCAR reanalyzed data with a temporal resolution of 6h (Kalnay et al, 1996). The original land use category (25-Land USGS) of the model was modified to include completely the urban area of the city of San Luis Potosi by using satellite imagery to include correctly the UASLP in the domain D3 (Fig 5.1).

5.3. Results and Discussion

5.3.1 Atmospheric circulation

It is necessary to consider two fundamental aspects: the synoptic circulations and local factors to contextualize the atmospheric circulation in the UASLP. In the synoptic circulation, winter cold fronts propagate through the plains of the central-southeast region of USA in anticyclone motion, advancing southwards into Mexico. Some of the cold fronts reach Mexico through the coastal plains of the Gulf of Mexico, moving forward through the Eastern Sierra Madre to the highlands. This synoptic situation is dominated by westerly circulation causing regional winds flowing from the southwest in the valley of San Luis Potosi (Schultz et al, 1998; Cavazos, 1999). Cold air masses circulation is channeled by the complex topography in the highlands as the front progresses to the central part of Mexico. Another important feature is that the circulation associated with most of these cold air masses coincides in direction with the westerly jets in the upper troposphere producing a channeling in lower levels into the central plains through the lowlands of the Sierra Madre.

Thus, channeled winds flow dominantly from the west-southwest, although it varies from front to front (Perez, 1996, Magaña et al, 1999; Pineda-Martínez et al, 2007).

In summer, upper westerly jet disappears (Cavazos and Hastenrath 1990), trade winds are dominant and flow into the highland through the Eastern Sierra Madre in lower layers of the atmosphere. This prevailing synoptic configuration is intermittently modified by cyclone systems and tropical waves propagating along the coastal areas of the Gulf of Mexico and affecting the circulation patterns landwards. From this general circulation analysis, we state that southerly and southeasterly winds flow consistently in the UASLP. Therefore, we present the hypothesis of a preferential transport of PM₁₀ from the southeast to the northwestern part of the UASLP, guided by the foothills of the mountain chain Sierra de San Miguelito. A second and even more dominant circulation pattern is related to local effects like convergence and divergence processes and anabatic and katabatic winds in the UASLP. The convergence induced by the mountain-valley circulation causes regional easterly winds, generating a re-circulation in the UASLP; these processes are unfavorable to the dispersion and to the transport of PM₁₀ beyond the urban area.

5.3.2 Model validation with observed meteorological data

Since it is necessary to have certainty and precision in the results, the model performance was analyzed by comparing calculated values of several meteorological variables with data obtained at the meteorological observatory in the UASLP. Table 5.1 presents a summary of Root Mean Square Error (RMSE) among model outputs and observed data. The RMSE was calculated for monthly averages of temperature, relative humidity and wind speed.

Table 5.1 RMSE values of temperature (RMSEt), Relative Humidity (RMSErh) and Wind speed (RMSEw).

Run ID	RMSEt	RMSErh	RMSEw
200306	2.06	5.85	1.92
200307	1.26	11.03	2.05
200308	1.27	8.15	1.78
200309	1.48	6.98	1.71
200311	1.45	9.56	3.35
200312	1.97	13.74	3.11
200401	1.69	12.93	3.26
200402	2.04	16.83	3.96
200403	1.70	14.93	3.14

The estimated RMSE for monthly averages are of the same order as those reported in other works (Jazcilevich et al, 2002). For wind speed RMSE was 2.7m/s, for the temperature 1.66°C and 11.11% for the relative humidity. These values give us a measure of the model accuracy. The model satisfactory calculates the phase and intensity of the temperature. Considering the results showed in Table 5.1, all parameters presented an acceptable precision.

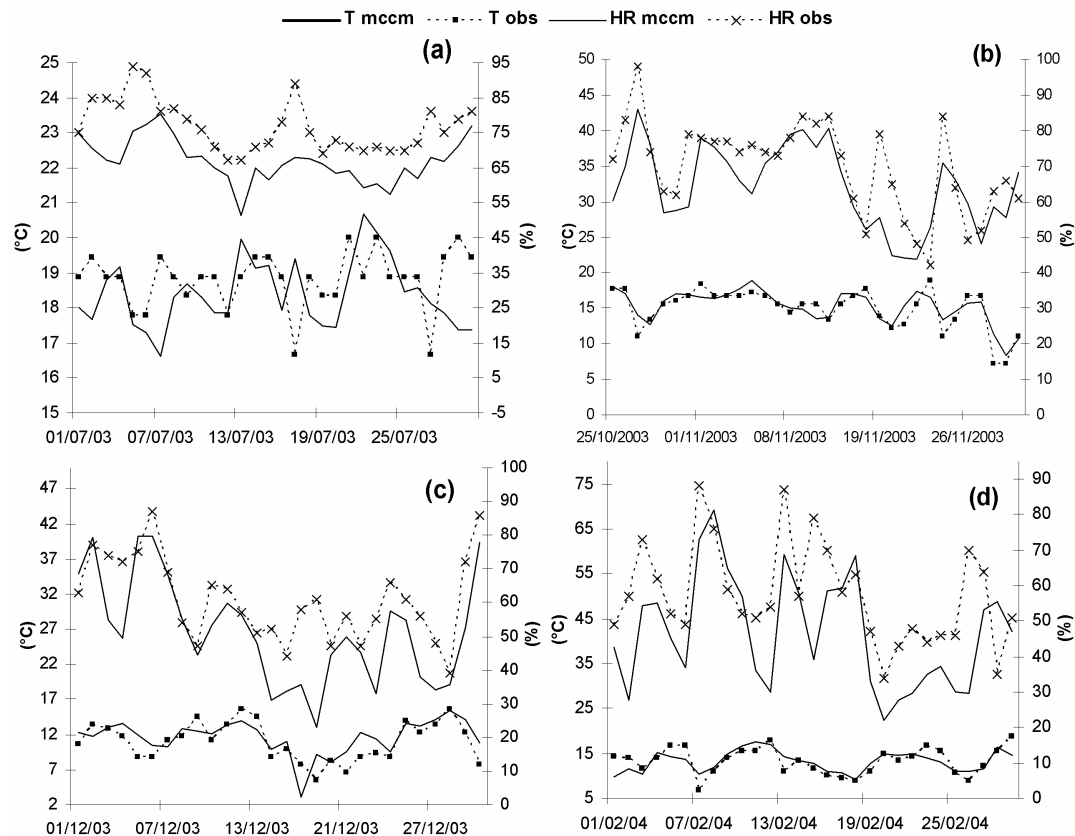


Fig. 5.2 Time series of temperature ($^{\circ}\text{C}$) observed data and MCCM output. Observed data of relative humidity (%) and MCCM output are also presented in a second scale. Four selected periods selected are shown for (a) July 2003, (b) October-November 2003, (c) December 2003 and (d) February 2004).

Figure 5.2 presents a comparison among calculated and measured temperature and relative humidity data for four periods in which concentrations of TSP were determined. The temperature and relative humidity for these periods are shown in connection with high TSP concentrations. The results for temperature, relative humidity are shown in the same periods of high TSP concentrations. In Fig. 5.2c, for instance, a cold front propagating on December 19 in the San Luis Potosi valley caused low temperature and relative humidity values and strong winds in the lead edge. Hence, it is possible to link the atmospheric

behavior to the increase or reduction of concentrations of TSP by accumulation or dispersion in the lower atmospheric layers due to a stratified or turbulent atmosphere.

5.3.3 PM10/TSP

The aim of this study is to analysis the dispersion of particulate matter, their relation with atmospheric circulation and physicochemical properties. TSP samples were collected in order to obtain the most of the information about the particles, including size ranges and chemical composition. Although, there is a national urban air quality network for many cities in Mexico (SINAICA), PM10 monitoring was recently implemented for UASLP. PM10 and TSP have been simultaneously sampled for the year 2008. Both samplers are located in the same site in the urban area. Fig. 5.3a shows the daily average of TSP and PM10 that represents the 56.69% of the TSP for October 2008.

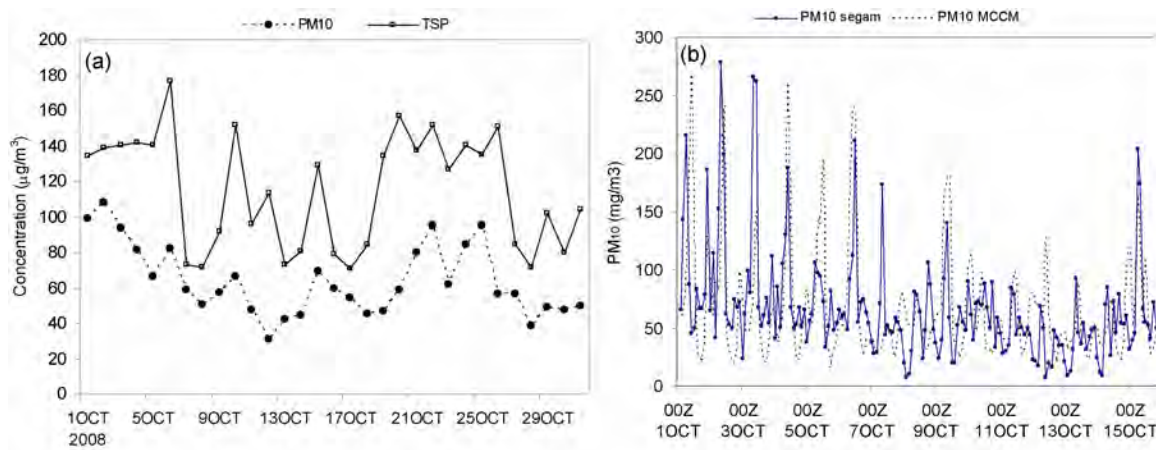


Fig. 5.3 (a) Measures data of TSP/PM10 for October 2008 (b) PM10 field observations and MCCM output for October 2008.

For this study an initial emission inventory was proposed to simulate TSP events, which represented an acceptable approximation of the TSP behavior. The emissions rates were able to reproduce the daily cycle, at least in phase and concentrations and PM10/TSP

proportions similar to those calculated from measured data (Table 5.2). Thus, the same initial conditions for emission were used to evaluate PM₁₀ in recent monitoring. It was observed that the emissions were able to reproduce actual conditions (Fig. 5.3b). In Fig. 5.3b is shown a model test simulation for PM₁₀ from 1 to 15 October by applying the proposed emission inventory. It is observed the capability of MCCM not only for simulating daily variations but also concentrations (RSME=20.2).

Table 5.2 RMSE values of PM₁₀ and modeled PM₁₀ and observed TSP proportion

Run ID	RMSE _{PM₁₀}	PM ₁₀ /TSP
200306	7.48	0.45
200307	14.77	0.63
200308	24.73	0.75
200309	3.43	0.52
200311	18.64	0.62
200312	23.76	0.66
200401	39.53	0.83
200402	20.56	0.63
200403	39.28	0.38

The TSP annual mean concentration was 343 $\mu\text{g m}^{-3}$ above the maximum recommended guideline value of the Mexican Official Standard and World Health Organization of 90 $\mu\text{g m}^{-3}$ and 75 $\mu\text{g m}^{-3}$ respectively (NOM, 1993; WHO, 2002). It is possible to appreciate a large concentration of particulate matter in dry cold periods of November 2003 and February 2004 (Fig. 5.4). It can be associated with the intensity of winds ($>7 \text{ m s}^{-1}$) which favors the local resuspension and fugitive dust. While in the arid zones agriculture dust contribution is a major factor, it is not possible to specify its original source by a single inspection. It is possible to identify dust events by analyzing reported data from the Navy Aerosol Analysis and Prediction System (NAAPS) (Hogan and Rosmond, 1991). In the

sampled period there were not presences of fugitive dust by wind erosion affecting the study area. This means that local sources (urban) are the major contribution of PM in the UASLP. Thus, we have focused this study on the urban sources distribution and its implications in particles properties.

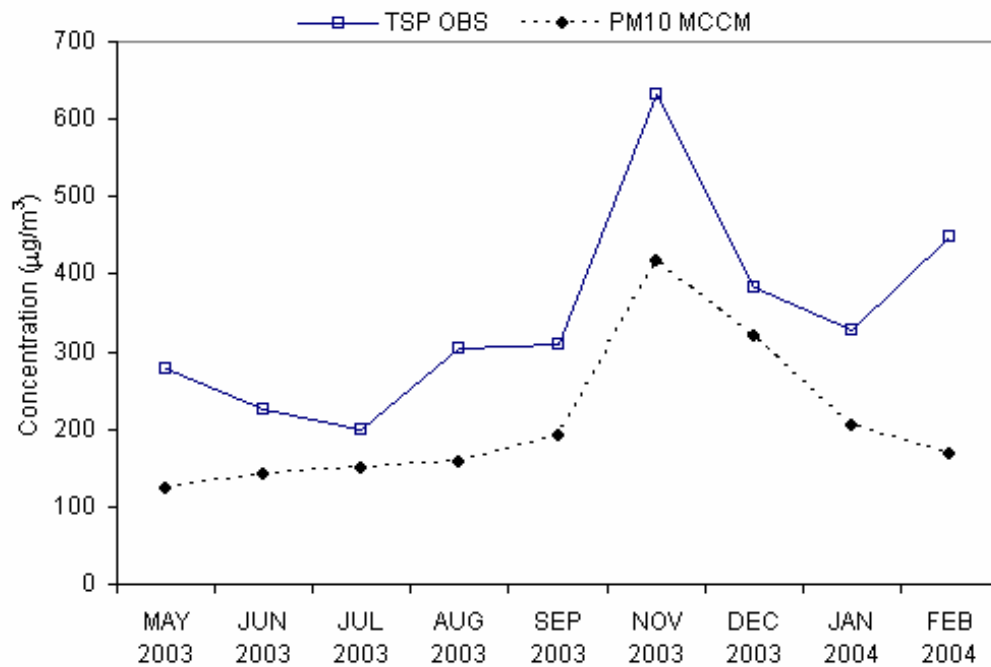


Fig. 5.4 Monthly means of measured PM10 data and modeled data for the period from May 2003 to February 2004.

In summer time, we observed that TSP/PM10 levels are significantly smaller than in the cold period. This result may be attributed to the influence of low winds ($<4 \text{ m s}^{-1}$) and to the humidity during the rainy season. Nevertheless, an isolated event on July 3, 2003 occurred in the summer rainy season. It was related to accumulation due to converging regional flow. It is discussed below, and the analysis revealed the main influence of urban sources on the studied area.

Figure 5.5 shows time series from representative stations T and B, for events with the highest measured of TSP and modeled PM10 concentrations. Daily averages give us important information about net transport and deposition processes of urban dust; for instance, some high and low TSP values were positively or negatively correlated with strong temperature and relative humidity changes, such as it is shown in the Fig. 5.2, where both cases were documented under wet and dry conditions. The meteorological variables are closely related to TSP concentrations for weather conditions influencing the process of dispersion-deposition.

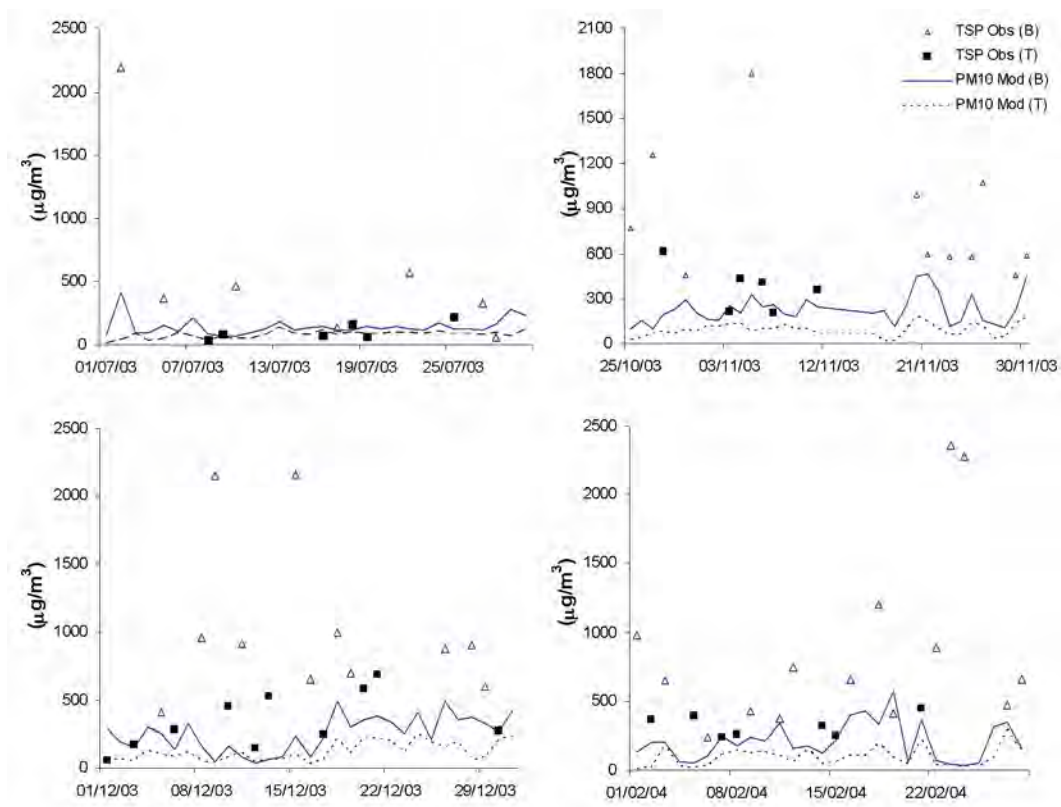


Fig. 5.5 TSP field observations and PM10 concentrations from MCCM output for T and B are shown for periods with maxima concentration (a) July 2003, (b) October-November 2003, (c) December 2003 and (d) February 2004.

As an assessment of the variability along the different seasons, PM10-TSP time series are shown for four selected periods in which maximum concentrations were measured (Fig. 5.5). These events occurred under different circulation conditions. Another approach is that PM10/TSP ratio is variable during the sampling period at difference of reported where TSP and PM10 shown a similar temporal behavior. It is appreciated in simultaneous sampling data. It can be related to intermittent sources of particulate matter greater than PM10 for instance local resuspension on roads or by construction industry sources nearby station B, for instance.

The time series for July 2003 (Fig. 5.5a) reveals an abrupt increase of the concentration of PM10 on July 2, after that the concentrations tend to stabilize for the rest of the month. This anomalous behavior is associated with an accumulation process within the urban area by converging winds. This is clearly seen in Fig. 5.6a which shows a complex pattern of currents that converge and diverge across the valley forming, by topographic effects, zones of accumulation and dispersion. On October 27 and November 5 high concentration events occurred under northerly winds, low temperatures and high values of relative humidity (see Fig. 5.2b and 5.5b), indicating the presence cold fronts. This motion leads to an accumulation of particle matter in the southern part of the city, mostly due to mountain barrier and to easterly winds in this area which converge with the northerlies.

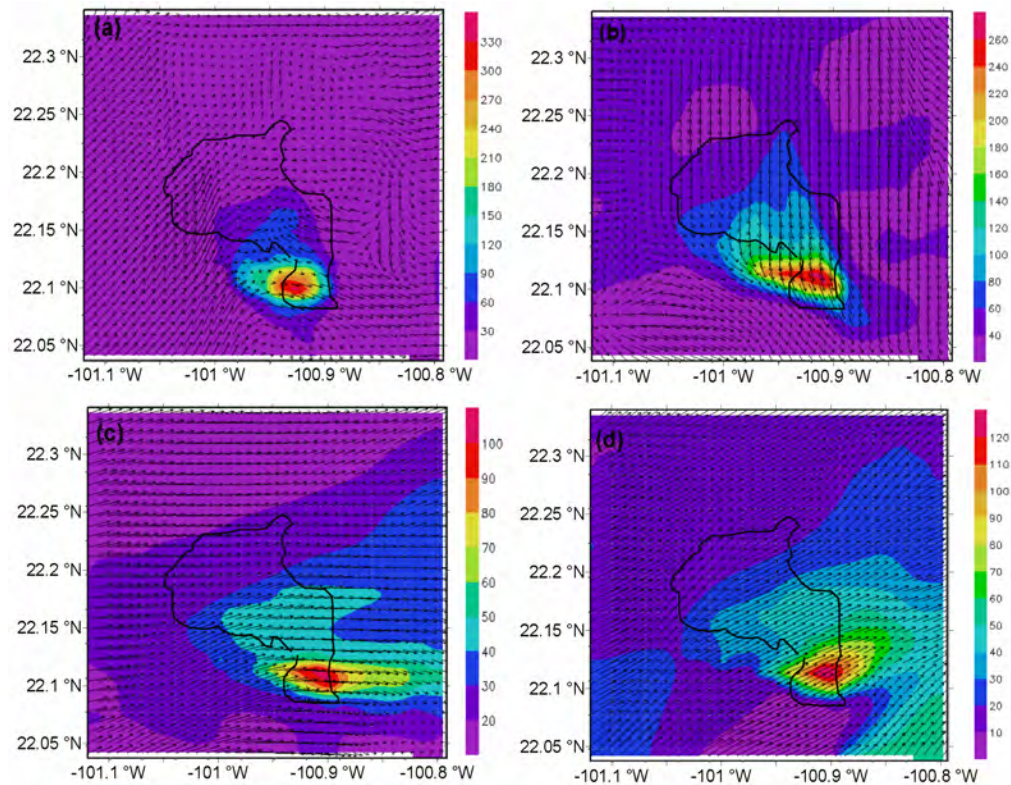


Fig. 5.6 MCCM domain 3 output of PM10 horizontal distribution in $\text{mg} \cdot \text{m}^{-3}$ (shaded color) and wind vectors for: (a) July 2 2003, (b) November 5 2003, (c) December 9 2003 and (d) February 23 2004.

The time series corresponding to December 2003 include values that are above the $500\mu\text{gTSP m}^{-3}$ in 7 days of the month (see Fig. 5.5c). At this time of the year there are more events with strong winds, with gusts reaching speeds higher than 10 m s^{-1} in short intervals, but sufficiently robust to re-suspend large amounts of sub-urban dust causing very high concentration of TSP. These winds are channeled in the northwest direction towards the city by the topographical configuration at the southwestern side UASLP (Fig. 5.6c, see also Fig. 5.1b). The maximum concentration values of TSP reached in calm periods are in this case by accumulation and entrapment and by atmospheric stability.

The maximum wind speed occurs regularly in January, February and with less intensity and frequency in March. In this time of the year there is a major incidence of dust in the northern region of Mexico. Since it is a time of drought, the incidence of strong winds increases significantly the re-suspension of agricultural dust in the surroundings of the UASLP. Statistically, the largest numbers of extreme wind events take place in February (even more than in January and March). An example of these events occurred on February 23, 2004 is shown in Fig. 5.6d, when westerly winds flowed strongly through the UASLP. When these phenomena occur, they dominate over local circulation effects. Under these conditions convergence and divergence processes induce high turbulence and vorticity by mechanic friction in the urban area, characterized by thermal contrasts related to soil properties. This turbulence contributes to the urban dispersion of the emissions.

Two examples of how the dispersion occurs under different seasonal conditions are presented in Fig. 5.7. In summer, there is a major dispersion of pollutants because the turbulence and thickness of the boundary layer is much larger (Fig. 7a). In winter the atmospheric stability in the presence of cold air masses leads to the accumulation of PM10 in the lower layers (Fig. 5.7b). Clearly, the height of PM10 plume is higher in summer than in winter.

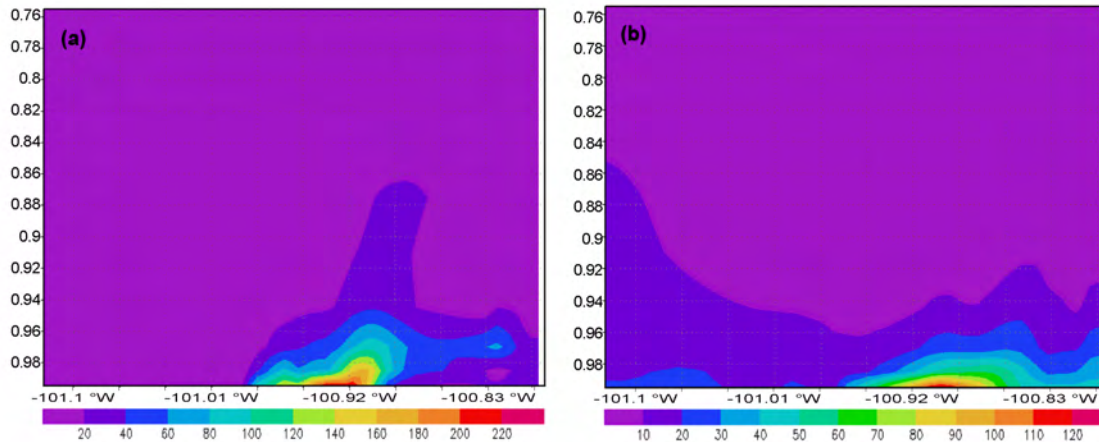


Fig. 5.7 West-East cross section at Lat 22.12 °N (through UASLP) of the vertical distribution in sigma levels of the PM10 modeled concentrations ($\mu\text{g m}^{-3}$): (a) July 2 2003 and (b) December 9 2003.

Annual background overall concentrations are caused mainly by industrial activities, transportation and resuspension in roads by vehicular traffic. This situation is enhanced in the dry season from October to March by sub-urban sources, by a decrease in the height of the boundary layer and atmospheric stability induced by cold air masses. It leads to entrapment and higher concentrations of PM10. As it has been established, the atmospheric circulation in the UASLP throughout a year is quite variable but it shows seasonal preferential patterns: northeasterly winds in winter and southeasterly in summer (most frequently). However, monthly averages for the two specified seasons reveal that overall prevailing winds flow from the southeast (Fig. 8). The importance of presenting monthly average is to focus this research in terms of the spatial and temporal distribution of PM10 and its relation with regional circulation. There seems to be a lack of this kind of studies in fast growing and developing cities of Mexico.

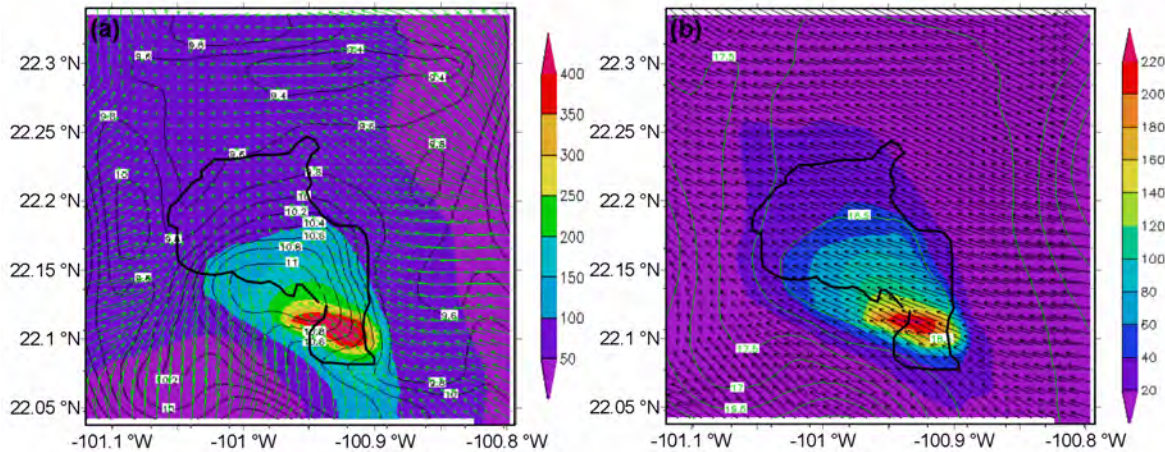


Fig. 5.8 Horizontal distributions of PM10 ($\mu\text{g} \cdot \text{m}^{-3}$) and wind vectors ($\text{m} \cdot \text{s}^{-1}$) of monthly means for (a) December 2003 and (b) August 2003.

5.3.4 TSP Characteristic

We obtained TSP sub-samples directly at chimneys and during the process of some specific industries such as the mechanic-metal industry, paint production, automotive assembly, steel processing, electronic devices production and steel manufacturing. These sub-samples were collected at the same time than the monitoring stations. The main objective of analyzing this supplementary information was to obtain a point for comparing samples found in the principal monitor in order to distinguish anthropogenic particles of natural ones. In previous works in San Luis Potosi, some characteristics of collected particulate matter have been reported from SEM analysis (Aragón-Piña et al., 2006). They showed that while natural particles presented morphological characteristics such as pollen and spores or mineral particles with well defined angles, the anthropogenic ones presented irregular morphology and were generally associated with heavy elements. In addition, particles such as quartz (SiO_2), calcite (CaCO_3) and fluorite (CaF_2) have been reported as a collateral waste of mining activities and anthropogenic particles rich in iron, carbon-sulfur, calcium,

copper, lead and arsenic which are generated by punctual sources such as steel manufacturing, tire industry and copper smelters

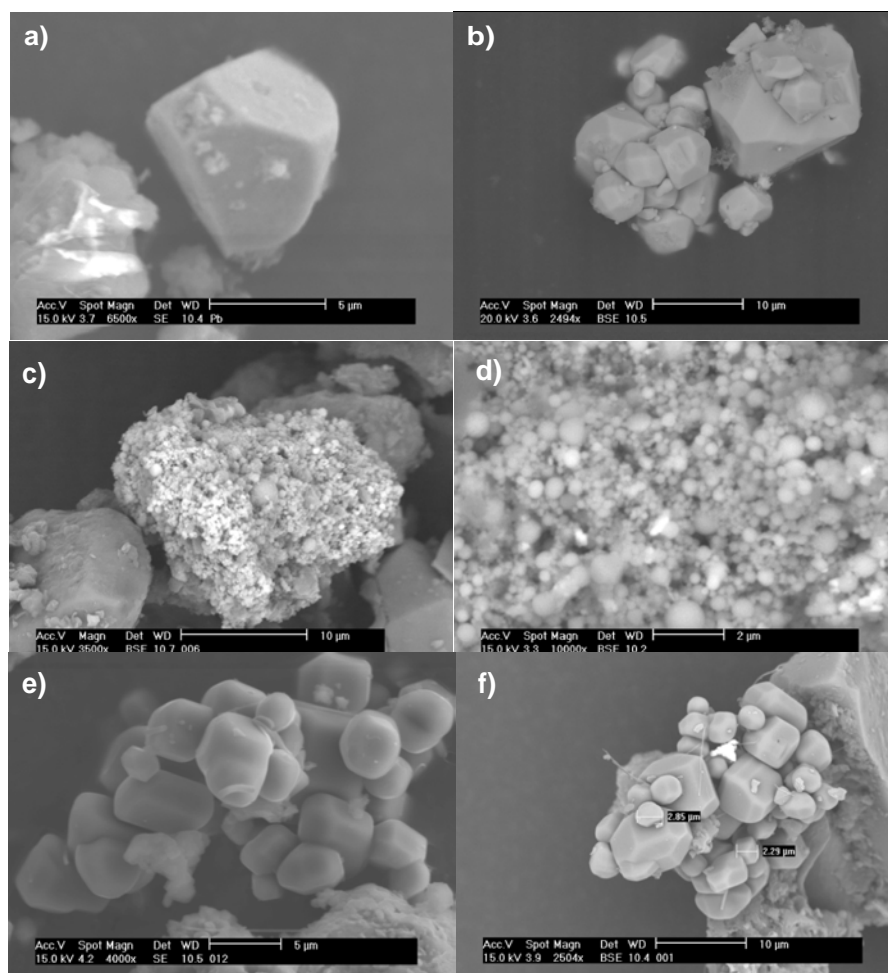


Fig. 5.9 Micrography of anthropogenic of air-transported and industry process particles: (a) lead oxide in T site, (b) particles found in battery manufacture, (c) agglomerates of iron and zinc oxides from T samples (d) agglomerates of particles from process of steel foundry, (e) calcium sulfate particles found in T and (f) particles of waste form chemical industry.

In Fig. 5.9 we shown a series of micrographies of particles found at the station T and sub-samples from punctual sources. The particles found in samples collected at T agree quite well with those captured in sub-samples from punctual sources. We found particles of lead oxide in T station samples presenting defined edges and angles, which are originated in

manufacture of batteries (Figs. 5.9a and 5.9b). The agglomerates of iron and zinc oxides of ultrafine sizes (less than 0.5 μm) were also observed at the station T. These are originated in process of the steel foundry (Figs. 5.9c and 5.9d). Particles of calcium sulfate, presenting a prismatic morphology, from waste of chemical industry of sulfuric acid were observed in both sites (Fig. 5.9e and 5.9f). As well as, particles of carbon-sulfur with traces of vanadium and nickel with porous and spherical morphology were observed at the site T, which are related to burning fuel oil at high temperature from industrial processes. The presence of all of them particles is explained by long-range transport from the IZ sites to the UASLP since there are not industrial sources that generate this kind of pollutants near T site.

5.4. Conclusions

We presented the study of transport and concentrations of PM₁₀ in the Urban Area of San Luis Potosi, Mexico, where not much is known about the effects of the atmospheric circulation on the transport of pollutants, particularly TSP. The city of San Luis Potosi is considered one of the most polluted cities in Mexico, taking into account only the concentrations of PM₁₀ as a criterion. We found an annual average of 343 $\mu\text{g m}^{-3}$ of TSP for the UASLP. The characteristics of the anthropogenic particles that were found at the station T are directly related to the particles originated in the Industrial Zone. It was possible to identify and to relate particles by SEM-EDS techniques with specific sources. We have shown that the location of the Industrial Zone in the UASLP is not favorable, since it contributes significantly to the pollution in the rest of the city by high concentrations of PM₁₀. The fundamental process is the presence of dominant easterly

winds which transport the particles from the Industrial Zone towards the UASLP. Atmospheric circulation described by numerical modeling for high concentration of TSP allow us to conclude that effects of bad ventilation cause the diminution of air quality in UASLP.

References

- Aragón-Piña A., Torres V.G. and Monroy F.M.G., 2000. Scanning electron microscope and statistical analysis of suspended heavy metal particles in air samples from a metallurgically active Mexican city. *Atmospheric Environment* 34, 4103-4112.
- Aragón-Piña A., Torres V.G., Santiago J.P. and Monroy F.M.G., 2002. Scanning and transmission electron microscope of suspended lead rich particles in the air of San Luis Potosi, Mexico. *Atmospheric Environment* 36, 5235-5243.
- Aragón-piña A. Campos-Ramos A.A., Leyva-Ramos R., Hernández-Orta M., Miranda-Ortiz N. and Luszczewski-Kudra A., 2006. Influencia de emisiones industriales en el polvo atmosférico de la ciudad de San Luis Potosí, México. *Revista Internacional de Contaminacion Ambiental* 22(1), 5-19.
- Cavazos, T., 1999. Large-scale circulation anomalies conducive to extreme precipitation events and derivation of daily rainfall in northeastern Mexico and southeastern Texas, *Journal of Climate* 12, 1506-1523.
- Chiriaco M., Vautard R., Chepfer H., Haeffelin M., Morille Y., Protat A. and Wanherdrick Y., 2004. The ability of MM5 to simulate thin clouds: systematic comparisons with lidar/radar measurements. *Air Chemistry, 5th WRF/14th MM5 PSUNCAR Users' Workshop, Colorado*

Garreaud, R. D., 1999. Cold air incursions over subtropical and tropical South America. A numerical case study. *Monthly Weather Review* 127, 2823–2853.

Grell, G.A., Dudhia, J., Stauffer, D.R., 1994. A description of the .fifth-generation Penn State/NCAR mesoscale model (MM5). NCAR Technical Note, NCAR/TN-398+STR, Boulder, CO.

INEGI (Instituto Nacional de Estadística Geografía e Informática), 2002. Síntesis de información Geográfica del Estado de San Luis Potosí. Aguascalientes, México, 15-20, 23-32,

IPCC (Intergovernmental Panel on Climate Change). *Climate Change, 2007. Synthesis Report*

Jazcilevich, A.D., García, A.R., and Ruíz-Suárez, L.G., 2002. A modeling study of air pollution modulation through land-use change in the Valley of Mexico. *Atmospheric Environment*, 36 (14), 2297-2307.

Jazcilevich, A.D., García, A.R., Ruiz-Suárez, L.-G., 2003. An air pollution modeling study using three surface coverings near the New International Airport of Mexico City. *Journal of the Air & Waste Management Association*, 53 (10), 1280-1287.

Kalnay, E., M. Kanamitsu, R. Kistler, W. Collins, D. Deaven, L. Gandin, M. Iredell, S. Saha, G. White, J. Woollen, Y. Zhu, A. Leetmaa, B. Reynolds, M. Chelliah, W.

- Ebisuzaki, W. Higgins, J. Janowiak, K. Mo, C. Ropelewski, J. Wang, R. Jenne, and D. Joseph, 1996. The NCEP/NCAR 40-Year Reanalysis Project. *Bulletin of the American Meteorological Society* 77, 437–471.
- Korhonen, H., Lehtinen, K., and Kulmala, M., 2004. Aerosol dynamics model UHMA: Model development and validations. *Atmospheric Chemistry and Physics* 4, 757–771.
- Kulmala M., Suni T., Lehtinen K. E. J., Dal Maso M., Boy M., Reissell A., Rannik U., Aalto P., Keronen P., Hakola H., Bäck J., Hoffmann T., Vesala T., and Hari P., 2003. A new feedback mechanism linking forests, aerosols, and climate *Atmospheric. Chemistry and Physics Discussions* 3, 6093–6107.
- Leyva R.A., Luszczewski-Kudra A., Monsiváis J.M., Flores H.C., Hernández M.G., 1996. Muestreo Local de aire en San Luis Potosí (Zona Industrial Minera), Vogel et al (Eds.) *Second Inter-American Environmental Congress*, ITESM, México, pp 180-183.
- Magaña, V., Amador J. and Medina S., 1999. The mid-summer drought over Mexico and Central America. *Journal of Climate* 12, 1577-1588.
- NOM-035-ECOL-1993 Norma Oficial Mexicana, métodos de medición para determinar la concentración de partículas suspendidas totales en el aire ambiente y el procedimiento para la calibración de los equipos de medición.

Perez G.I, 1996. Major cold air outbreaks affecting coffee and citrus plantations in the eastern and northeastern Mexico. *Atmosfera* 9, 47-68.

Pineda-Martínez L.F., Carbajal N. and Medina-Roldán E., 2007. Regionalization and classification of bioclimatic zones applying principal components analysis (PCA) in the central-northeastern region of México. *Atmosfera* 20, 111-222

Querol X., Alastuey A., Rodríguez S., Viana M. M., Artiñano B., Salvador P., Mantilla E., Garcia Do Santos S., Fernyez Patier R., De la Rosa J., Sanchez De la Campa A. and Menendez M., 2004b. Levels of PM in rural, urban and industrial sites in Spain. *The Science of Total Environment* 334-335, 359-376.

SEDECO (Secretaria de Desarrollo Económico), 2004. Directorio de empresas que operan en las zonas y parques industriales de la ciudad de San Luis Potosí. San Luis Potosí, México.

Stockwell W.R., Middleton R.P., Chang J.S. and Tang X., 1990. The second generation regional acid deposition model chemical mechanism for regional air quality modeling. *Journal of Geophysical Research* 95, 16343-16367.

Schultz, D.M., Bracken W.E. and Bosart L.F., 1998. Planetary- and synoptic-scale signatures associated with Central American cold surges. *Monthly Weather Review* 126, 5-27.

Wesley M.L.,1989. Parameterization of surface resistance to gaseous dry deposition in regional numerical models. *Atmospheric Environment* 16, 1293 .1304.

WHO 2002. Guidelines for concentration and exposure-response measurement of fine and ultra fine particulate matter for use in epidemiological studies. Published on behalf of the European Commission.

Chapter 6

General Conclusion

In the first part of this thesis the main approach was to obtain a bioclimatic regionalization for Mexico including new criterion in clustering method. Dominant vegetation and topographic features provide support of the distributions of climate regions in Mexico that include some environmental aspects. The land vegetation cover plays an important role for such as aspects. In a scenario of global climate change, it is important to establish frameworks to address these concerns for this issue. From a scientific point of view it is important to know and study all aspects related regional climatic trends in human impacted areas. However, in terms of local and regional scales the knowledge can be addressed to specific issues to study their effects at these scales. In this thesis we analyzed the relationship among impacts on weather and regional climate at relatively small time and spatial scales. The variations on soil surface properties were identified as a potential forcings source at different scales; which influence important aspects such as the energy balances, soil loss and air quality. Moreover, the alterations in the surface properties by changes in the vegetation composition have implications for mesoscale flows inducing alterations in energy balance for the first sub-surface layers of soil. The change in vegetation cover alters the conditions of the immediate surface layer, these mechanisms works as a source of disturbance into the atmosphere. This layer is very important for horizontal and vertical diffusion of heat and moisture into the atmosphere.

We have pointed out the need of obtaining information of heat and moisture fluxes under different conditions such as extreme weather events. Finally, this is a contextual framework for future studies in climate studies considering the environmental and ecological dimension as well as influence of human activities on the environment.